NREL
NATIONAL RENEWABLE ENERGY LABORATORY

Overview and Meteorological Validation of the Wind Integration National Dataset Toolkit

C. Draxl, B.-M. Hodge, and A. Clifton
National Renewable Energy Laboratory

J. McCaa
3TIER By Vaisala

NREL is a national laboratory of the U.S. Department of Energy
Office of Energy Efficiency & Renewable Energy
Operated by the Alliance for Sustainable Energy, LLC

This report is available at no cost from the National Renewable Energy Laboratory (NREL) at www.nrel.gov/publications.

Technical Report
NREL/TP-5000-61740
April 2015

Contract No. DE-AC36-08GO28308

NREL
NATIONAL RENEWABLE ENERGY LABORATORY

Overview and Meteorological Validation of the Wind Integration National Dataset Toolkit

C. Draxl, B.-M. Hodge, and A. Clifton
National Renewable Energy Laboratory

J. McCaa
3TIER By Vaisala

Prepared under Task No. WE11.0705

National Renewable Energy Laboratory
15013 Denver West Parkway
Golden, CO 80401
303-275-3000 • www.nrel.gov

Technical Report
NREL/TP-5000-61740
April 2015

Contract No. DE-AC36-08GO28308

This report is available at no cost from the National Renewable Energy Laboratory (NREL) at www.nrel.gov/publications.

Available electronically at http://www.osti.gov/scitech

Available for a processing fee to U.S. Department of Energy and its contractors, in paper, from:

U.S. Department of Energy
Office of Scientific and Technical Information

P.O. Box 62
Oak Ridge, TN 37831-0062
phone: 865.576.8401
fax: 865.576.5728
email: mailto:reports@adonis.osti.gov

Available for sale to the public, in paper, from:

U.S. Department of Commerce
National Technical Information Service
5285 Port Royal Road
Springfield, VA 22161
phone: 800.553.6847
fax: 703.605.6900
email: orders@ntis.fedworld.gov
online ordering: http://www.ntis.gov/help/ordermethods.aspx

Cover Photos: (left to right) photo by Pat Corkery, NREL 16416, photo from SunEdison, NREL 17423, photo by Pat Corkery, NREL 16560, photo by Dennis Schroeder, NREL 17613, photo by Dean Armstrong, NREL 17436, photo by Pat Corkery, NREL 17721.

NREL prints on paper that contains recycled content.

Acknowledgments

This work was supported by the U.S. Department of Energy (DOE) under Contract No. DE-AC36-08-GO28308 with the National Renewable Energy Laboratory. Funding for the work was provided by the DOE Office of Energy Efficiency and Renewable Energy, Wind and Water Power Technologies Office.

3TIER By Vaisala developed the Wind Integration National Dataset (WIND) Toolkit under contract from the National Renewable Energy Laboratory (NREL). Their experience in wind energy and numerical weather prediction was invaluable for the successful completion of this project.

The authors would like to thank all of the technical review committee participants who helped shape the WIND Toolkit project including Jim Wilczak (National Oceanic and Atmospheric Administration), Wei Yu (Environment Canada), Mark Ahlstrom (WindLogics), Gary Jordan (NREL contractor), Jack King (RePPAE), Dan Beckstead, Keegan Moyer, and B. Nickell (Western Electricity Coordinating Council), J. Caspary (Southwest Power Pool Electric Energy Network), Jimy Dudhia (National Center for Atmospheric Research), Joel Cline (DOE), Jason Schmidt (Ventexx), Sara Harrold (3TIER By Vaisala), Kara Clark, John Michalakes, Kirsten Orwig, Dennis Elliott, Keith Searight, Pat Moriarty, Brian Smith, Julie Lundquist, Aaron Bloom, Debbie Lew, Avi Purkayastha, Billy Roberts, Andrew Platt, Wes Jones, and Marissa Hummon (NREL).

List of Acronyms

DOE	U.S. Department of Energy
EWITS	Eastern Wind Integration Transmission Study
MB	Megabyte
MERRA	Modern-Era Retrospective Analysis
MCP	Measure-correlate-predict
NREL	National Renewable Energy Laboratory
NWP	Numerical weather prediction
NWTC	National Wind Technology Center
PB	Petabyte
SPP	Southwest Power Pool Electric Energy Network
SIND	Solar Integration National Dataset
TB	Terabyte
WIND	Wind Integration National Dataset
WRF	Weather Research and Forecasting model
WWSIS	Western Wind and Solar Integration Study

Executive Summary

Regional wind integration studies in the United States require detailed wind power output data at many locations to perform simulations of how the power system will operate under high-penetration scenarios. The wind data sets that serve as inputs to these studies must realistically reflect the ramping characteristics, spatial and temporal correlations, and capacity factors of the simulated wind plants, as well as be time-synchronized with available load profiles.

The Wind Integration National Dataset (WIND) Toolkit described in this report fulfills these requirements, and constitutes a state-of-the-art national wind resource data set covering the contiguous United States from 2007 to 2013 for use in a variety of next-generation wind integration analyses and wind power planning. The toolkit is a wind resource data set, wind forecast data set, and wind power production and forecast data set derived from the Weather Research and Forecasting (WRF) numerical weather prediction model. WIND Toolkit data are available online for over 116,000 land-based and 10,000 offshore sites representing existing and potential wind facilities.

The WIND Toolkit wind resource data was generated on a 2-kilometer (km) by 2-km grid with a 20-meter (m) resolution from the ground to 160 m above ground, and includes meteorological and power data every 5 minutes. A state-of-the-art forecast data set was also created on a 6-km grid at 1-hour, 4-hour, 6-hour, and day-ahead forecast horizons using industry best practices. During this process, a team of developers focused on mimicking state-of-the art forecast accuracy. The power data were created using data from actual and hypothetical wind farms for 126,000 land-based and offshore wind power production sites. Barometric pressure, wind speed and direction (at 100 m above ground level), relative humidity, temperature, and air density data is available via an online interface.

The conversion from wind to power included wind speed adjustment for wakes with an empirical function, application of power curves using different power curves for offshore and class 1–3 wind sites, and statistical adjustment to power. We used methods that respect the spatio-temporal correlations of typical forecast errors at all delivered horizons. We further applied statistical models at each site for horizons of <= 6h and created probabilistic forecasts using nonparametric error quantiles. Therefore, each power forecast contains a deterministic best-estimate value and the P10/P90 probability of exceedance values.

Through this work, the research team discovered that creating and storing many terabytes of multiyear wind resource output data is challenging. As a result, we used parallel asynchronous I/O (parallel-netcdf combined with WRF Quilt-I/O) to keep pace with the continuous generation of output data resulting from very high spatial and temporal resolutions for a large geographical area (continental United States). This document describes the selections of WRF settings to optimize the model output for wind turbine arrays and includes lessons learned from past projects.

In addition, this document shows a comparison of observational data from six tall towers and three buoys with data from the WIND Toolkit, and thus serves as a validation report of the toolkit's meteorological data set. In this context, "validation" is taken to mean: "confirming that the WIND Toolkit meets the needs of a wind integration study by accurately capturing local

wind conditions and their variability over a wide range of time scales." As described in this report, the WIND Toolkit meteorological data set appears to be an accurate description of the climate and weather at each of the sites that were investigated. Results also indicated that there is no obvious relationship between model performance and terrain. Based on previous experience, the data set is likely to be appropriate for conducting grid integration studies.

The power data set is validated in a separate document (King et al. 2014). Users are reminded that the WIND Toolkit should be used with caution and re-validated for any other application or location.

Table of Contents

List of Figures **8**
List of Tables **10**
1 Introduction **11**
2 Data and Methods **13**
2.1 Site Selection 13
2.2 Data Extraction and Web Interface 14
2.3 Modeling Wind Resource and Forecast Data Sets 16
3 Validation Data Sets **21**
3.1 Observational Data 21
3.2 Reanalysis Data 27
3.3 Quality Control of Observations and Model Data 27
3.4 Error Metrics 28
4 Validation of the National Wind Resource Data Set **29**
4.1 General Validation 29
4.2 Model Restarts 54
4.3 Validation of Power Production Simulations 55
5 Discussion **56**
6 Summary and Conclusion **60**
References **61**
Appendix **63**
WRF Namelist 63
Diurnal Cycles Per Month 65

List of Figures

Figure 1. Map of the final 126,000+ site locations, showing the site density 14
Figure 2. Screenshot of the Wind Prospector data query interface; each dot represents a site, can be clicked on, and allows the data to be downloaded 15
Figure 3. WRF simulation domains 17
Figure 4. Terrain map of the area around the NWTC; the blue cross denotes the location of the measurement tower 22
Figure 5. Terrain map of the area around the measurement station at Cape May Peninsula, New Jersey; the blue cross denotes the location of the measurement tower 23
Figure 6. Terrain map of the area surrounding Butler Grade; the red cross denotes the location of the measurement tower 24
Figure 7. Terrain map of the area surrounding Bovina and Cochran County; blue crosses indicate where the measurement towers are located 25
Figure 8. Terrain map of the area surrounding Megler; the measurement tower is indicated by the blue cross 26
Figure 9. Histograms for observed and modeled wind speeds at Bovina at 50 m (left) and 100 m (right) 30
Figure 10. Histograms of observed and modeled wind speeds at the NWTC (left) and Butler Grade (right) 30
Figure 11. Histograms of observed and modeled wind speeds at Cape May (left) and Cochran (right) 30
Figure 12. Histograms of observed and modeled wind speeds at New York Harbor at 10 m (left) and 50 m (right) 31
Figure 13. Histograms of observed and modeled wind speeds at Portland at 10 m (left) and 50 m (right) 31
Figure 14. Histograms of observed and modeled wind speeds at Santa Maria at 10 m (left) and 50 m (right) 31
Figure 15. Histograms of observed and modeled wind speeds at Megler 32
Figure 16. Quantile-quantile plot for Bovina at 50 m (left) and 100 m (right) 33
Figure 17. Quantile-quantile plot for New York Harbor at 10 m (left) and 50 m (right) 33
Figure 18. Quantile-quantile plot for Portland at 10 m (left) and 50 m (right) 33
Figure 19. Quantile-quantile plot for Santa Maria at 10 m (left) and 50 m (right) 34
Figure 20. Quantile-quantile plot for Butler Grade (left) and Cape May (right) 34
Figure 21. Quantile-quantile plot for Cochran (left) and Megler (right) 34
Figure 22. Quantile-quantile plot for NWTC 35
Figure 23. Wind roses for modeled (left) and observed wind speeds (right) for Bovina at 50 m 36
Figure 24. Wind roses for modeled (left) and observed wind speeds (right) for Bovina at 100 m 36
Figure 25. Wind roses for wind speeds modeled by MERRA (top left), the WIND Toolkit at 60 m (top right), the WIND Toolkit at 10 m (lower left), and observed wind speeds at 5 m (lower right) for New York Harbor 37
Figure 26. Wind roses for wind speeds modeled by MERRA (top left), the WIND Toolkit at 60 m (top right), the WIND Toolkit at 10 m (lower left), and observed wind speeds at 5 m (lower right) for Portland 38
Figure 27. Wind roses for modeled (left) and observed wind speeds (right) for Butler Grade 39
Figure 28. Wind roses for wind speeds modeled by MERRA (top left), the WIND Toolkit at 60 m (top right), the WIND Toolkit at 10 m (lower left), and observed wind speeds at 5 m (lower right) for Santa Maria 39
Figure 29. Wind roses for modeled (left) and observed wind speeds (right) for Cape May 40
Figure 30. Wind roses for modeled (left) and observed wind speeds (right) for Cochran 40
Figure 31. Wind roses for modeled (left) and observed wind speeds (right) for Megler 40
Figure 32. Wind roses for modeled (left) and observed wind speeds (right) for the NWTC 41
Figure 33. Diurnal cycle of wind speed bias (top), CRMSE (middle), and RMSE (bottom) for the summer months for Bovina at 100 m 49
Figure 34. Diurnal cycle of wind speed bias (top), CRMSE (middle), and RMSE (bottom) for the winter months for Bovina at 100 m 50

Figure 35. Annual cycle of wind speed bias (a), CRMSE (b), RMSE (c), and rank correlation (d) for Bovina at 50 m (left) and 100 m (right) 51
Figure 36. Annual cycle of wind speed bias (a), CRMSE (b), RMSE (c), and rank correlation (d) for New York Harbor (left) and Portland (right). The 50-m data are compared to MERRA. 52
Figure 37. Annual cycle of wind speed bias (a), CRMSE (b), RMSE (c), and rank correlation (d) for Santa Maria (left) and Butler Grade (right) 52
Figure 38. Annual cycle of wind speed bias (a), CRMSE (b), RMSE (c), and rank correlation (d) for Cape May (left) and Cochran (right) 53
Figure 39. Annual cycle of wind speed bias (a), CRMSE (b), RMSE (c), and rank correlation (d) for Megler (left) and the NWTC (right) 54
Figure 40. Times series during times of model restarts for 2 months in 2007 at the NWTC at 80 m; the model data at the nearest grid point from the NWTC are in blue and green, and the observations are in red 55
Figure 41. Diurnal cycles of wind speed at the lowest available resolution (left) and hourly averages (right) 58
Figure 42. Annual cycle of wind speed at the lowest resolution (left) and hourly resolution (right); the same legend in Figure 41 applies 58
Figure A1. Diurnal cycle of wind speed bias (top), centered-root-mean-square error (CRMSE) (middle), and root-mean-square error (RMSE) (bottom) for the summer months for Butler Grade 65
Figure A2. Diurnal cycle of wind speed bias (top), CRMSE (middle), and RMSE (bottom) for the winter months for Butler Grade 66
Figure A3. Diurnal cycle of wind speed bias (top), CRMSE (middle), and RMSE (bottom) for the summer months for Cape May 67
Figure A4. Diurnal cycle of wind speed bias (top), CRMSE (middle), and RMSE (bottom) for the winter months for Cape May 68
Figure A5. Diurnal cycle of wind speed bias (top), CRMSE (middle), and RMSE (bottom) for the summer months for Cochran 69
Figure A6. Diurnal cycle of wind speed bias (top), CRMSE (middle), and RMSE (bottom) for the winter months for Cochran 70
Figure A7. Diurnal cycle of wind speed bias (top), CRMSE (middle), and RMSE (bottom) for the summer months for Megler 71
Figure A8. Diurnal cycle of wind speed bias (top), CRMSE (middle), and RMSE (bottom) for the winter months for Megler 72
Figure A9. Diurnal cycle of wind speed bias (top), CRMSE (middle), and RMSE (bottom) for the summer months for the National Wind Technology Center (NWTC) 73
Figure A10. Diurnal cycle of wind speed bias (top), CRMSE (middle), and RMSE (bottom) for the winter months for the NWTC 74
Figure A11. Diurnal cycle of wind speed bias (top), CRMSE (middle), and RMSE (bottom) for the summer months for New York Harbor at 10 m 75
Figure A12. Diurnal cycle of wind speed bias (top), CRMSE (middle), and RMSE (bottom) for the summer months for New York Harbor at 50 m; WIND Toolkit model data are compared to Modern-Era Retrospective Analysis (MERRA) 76
Figure A13. Diurnal cycle of wind speed bias (top), CRMSE (middle), and RMSE (bottom) for the winter months for New York Harbor at 10 m 77
Figure A14. Diurnal cycle of wind speed bias (top), CRMSE (middle), and RMSE (bottom) for the winter months for New York Harbor at 50 m; WIND Toolkit data are compared to MERRA 78
Figure A15. Diurnal cycle of wind speed bias (top), CRMSE (middle), and RMSE (bottom) for the summer months for Portland at 10 m 79
Figure A16. Diurnal cycle of wind speed bias (top), CRMSE (middle), and RMSE (bottom) for the summer months for Portland at 50 m; WIND Toolkit data are compared to MERRA 80
Figure A17. Diurnal cycle of wind speed bias (top), CRMSE (middle), and RMSE (bottom) for the winter months for Portland at 10 m 81
Figure A18. Diurnal cycle of wind speed bias (top), CRMSE (middle), and RMSE (bottom) for the winter months for Portland at 50 m; WIND Toolkit data are compared to MERRA 82
Figure A19. Diurnal cycle of wind speed bias (top), CRMSE (middle), and RMSE (bottom) for the

summer months for Santa Maria at 10 m 83
Figure A20. Diurnal cycle of wind speed bias (top), CRMSE (middle), and RMSE (bottom) for the summer months for Santa Maria at 50 m WIND Toolkit data are compared to MERRA..... 84
Figure A21. Diurnal cycle of wind speed bias (top), CRMSE (middle), and RMSE (bottom) for the winter months for Santa Maria at 10 m 85
Figure A22. Diurnal cycle of wind speed bias (top), CRMSE (middle), and RMSE (bottom) for the winter months for Santa Maria at 50 m WIND Toolkit data are compared to MERRA 86

List of Tables

Table 1. Data Variables Available via the Online Data Extraction Tool and Stored at NREL 15
(All parameters are available every 5 min, except for the wind power forecasts, which are available every hour.) 15
Table 2. Configurations for Sensitivity Study 19
Table 3. Sites, Including Their Longitude, Latitude, Measurement Height, Temporal Resolution, Available Period, and Data Availability 21
Table 4. Error Metrics Used in the Validation Process 28
Table 5. Mean Observed Wind Speeds and Error Metrics using Hourly Values 42
Table 6. Mean Observed Wind Speeds and Error Metrics using 5/10-min Intervals 43
Table 7. Bias (Model – Obs) in m/s Per Month for All Sites using the Lowest Resolution Available (5/10 min) in the Observations (Table 3) 44
Table 8. Bias (Model – Obs) in m/s Per Month for All Sites using Hourly Averages..... 45
Table 9. RMSE in m/s for Each Month at the Lowest Available Common Resolution (Table 3) 46
Table 10. RMSE in m/s for Each Month for Hourly Averages 47

1 Introduction

Conducting integration studies of high-penetration renewable energy futures requires wind and solar power data at a resolution of only a few kilometers to accurately predict the wind and solar output in an area of interest. To conduct simulations of power system plants at these high penetrations, wind power output at a minimum of 1-hour temporal resolution is needed for a very large number of disparate locations. Because these future wind plants do not yet exist, a team of researchers had to simulate the data used for this study. Another requirement is that the wind power output should reflect the same weather conditions as the historical load data, which is heavily influenced by the prevailing weather conditions.

A dearth of high-quality wind resource data for future wind sites poses one of the largest challenges in wind integration studies. Although observational data is preferred, it is not available for all locations that are being considered for future high-penetration scenarios. Furthermore, observed data has some limitations. For example, wind speed data may be available at one location where a future wind plant is envisioned; however, it may be near ground level. There can be significant differences between ground-level wind speeds and hub height wind speeds, and even then the single measurement point is not sufficient enough to represent the conditions within a turbine array simultaneously. To make the best use of limited data sets, some statistical techniques have been developed. Measure-correlate-predict (MCP) is one method that can be used to compare the differences between observed winds at two locations during a short time period, and then to produce longer time series based on the relationships identified. This technique is best used for single locations that are geographically proximate to the desired location.

Reanalysis data sets (NOAA 2014b) help facilitate analyses for wind resource assessments or grid integration in which observational data are not available; however, these data sets have many of the same flaws concerning the discrepancy of conditions at geographically proximate locations. In addition, reanalysis data sets often contain substantial biases (Pryor et al. 2009) and have a resolution that is too coarse for integration studies. Mesoscale numerical weather prediction (NWP) models can be used to downscale reanalysis data sets while adding physical phenomena, due to their smaller spatial and temporal time scales, including the consideration of local topographical features.

Using mesoscale models also provides the advantage of being able to simulate a large number of locations while maintaining the correlation of weather phenomena and their influence on local conditions from one location to the next. This spatial and temporal correlation is essential for integration studies (Lew et al. 2011). Lew et al. demonstrated some difficulties when utilizing NWP models as the basis for wind integration input data sets. Specifically, mesoscale NWP models need to be nested/run regionally and restarted periodically because of computational limitations. When spliced together, these temporal and spatial seams had some unintended consequences, such as false ramps, that resulted in unrealistic outcomes (e.g., higher reserve requirements) during the power system modeling. These undesirable data characteristics had to be corrected, or, if corrections were ineffective, sections of the data had to be removed.

Wind integration studies driven by simulated meteorological data have been carried out several times. As part of the first phase of the Western Wind and Solar Integration Study (WWSIS),

3TIER created a data set using a mesoscale NWP model (Potter et al. 2008). This data set provided hourly wind power data for approximately 30,000 sites in the Western Interconnection from 2004 to 2006. These data sets were the first of their kind and their output has subsequently been used in many different types of research. Other studies have been performed to describe the wind climate in the continental United States (Pryor et al. 2009; National Renewable Energy Laboratory 2014); however, improvements to the data set were needed as renewable integration studies progressed. Some of the user-requested improvements included more recent years of simulated data, a larger number of years for the evaluation of inter-annual variability, a minimization of false ramps and spatial seams, a more thorough incorporation of solar power inputs, and higher temporal resolution data.

The U.S. Department of Energy (DOE) wind and solar programs funded two projects in 2013 to develop updated data sets: the Wind Integration National Dataset (WIND) Toolkit and the Solar Integration National Dataset (SIND) Toolkit. The WIND Toolkit consists of a wind resource and forecast data set. Wind resource data was generated on a 2-kilometer (km) by 2-km grid with a 20-meter (m) resolution from the ground to 160 m above ground, and includes meteorological and power data every 5 minutes. The forecast data set was created on a 6-km grid at 1-hour, 4-hour, 6-hour, and day-ahead forecast horizons using industry best practices. A team of developers focused on mimicking the state of the art in forecast accuracy. The power data were created using data from actual and hypothetical wind plants for 126,000 land-based and offshore wind power production sites. The WIND Toolkit provides barometric pressure, wind speed and direction (at above ground level), relative humidity, temperature, and air density data via an online interface. Issues from previous data sets were addressed in the WIND Toolkit. The data were created to realistically reflect the ramping characteristics, spatial and temporal correlations, and capacity factors of the simulated wind plants, and to be time synchronized with available load profiles.

This manuscript provides an overview and validation of the WIND Toolkit meteorological data set. An extensive validation of the power data set is available in a separate report (King et al. 2014). Section 2 of this report describes the creation of the meteorological data set. Section 3 describes the data sets used in the validation, before we present the results of the validation in Section 4. A discussion is provided in Section 5, and a summary and conclusion in Section 6.

2 Data and Methods

2.1 Site Selection

The site selection process was an important component of the data set generation process. The goal of the site selection methodology was not to recommend future wind plant sites, but to select likely locations. Based on common-practice siting criteria, a total of 112,471 land-based and 14,221 offshore sites were chosen (Figure 1). These sites included existing wind plants, likely future locations, and previous WWSIS and Eastern Wind Integration and Transmission Study (EWITS) locations. Each site was defined by a 2-km by 2-km grid cell in the NWP data set, and it was assumed that eight 2-megawatt (MW) wind turbines were the maximum number of turbines that could be accommodated per grid cell. Certain onsite locations were excluded from consideration because of certain environmental and land-use criteria, and wind speed. These locations included most federal lands and all National Park Service Fish and Wildlife Service-managed lands, open water areas, areas with a slope greater than 20%, and those areas within a buffer area around developed land and airports. Although the location of existing transmission lines is an important consideration when building a new wind plant, the large number of locations needed precluded transmission availability as a feasible criterion; however, because of the large number of sites, users will have the ability to choose sites that most adequately correspond with their expected, planned, or simulated transmission build-out scenarios. For the selection of the 10,000+ offshore sites, the main selection criteria included the wind resource, distance from shore, and bathymetry. All of the sites were at least 8-km offshore. More information about the site selection process can be found in the WIND Toolkit final report (McCaa et al. 2015).

We ran the site selection model using 3TIER's 90-m continental United States wind resource data set for mean annual wind speeds. Based on the exclusions and the buildable land area in each cell, as well as the turbine type implied by the class of wind speed, each of the grid cells was provided with an effective mean generation. For offshore locations, a class 1 offshore turbine was assumed. The sites were then ranked and the best 100,000+ sites chosen, taking care to choose a geographically diverse data set while enabling users to define plant build-outs by clustering sites.

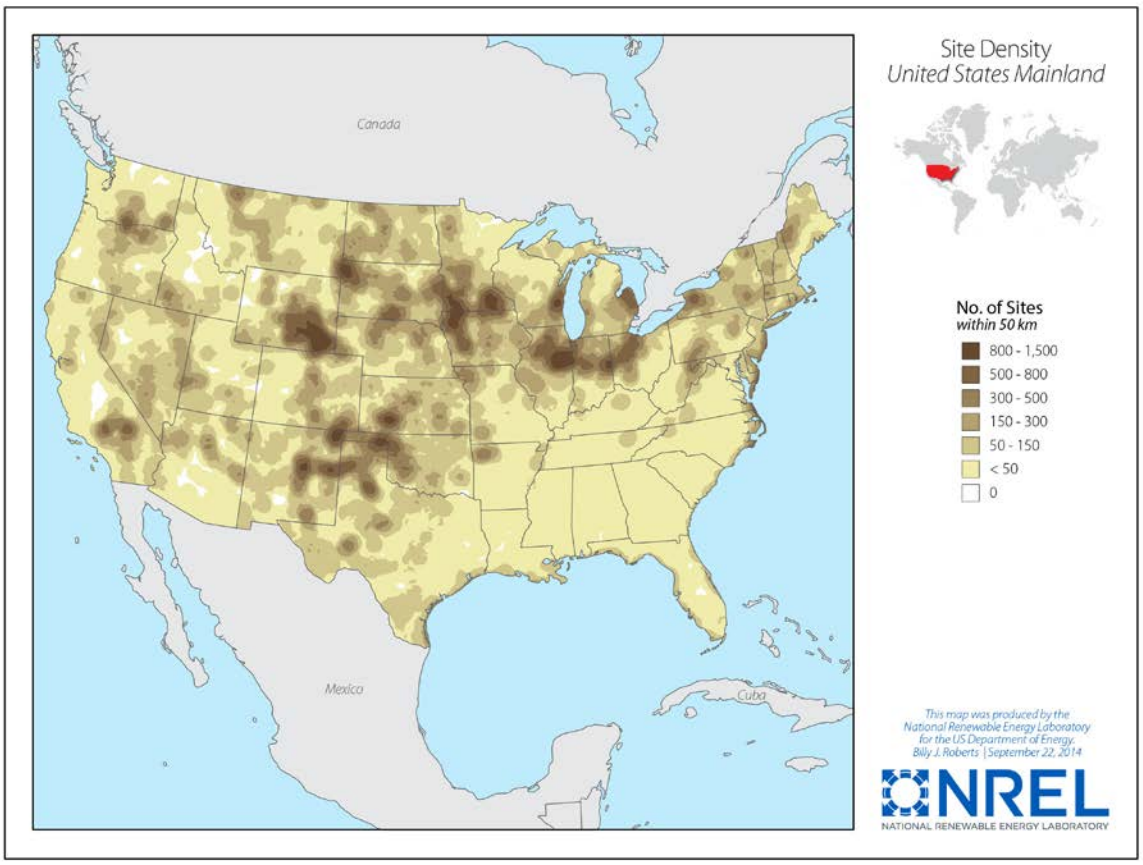

Figure 1. Map of the final 126,693 site locations, showing the site density

2.2 Data Extraction and Web Interface

Wind power forecasts as well as simulated wind power production, production time series of wind speed and direction, 2-m temperature, surface air pressure, air density, and capacity factor data can be downloaded freely from http://maps.nrel.gov/wind_prospector. This data extraction tool is intended to help grid operators with their planning efforts by providing data that are important for grid integration studies. Concerning the forecast data set, note that the purpose of the WIND Toolkit is not to create the most accurate forecasts possible, but one that best reflects current forecast error accuracies. This is important so that wind integration studies conducted with the data provide an accurate view of the impact of state-of-the-art wind power forecasting on power system operations.

The tool's graphical interface makes it easy for users to select data from the 126,000+ sites (Figure 2). The WIND Toolkit was created and funded to be a state-of-the-art wind integration data set to be used by everyone in the wind energy community. As a result, we additionally store an extended meteorological data set at the National Renewable Energy Laboratory (NREL) at every grid point, which is not available via the data query interface because of the extensive size of the data set (Table 1).

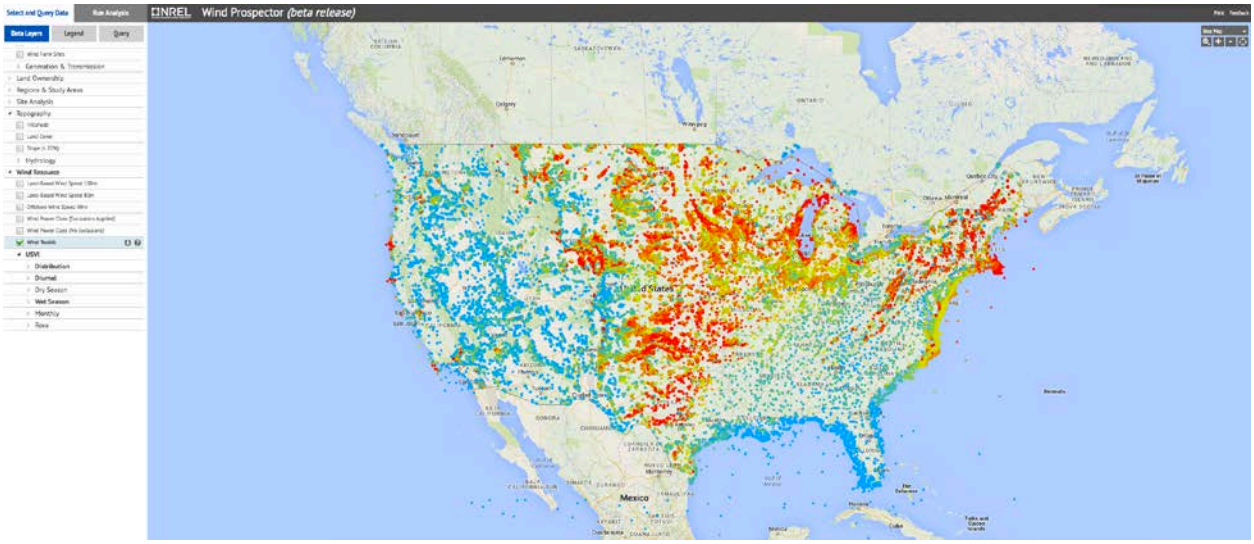

Figure 2. Screenshot of the Wind Prospector data query interface; each dot represents a site, can be clicked on, and allows the data to be downloaded

Table 1. Data Variables Available via the Online Data Extraction Tool and Stored at NREL

All parameters are available every 5 min, except for the wind power forecasts, which are available every hour.

Data Available via Data Interface	Data Stored at NREL
Wind speed at 100 m (m/s)	Wind speed at 10 m, 40 m, 60 m, 80 m, 100 m, 120 m, 140 m, 160 m, 180 m, 200 m
Wind direction at 100 m (degrees)	Wind direction at 10 m, 40 m, 60 m, 80 m, 100 m, 120 m, 140 m, 160 m, 180 m, 200 m
Temperature at 2 m (K)	Temperature at 2 m, 10 m, 40 m, 60 m, 80 m, 100 m, 120 m, 140 m, 160 m, 180 m, 200 m
Surface pressure (Pa)	Relative humidity at 2 m and 10 m
Air density at hub height (kg/m^3)	Precipitation rate at the surface
Wind power forecasts for 1-h, 4-h, 6-h, and 24-h forecast horizon (MW)	Shortwave downward radiation, diffuse irradiance, direct normal irradiance, global horizontal shortwave irradiance
Wind power (MW)	1/L (atmospheric stability)
Time [Coordinated Universal Time (UTC)]	Upward heat flux at the surface
	Boundary layer height
	Surface skin temperature
	u_* in similarity theory
	Pressure at 100 m and 200 m

2.3 Modeling Wind Resource and Forecast Data Sets

The WIND Toolkit was produced with the Weather Research and Forecasting (WRF) model (Skamarock et al. 2008) version 3.4.1, which provides high-resolution (2 km) NWP output over a 7-year timeframe (2007–2013). The wind resource data are available at a 5-min temporal resolution. Forecasts were created for the 1-h, 4-h, 6-h, and day-ahead forecast horizons. This report covers the validation of the meteorological data set only, focusing mainly on the wind speed and wind direction data. We identified wind data to be of main interest to the community. The additional available parameters in the meteorological data set include barometric pressure, relative humidity, temperature, and air density. Performing an extensive physical validation of those additional parameters was beyond the scope of this report.

In this section we describe the WRF setup and model output. Creating and storing many terabytes of multiyear and high temporal and spatial resolution wind resource output data requires innovative solutions. As a result, we used parallel asynchronous I/O to keep pace with the continuous generation of output data.

2.3.1 WRF Setup

The WRF model setup for the wind power production time series consisted of a main grid with a horizontal grid spacing of 54 km and three nested domains of 18, 6, and 2 km (Figure 3). The innermost domain covers the whole contiguous U.S. to eliminate spatial seams in the data. For the forecasts, only the three outermost nested grids were used, which corresponds well with operational forecast grid spacing. The model levels in the lower levels of the atmosphere are at approximately 15 m, 47 m, 80 m, 112 m, 145 m, and 177 m. Model output was then interpolated with the power law (IEC 2005) to 10 m, 40 m, 60 m, 80 m, 100 m, 120 m, 140 m, 160 m, and 200 m. Only the 100-m model output is available publically because of storage restrictions.

For the wind power production time series, the WRF model was initialized and forced at the boundaries with the European Centre for Medium-Range Weather Forecasts Interim Reanalysis (ERA-Interim) data set. The model terrain, roughness, and soil properties were obtained from the U.S. Geological Survey GTOPO30 data, and land use classifications come from the 3-second National Land Cover Dataset (NLCD). In addition, grids were continuously relaxed toward the 6-hourly ERA-Interim reanalysis to prevent drift of the simulations from the analyzed synoptic patterns. We used scale-selective grid nudging, a technique that continuously relaxes the model solution toward large-scale observed analysis fields while preserving small-scale structures within the WRF domain. The model was restarted every month to avoid excessive drift, and the simulations included a spin-up period of 48 h over the last days of the previous month. The model physics options were based on a sensitivity study carried out for this project (Section 2.2.3), and included the Noah land surface model (LSM), the Yonsei University (YSU) boundary layer scheme (Hong et al. 2006), and topographic wind enhancement (Jiminez and Dudhia 2012). Model output statistics and postprocessing techniques were applied to power data before the data were made available. Meteorological data are raw model output. For this study, we took the model data from the raw model output and bi-linearly interpolated the data between the grid points that were located the closest to the observations.

For the forecasts, WRF was initialized and forced at the boundaries with the National Oceanic and Atmospheric Administration (NOAA) Reforecast2 Global Ensemble Forecast System

Control 1-degree, and the National Centers for Environmental Prediction real-time global 1/12th-degree sea surface temperature analysis. Scale-selective grid nudging was employed using the GEFS analysis. The runs were initialized daily at 00 Coordinated Universal Time (UTC). The forecasts were post-processed to respect the spatial-temporal correlations of typical forecast horizons, and each forecast contains a deterministic value and the P10/P90 probability of exceedance values. The probabilities were calculated with nonparametric error quantiles. Power forecasts at 1-h, 4-h, 6-h, and 24-h lead times were produced to correspond to each hour of the wind power production data set.

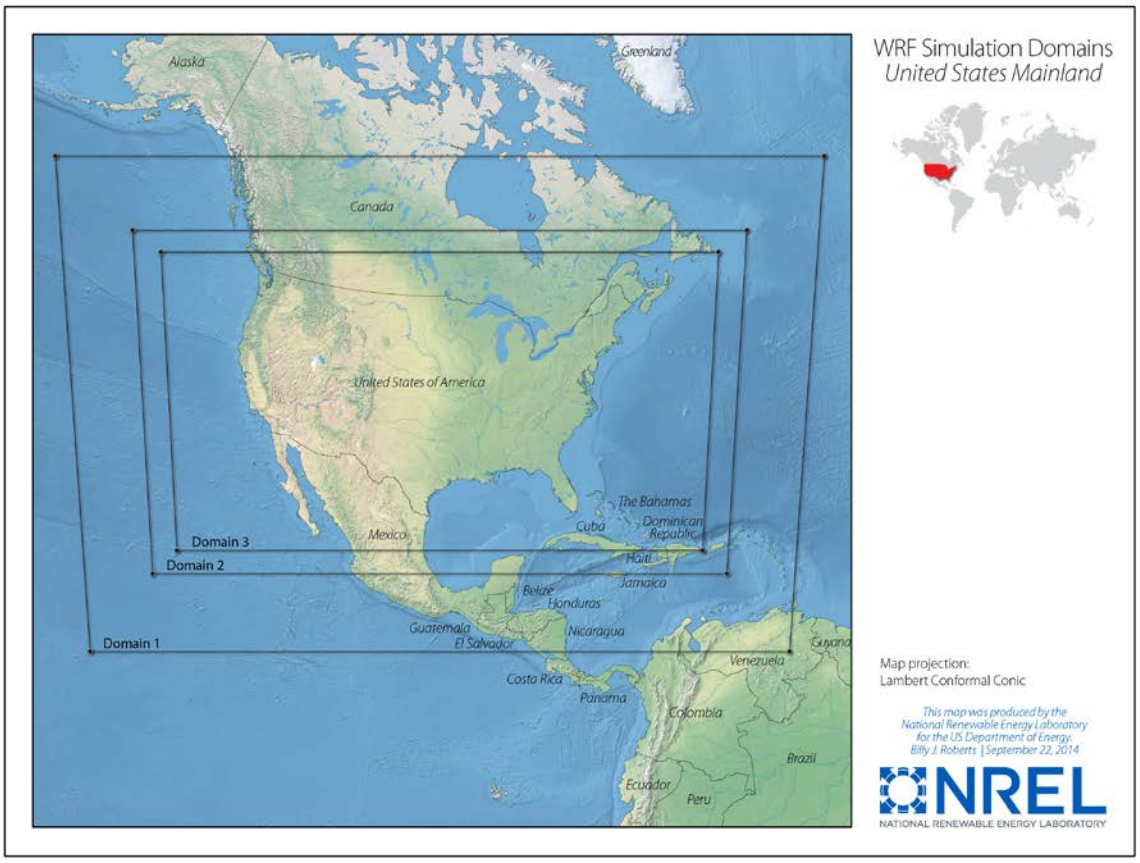

Figure 3. WRF simulation domains

2.3.2 High- Performance Computing System

Part of the simulation runs were performed on the Red Mesa High-Performance Computing (HPC) system at Sandia National Laboratories, and part on the Peregrine, HPC system at NREL. Although Red Mesa's nodes had eight computing Intel Nehalem cores at 2.93 gigahertz (GHz) (packaged as 2 CPUs), with 12 gigabytes (GB) of memory per node and a Lustre Parallel Filesystem, Peregrine's nodes were equipped with two 8-core Intel SandyBridge processors at 16 cores/node, and 32 GB of memory per node. Ultimately, all the data were transferred to Peregrine and the files were checked to make sure the simulations were consistent between the two HPC systems.

Parallel Asynchronous I/O

Creating and storing many terabytes of multiyear and high-resolution wind resource output data requires innovative solutions. The 2-km domain consists of 200 million grid points (3,007 x 1,633 horizontally and 41 vertical levels), which with output every 5 minutes at 16 GB per write would result in 10.6 petabytes (PB) for a 6-year simulation. Eliminating unnecessary fields in output reduces that to 2.7 PB. Such a simulation would require more than 3 years to run on a standard HPC system. The reason for this long runtime is because of the way the WRF model writes data to disk. The numerical part of the code completes a cycle before the buffer has completely written it to disk, which indicates an I/O problem (a performance bottleneck). Therefore, parallel asynchronous I/O (Parallel netCDF (pnetCDF) combined with WRF quilt-I/O) (Li et al. 2003) was used to keep pace with the continuous generation of output data. This method improved the output speed 50:1, making this project feasible.

2.3.3 Selection of WRF Configuration

Because of the large cost of the production runs for the final meteorological data set, it is important to have as much confidence as possible in the configuration of the NWP model before the main simulations commence. Keeping in mind that the focus of the data set is for it to be used as a tool for wind integration studies, the configuration selection we chose centered on numerical stability (particularly with regard to near-surface winds) and fidelity to historical wind speed observations. The sensitivity studies were carried out at a coarse resolution (18 km), and full-resolution simulations were tested for the most promising configuration from the set of coarse runs.

Eight WRF model configurations were tested (Table 2). All configurations share the following properties: the primary driver for the simulations is the ERA-Interim data set. Height, roughness, and soil properties of the earth's surface for the period of simulation are described using the U.S. Geological Survey GTOPO30 data set. The surface layer scheme is the Monin-Obhukov similarity model. Three full years of simulation have been conducted for each model configuration. The configurations were set up in a way that only one element was changed. The eighth configuration included a combination of promising elements from the other seven configurations and was used for subsequent tests at the full 2-km resolution.

Configuration 1 consists of 31 vertical levels and uses the YSU boundary layer scheme, a 5-layer soil diffusivity model (thermal diffusion scheme), and traditional Newtonian relaxation (nudging). The YSU scheme was chosen because it is a widely accepted scheme, and often serves as a baseline. For configuration 2, the number of vertical levels was increased to 51, using a set of levels used in vertical-level sensitivity testing conducted at the Developmental Testbed Center of the National Center for Atmospheric Research (2010). In configuration 3, scale-selective nudging was enabled. When WRF simulations are underway, grids are continuously relaxed, or nudged, toward the large-scale reanalysis to prevent drift of the simulations away from the analyzed synoptic patterns. Domain-resolution-dependent nudging, or scale-selective nudging, allows us to nudge very large domains based on the quantity of wavenumbers resolvable within the domain. Configuration 4 uses the Noah LSM, which simulates soil temperature and moisture in four layers as well as snowpack variables, canopy water content, and the energy flux and water flux terms of both the surface energy and water balance equations. By contrast, the thermal diffusion scheme is much simpler and uses soil temperature in five

layers. The quasi-normal scale elimination (QNSE) boundary layer scheme was used in configuration 5. This planetary boundary layer parameterization was chosen because it includes a turbulent kinetic energy prediction option, and has shown to maintain a meaningful mixed layer in the presence of strong stratification. For configuration 6, the number of full eta levels was increased to 41 in an attempt to concentrate levels near the surface while maintaining numerical stability. Topographic wind enhancement was included in configuration 7 to improve the effects of local complex topography on near-surface winds. This configuration was run at 41 levels as well. Configuration 8 is comprised of configuration 1 and changes made to it in configuration 3, 4, 6, and 7, based on their mildly positive impacts from the earlier testing. This configuration includes scale-selective grid nudging, the Noah LSM, the YSU boundary layer scheme, 41 vertical levels, and topographic wind enhancement.

Table 2. Configurations for Sensitivity Study

Configuration	Vertical Levels	Planetary Boundary Layer Scheme	LSM	Topographic Wind Enhancement	Nudging
Config 1	31	YSU	Thermal diffusion scheme	-	Traditional Newtonian relaxation
Config 2	51	YSU	Thermal diffusion scheme	-	Traditional Newtonian relaxation
Config 3	31	YSU	Thermal diffusion scheme	-	Scale-selective grid nudging
Config 4	31	YSU	Noah LSM	-	Traditional Newtonian relaxation
Config 5	31	QNSE	Thermal diffusion scheme	-	Traditional Newtonian relaxation
Config 6	41	YSU	Thermal diffusion scheme	-	Traditional Newtonian relaxation
Config 7	41	YSU	Thermal diffusion scheme	yes	Traditional Newtonian relaxation
Config 8	41	YSU	Noah LSM	yes	Scale-selective grid nudging

In addition to internal consistency checks, we looked at the agreement between simulated and observed monthly mean wind speed and annual diurnal cycle at 20 meteorological towers across the United States. Quantitative metrics such as the monthly Pearson correlation coefficient at each site were also considered.

Configuration 8 represents a good balance between the improved bias and diurnal cycle representation of configuration 4 (use of the Noah LSM) and the increase in hourly wind speed changes contributed by configuration 3 (the spectral nudging approach). The increase in vertical levels near the surface (at approximately 15 m, 47 m, 80 m, 112 m, 145 m, and 177 m above ground) will allow more information to be extracted at the multiple levels of interest for integration studies, and the topographic wind adjustment should reduce bias in complex terrain. Further bias reductions were revealed when using a higher resolution. As a result, configuration 8 was used for the creation of the WIND Toolkit.

3 Validation Data Sets

A data set is only considered valuable if its deficiencies are known, because corrective actions can be taken to eradicate those deficiencies. Therefore, we present the results from an analysis of wind speeds and directions (e.g., diurnal and annual cycles, frequency distributions, and error metrics of wind speed). The users can then draw conclusions as to the applicability of the data for their site of interest. We acknowledge that validation requirements will differ depending on the application of the data. With this report, we present a validation approach that we believe to be relevant to a broad wind energy community.

This section describes the comparison of the WIND Toolkit wind speeds and directions against observations from six tall towers and three buoys. Reanalysis data collected at the offshore sites were also used to validate the WIND Toolkit. Power data were validated separately against real power output from existing wind plants (King et al. 2014).

3.1 Observational Data

Six sites on land and three offshore were used to validate the WIND Toolkit meteorological data. The sites were chosen in different regions of the continental United States to catch different climatological and weather conditions, as well as terrain. The sites and the available data are summarized in Table 3.

Table 3. Sites, Including Their Longitude, Latitude, Measurement Height, Temporal Resolution, Available Period, and Data Availability

Site	Longitude [°]	Latitude [°]	Height [m]	Temporal Resolution	Time Series [YYYYMMDD]	Data Availability
National Wind Technology Center	-105.23	39.91	80	1 min	20070101-20130101	99.0%
Cape May	-74.89	38.94	100	10 min	20070924-20091215	76.8%
Butler Grade	-118.68	45.95	62.5	10 min	20061231-20111101	97.7%
Bovina (100m)	-102.88	34.52	50, 100	10 min	20090616-20121009	79.1%
Megler	-123.88	46.27	53.3	5 min	20100201-20121102	98.7%
Cochran	-102.76	33.73	70	10 min	20080229-20120629	91.7%
Santa Maria	-120.99	35.00	5	10 min	20061231-20121231	100%
Portland	-70.14	43.53	5	10 min	20061231-20121227	100%
New York Harbor	-73.70	40.37	5	10 min	20081030-20121231	100%

3.1.1 Sites On Land

3.1.1.1 National Wind Technology Center

The National Wind Technology Center (NWTC) is located in Colorado at the foot of the Rocky Mountains at an elevation of ~1,850 m above sea level (Figure 4). The NWTC location is dominated by strong westerly winds, typically resulting from a drainage flow out of the nearby Eldorado Canyon. The site itself is flat and undeveloped, and the mean wind speed is low, but winds can be extremely gusty and turbulent (Clifton et al. 2012). An 80-m meteorological tower monitors the wind flow at a 1-min resolution, and serves as the control against which the raw model output of the WIND Toolkit was compared.

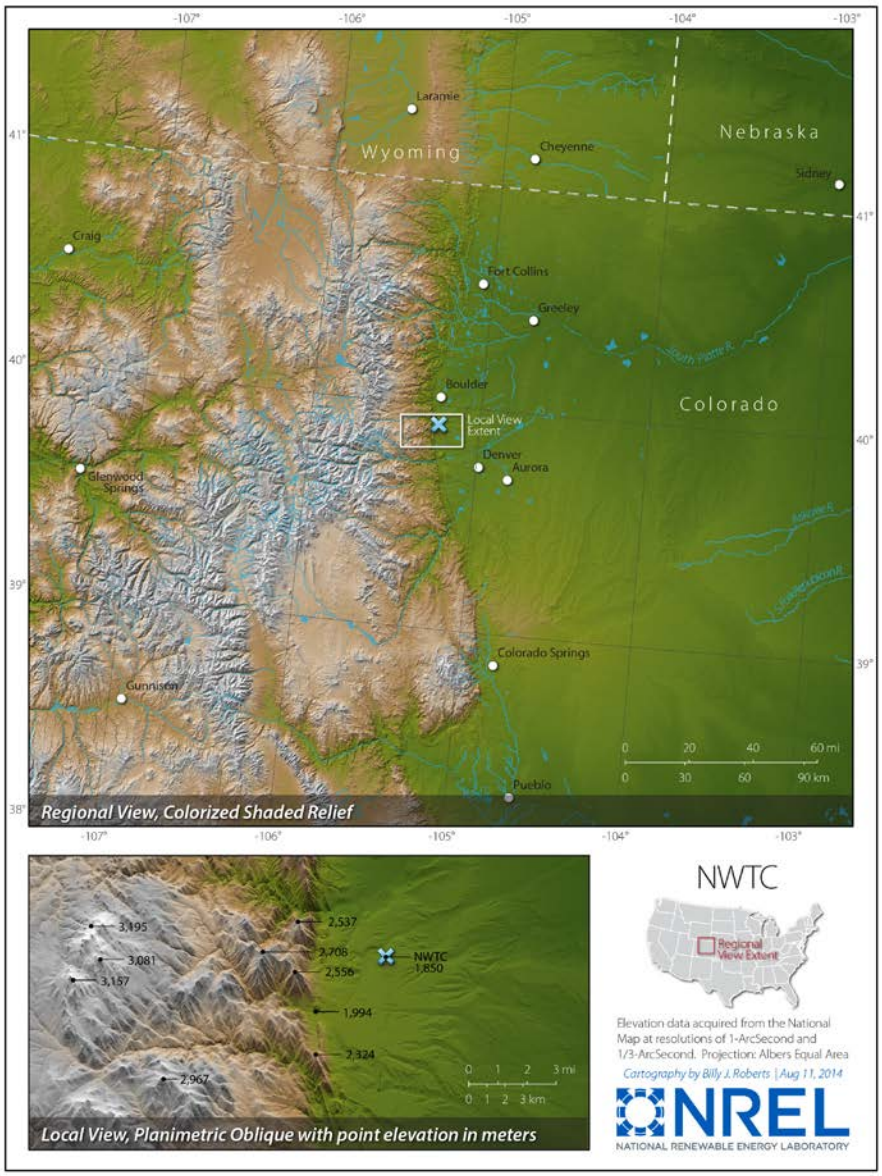

Figure 4. Terrain map of the area around the NWTC; the blue cross denotes the location of the measurement tower

3.1.1.2 Cape May

Cape May is a city at the southern tip of Cape May Peninsula, New Jersey (Figure 5), where the Delaware Bay meets the Atlantic Ocean. Cape May is generally low lying, with its highest point approximately 4 meters above sea level. The measurement tower for this location is positioned directly by the ocean. The 10-min sustained wind speed and direction data were measured at | 100 m.

Figure 5. Terrain map of the area around the measurement station at Cape May Peninsula, New Jersey; the blue cross denotes the location of the measurement tower

3.1.1.3 Butler Grade

Butler Grade is in the vicinity of the Columbia River Gorge, which is a canyon of the Columbia River in the Pacific Northwest of the United States (Figure 6). It cuts through the Cascade Range, a mountain range that extends from British Columbia to Northern California. Atmospheric pressure gradients east and west of the Cascade Range lead to channeling of the flow through the Columbia River Gorge, leading to high wind speeds in the canyon and the site of Butler Grade. The measurement tower is situated in undeveloped terrain. The data were available at 62.5 m at a 10-min resolution.

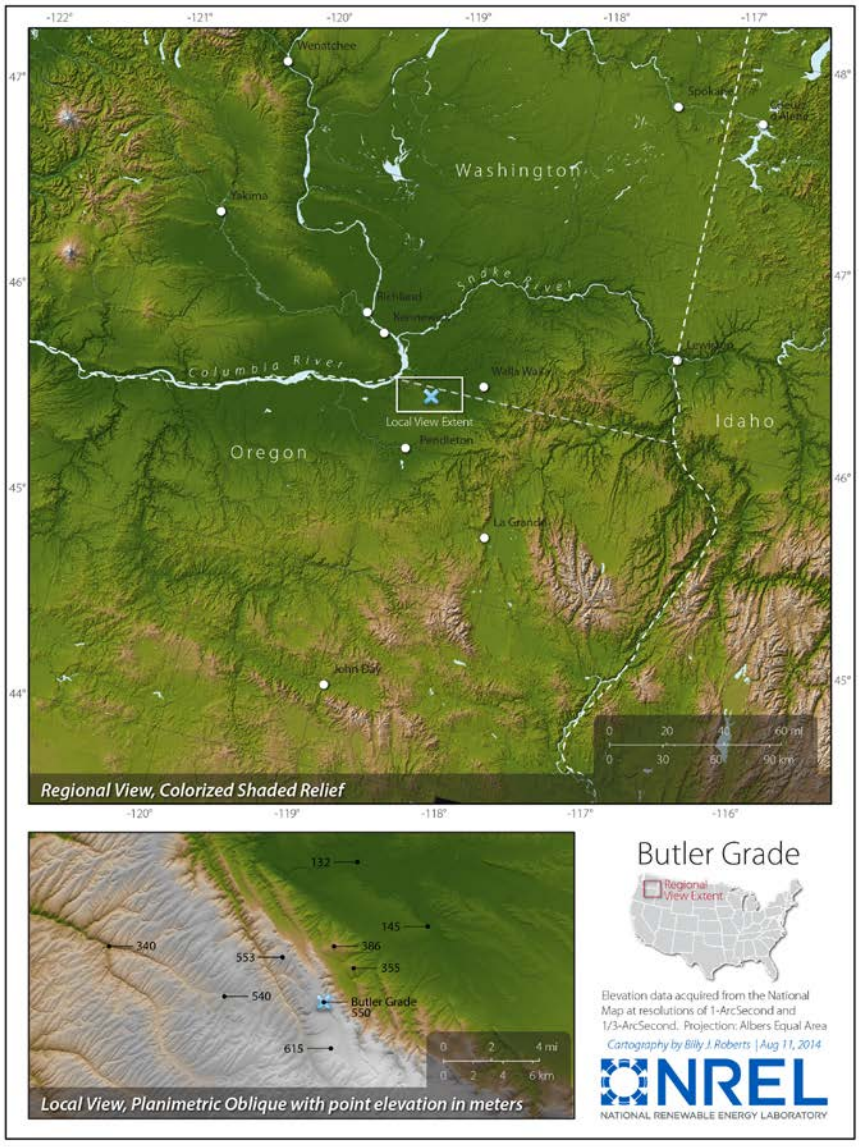

Figure 6. Terrain map of the area surrounding Butler Grade; the blue cross denotes the location of the measurement tower

3.1.1.4 Bovina

Bovina is located in Texas (Figure 7), with flat farmland surrounding the measurement site. For this site, 10-min sustained wind speeds and wind direction data were available at 50 m and 100 m.

3.1.1.5 Cochran

Cochran is located in flat farmland just outside of Morton, Texas (Figure 7). Measurements for this site were available at 70 m at a 10-min resolution.

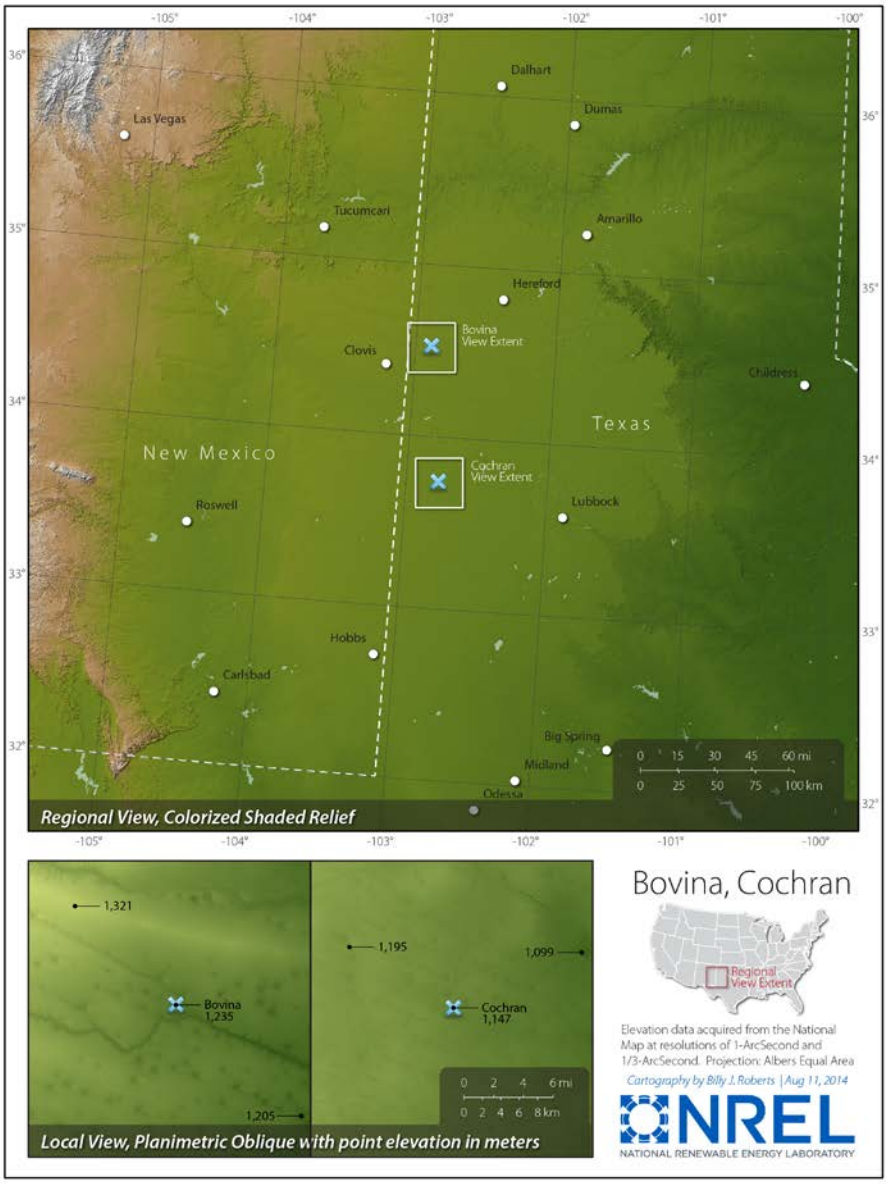

Figure 7. Terrain map of the area surrounding Bovina and Cochran County; blue crosses indicate where the measurement towers are located

3.1.1.6 Megler

Megler is located at the mouth of the Columbia River on the West Coast in Washington state (Figure 8). The measurement site is located on the northern side of the river in relatively tree-rich and hilly terrain, and is influenced by the ocean's climate and weather. Measurements are available at 53 m at a 5-min resolution.

Figure 7. Terrain map of the area surrounding Megler; the measurement tower is indicated by the blue cross

3.1.2 Offshore Sites

Three offshore validation sites were chosen to estimate model performance over the ocean. Buoy measurements were available at 5 m from the National Buoy Data Center (National Oceanic and Atmospheric Administration 2014a). To estimate wind speeds at hub height from these measurements, wind speed, temperature, and the wave state data are needed (e.g., Patton et al. 2014). Unfortunately, this information was not available for this study. As a result, the three

offshore sites were validated with available buoy measurements and model data at 10 m; however, because 10 m is not a good representative for wind energy purposes, the WIND Toolkit data were compared at 50 m to hourly Modern-Era Retrospective Analysis (MERRA) National Aeronautics and Space Administration (NASA) data (see Section 3.2). Details on the three offshore sites are as follows.

3.1.2.1 Santa Maria

Santa Maria is located off the California coast at 35 degrees north. The data for this site were obtained from the National Buoy Data Center. The device (buoy) measures wind speed and direction at 5 m at a temporal resolution of 10 min.

3.1.2.2 Portland

The Portland site is situated off the U.S. East Coast at 43.5 degrees north (Maine). The device (buoy) measures wind speed and direction at 5 m at a temporal resolution of 10 min.

3.1.2.3 New York Harbor

The New York Harbor offshore site is located by the New York Harbor entrance. The device (buoy) measures wind speed and direction at 5 m at a temporal resolution of 10 min.

3.2 Reanalysis Data

MERRA data are freely available, high-quality global reanalyses of weather occurring since 1979, built from version 5 of the Goddard Earth Observing System Data Assimilation System (GEOS-5 DAS) (Rienecker et al. 2011). There are 72 vertical levels in the system, which extend through the stratosphere, with data assimilation occurring over a range of these levels. GEOS-5 DAS assimilates observations from many sources: radiosondes, wind profilers, aircrafts, ships, buoys, radars, land surface stations, and virtually every existing major satellite data set. MERRA is one of the few global atmospheric reanalyses that use data from the entire constellation of NASA Earth Observing System satellites.

We compared MERRA data with the WIND Toolkit data at three offshore sites because observations were only available at 5 m, which is not representative of current turbine hub heights. We acknowledge that the MERRA data set is also simulated data, and can serve only as a comparison data set. An assessment of MERRA data versus WIND Toolkit data for land-based sites is underway.

3.3 Quality Control of Observations and Model Data

All of the observations were quality controlled both visually and automatically with Windographer software to remove outliers, missing and anomalous values, and icing periods.

The model data were not quality controlled in a meteorological sense, but were checked for integrity. NREL produced two files for each output time, one with limited variables that would be made available via the online extraction tool, and another with extended variables that are stored at NREL. We conducted simple checks for integrity based on known good files including checking size and the ability to read the header. The data (500,000 files) were then compressed and transferred from Sandia National Laboratories to temporary, large, long-term storage at NREL. After storing and archiving data, we verified its size and netCDF format. Part of the data

set was created on the Peregrine HPC system at NREL, therefore, comparisons were performed to ensure homogeneity of both data sets.

3.4 Error Metrics

To validate the wind speed data delivered by the WRF model runs, we calculated frequency distributions, diurnal and annual cycles, and error metrics. The latter comprise the root-mean-square error (RMSE), the bias, the centered-root-mean-square error (CRMSE), the rank correlation, the mean absolute error, and the percentage error (Table 4). Unless otherwise noted, the 5-min instantaneous model output was compared to the lowest available resolution of the observations (Table 3), yet at least to 5-min averages. Additional comparisons of hourly averages for both model and observation data were also performed.

Table 4. Error Metrics Used in the Validation Process

Metric	Description
Root-mean-squared-error (RMSE)	$RMSE^2 = \frac{1}{N_p}\sum_{k=0}^{N_p}(F_k - O_k)^2 = CRMSE^2 + BIAS^2$ N_p is the number of available forecast (F) – observation (O) pairs. The RMSE can be split into the systematic and random components (bias and CRMSE) of the RMSE (Taylor 2012).
Bias (BIAS)	$BIAS = \bar{F} - \bar{O}$; $\bar{F}$ and $\bar{O}$ are the forecast and observation averages over N_p values. The bias is the systematic component of the error and describes the differences in the mean of two time series.
Centered-root-mean-squared-error (CRMSE)	$CRMSE = \sqrt{\frac{1}{N_p}\sum_{k=1}^{N_p}[(F_k - \bar{F}) - (O_k - \bar{O})]^2}$ The CRMSE is the random component of the error, and describes the centered pattern of the error, the differences in wind speed variations around the mean.
Rank correlation	The rank correlation is a nonparametric statistic that reflects the strength of a monotone relationship between two variables (Wilks 2005). High correlation values indicate better pattern similarity.
Mean absolute error (MAE)	$MAE = \frac{1}{N_p}\sum_{k=1}^{N_p}\lvert F_k - O_k\rvert$. The MAE is a mean of the absolute errors.
Percentage error	The percentage error is the mean of the absolute errors in percent of the observed wind speed.

An analysis of other variables of the final data set such as temperature, boundary layer height, pressure, relative humidity, Monin-Obukhov length, solar radiation, and precipitation would lead to conclusions and an improved understanding of the behavior of the model; however, that analysis was beyond the scope of this study. Besides, observed data for the above were not available.

4 Validation of the National Wind Resource Data Set

4.1 General Validation

The observations, MERRA data, and WIND Toolkit data were compared using frequency distributions, quantile-quantile plots, wind roses, and error metrics (RMSE, bias, CRMSE, rank correlation, MAE, percentage error, and Renyi entropy—as explained in Table 4) to understand the quality of the raw model data used in the WIND Toolkit.

4.1.1 Rank Histograms of Wind Speed

Rank histograms show whether the wind speed frequency distribution is well captured. Model data are instantaneous, and the averaging time periods for the observations are listed in Table 3.

Figure 9 to Figure 15 show the wind speed distributions at each site. The figures show that the distribution shapes are different for each location. The NWTC (Figure 10 left) shows the widest range of wind speeds, whereas the buoy at Santa Maria (Figure 14) reflects the lowest. Most sites show a Weibull-like distribution, which is the most typical for wind speed (Wilks 2005); however, Butler Grade (Figure 10 right) shows a bimodal distribution. This seems to be common for channeled flow (Draxl et al. 2010; Clifton et al. 2014). A comparison of different sites can be used to identify the effects of terrain on the results. Specifically, we found:

- The WRF model underestimated the frequency of low wind speeds up to 6 m/s at the NWTC and overestimated higher ones. In contrast, the opposite was seen at Butler Grade. Both sites are situated in complex terrain. This is an example of the difficulty encountered when drawing general conclusions for complex terrain based on this validation.

- At Bovina (Figure 9), a flatland site, the WRF model overestimates wind speed up to 10 m/s, and underestimates them above that wind speed. The underestimation is more pronounced at 100 m. On the other hand, at Cochran (Figure 11 right), which is also a flatland site, WRF overpredicts wind speeds above 6 m/s and underpredicts lower ones.

- At Cape May (Figure 11 left; a coastal site), the model performs very well, and the distribution is mostly Gaussian. A slight underprediction can be seen between 6 and 8 m/s. Megler, a site on the West Coast, shows contrasting results: an overprediction above 6 m/s and an underprediction below that value.

- The comparison between the 5-m buoy data and the model data for New York Harbor and Portland shows good agreement between the two sites (Figures 12 and 13).

WRF-modeled winds for wind speeds up to 9 m/s at all of the offshore sites were underestimated when compared to the MERRA data. At Santa Maria, the WRF model overestimates wind speeds above 4 m/s. Note that the MERRA data is modeled and serves here only as a proxy for truth data. Although there appears to be some over- and underestimation of frequencies in certain wind speed intervals, in general, the frequency distributions were well captured by the WRF model.

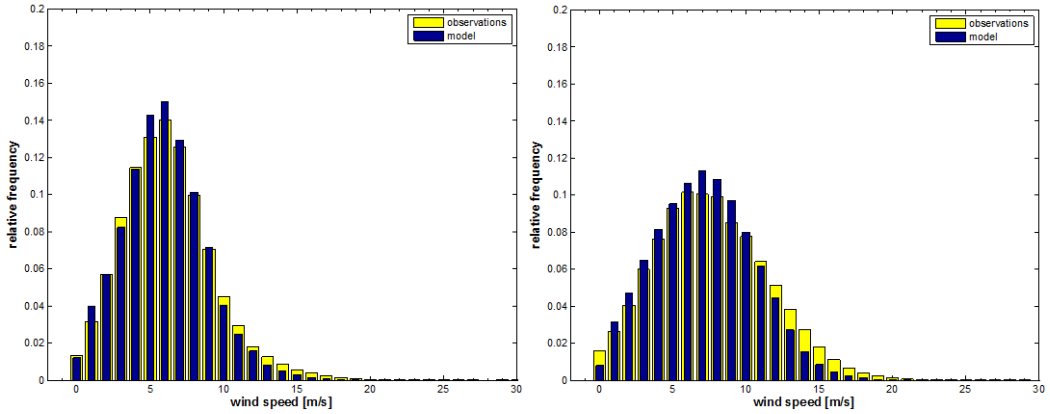

Figure 8. Histograms for observed and modeled wind speeds at Bovina at 50 m (left) and 100 m (right)

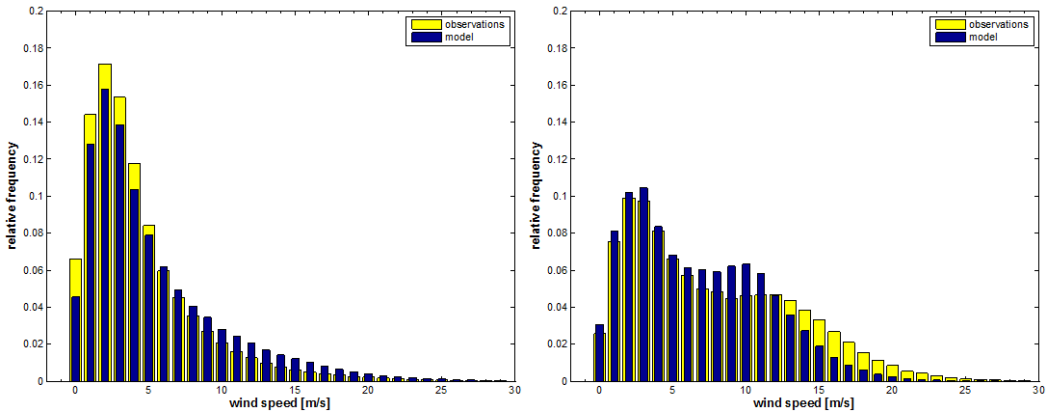

Figure 9. Histograms of observed and modeled wind speeds at the NWTC (left) and Butler Grade (right)

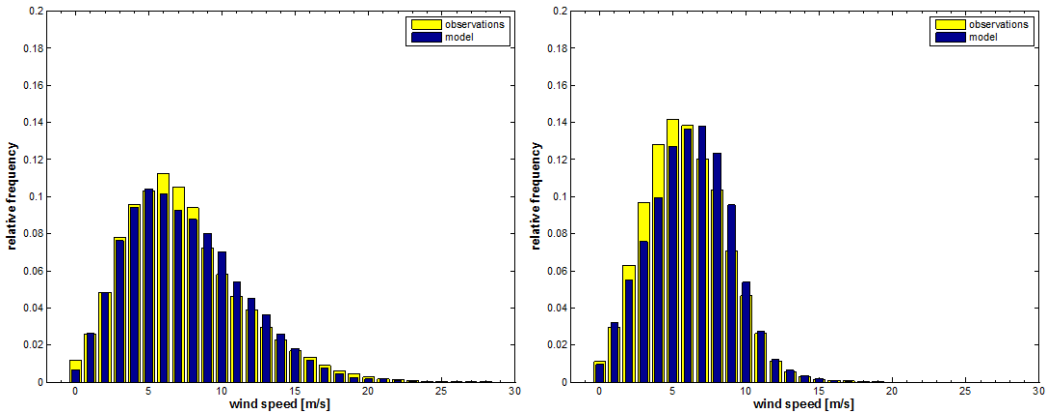

Figure 10. Histograms of observed and modeled wind speeds at Cape May (left) and Cochran (right)

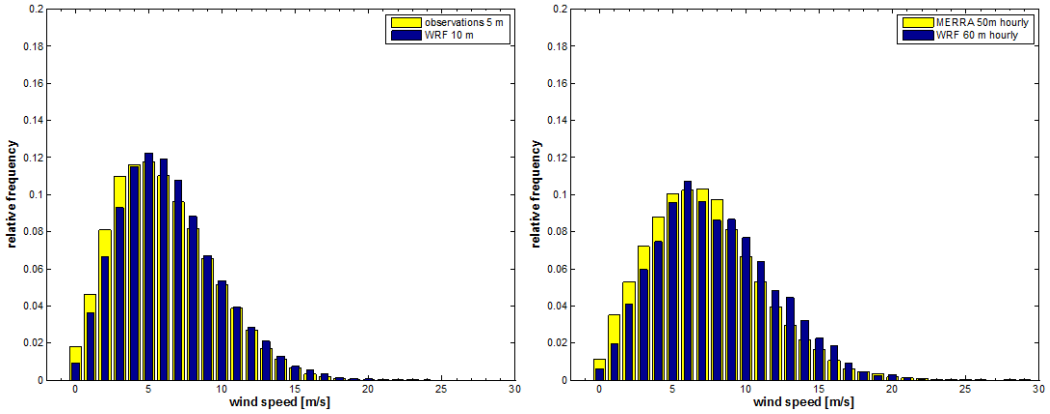

Figure 12. Histograms of observed and modeled wind speeds at New York Harbor at 10 m (left) and 50 m (right)

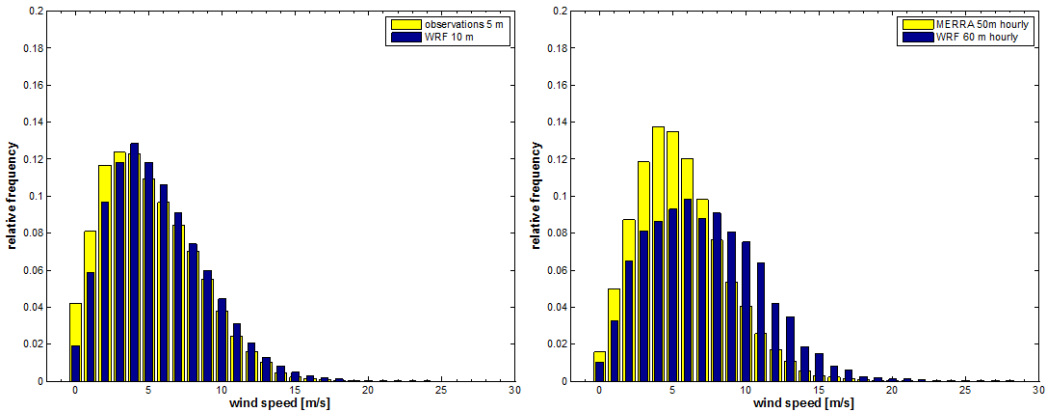

Figure 13. Histograms of observed and modeled wind speeds at Portland at 10 m (left) and 50 m (right)

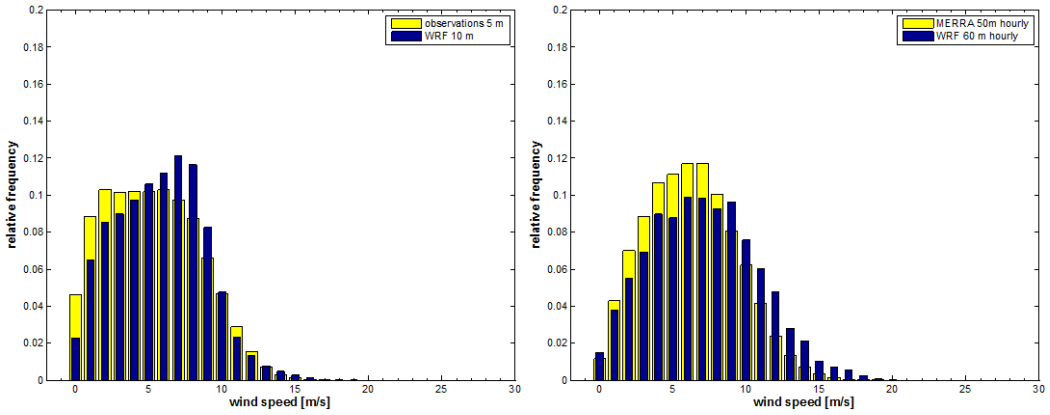

Figure 14. Histograms of observed and modeled wind speeds at Santa Maria at 10 m (left) and 50 m (right)

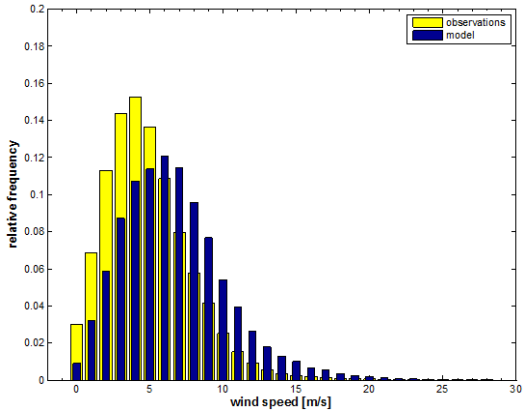

Figure 15. Histograms of observed and modeled wind speeds at Megler

4.1.2 Quantile-Quantile Plots of Wind Speed

The quantile-quantile (q-q) plot is a scatter plot (Wilks 2005). Each coordinate pair defining the location of a point consists of a data value, and the corresponding estimate for that data value derived from the quantile function of the observed distribution. If the points lie along the x=y line, then the model and observational data are equal, come from the same distribution, and should have similar means and variances. If the line is flatter than the $x=y$ line, the observed wind speeds are more dispersed; however, if the line is steeper, the modeled wind distribution is more dispersed/scattered/variable. Results are plotted from Figure 16 to Figure 22. The figures show the $x=y$ line (solid black) and a fit to the data (dashed red) to show how the observations and WIND Toolkit data distributions differ.

In general, results indicated that for all of the sites at lower wind speeds, the quantile function evaluated at the estimated empirical cumulative probabilities is close to the observed data values (i.e., the points are on or very close to the $x=y$ line). The higher the wind, the more the fitted distribution deviates from the $x=y$ line. This is an indication of the tail of the fitted gamma distribution being too thin. This is indeed most pronounced for the NWTC, whose tail is the largest (see histogram in Figure 10).

Curved lines on a q-q plot are an indication of one distribution being skewed. This is the case for Megler (Figure 21 right). In general, the figure shows that at higher winds the modeled distributions deviate from those observed regardless of terrain type. For Bovina, both at 50 m and 100 m, there is a higher incidence of observed high winds than in the modeled WIND Toolkit data—this results in a negative bias, which tends to occur during high wind speeds. At the buoy sites (Figure 17 to Figure 19), the response is the opposite: a higher incidence of simulated wind speeds during high winds (this is most pronounced for Portland, with New York Harbor at 50 m as the exception). Note again that the WIND Toolkit data were compared to MERRA data at 50 m and not observations. At Butler Grade (Figure 20 left), observed wind speeds are shown to be higher than simulated ones during high wind speeds. At Cape May (Figure 20 right), the points lie on the $x=y$ line up to 15 m/s, which means modeled and observed wind speeds should have the same distribution. Cochran (Figure 21, left) shows the same characteristics, but here it can be seen that the model is overpredicting during high wind speeds. At the NWTC (Figure 22), a higher incidence of simulated wind speeds is shown.

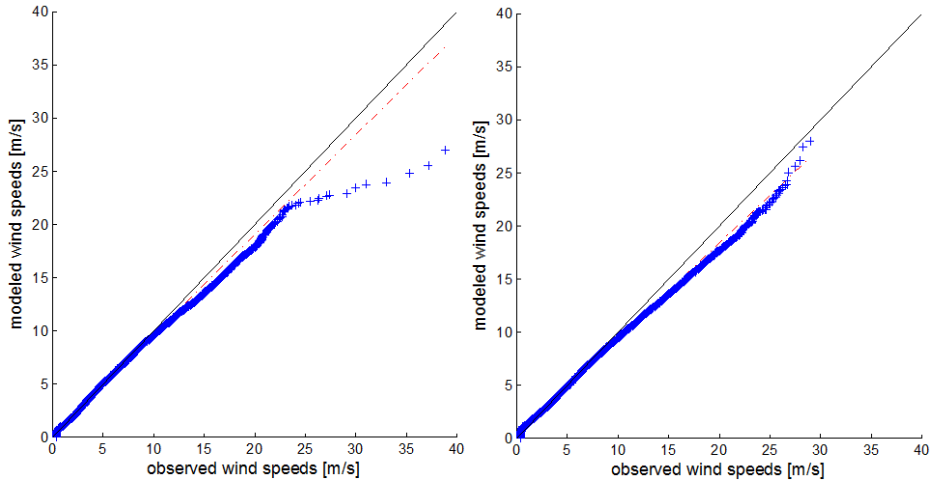

Figure 11. Quantile-quantile plot for Bovina at 50 m (left) and 100 m (right)

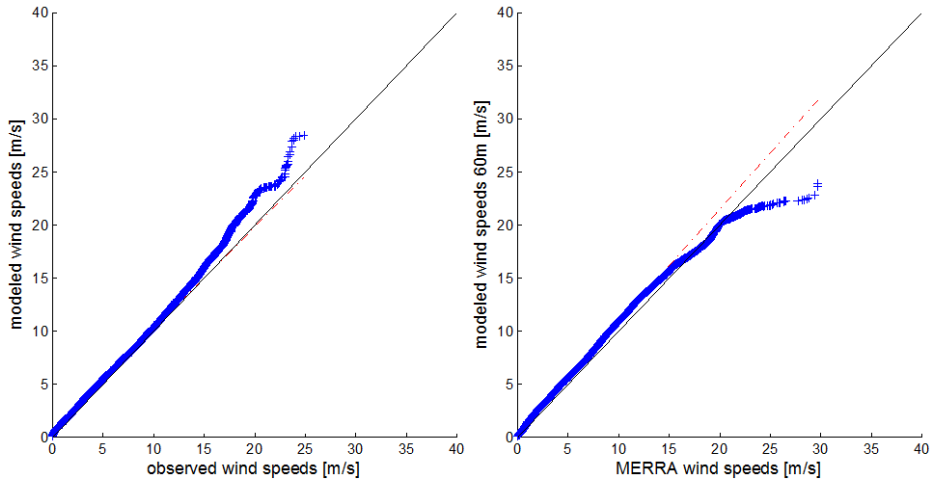

Figure 12. Quantile-quantile plot for New York Harbor at 10 m (left) and 50 m (right)

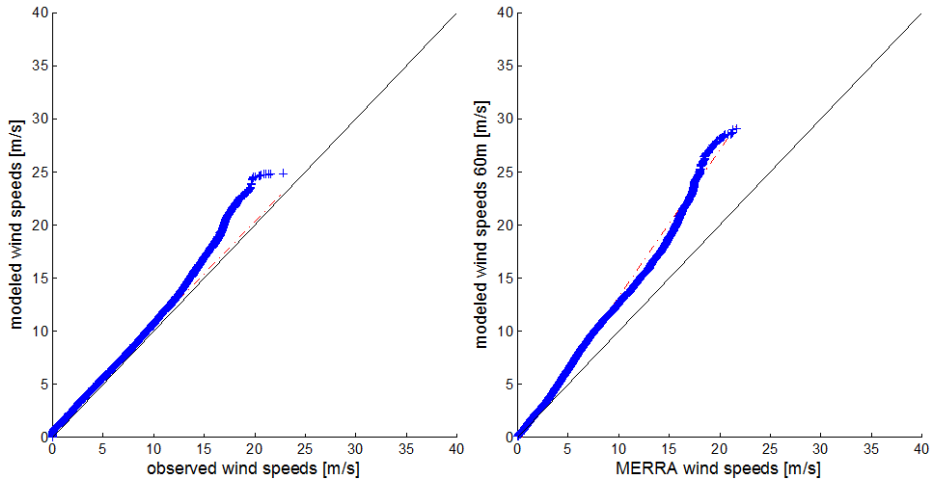

Figure 13. Quantile-quantile plot for Portland at 10 m (left) and 50 m (right)

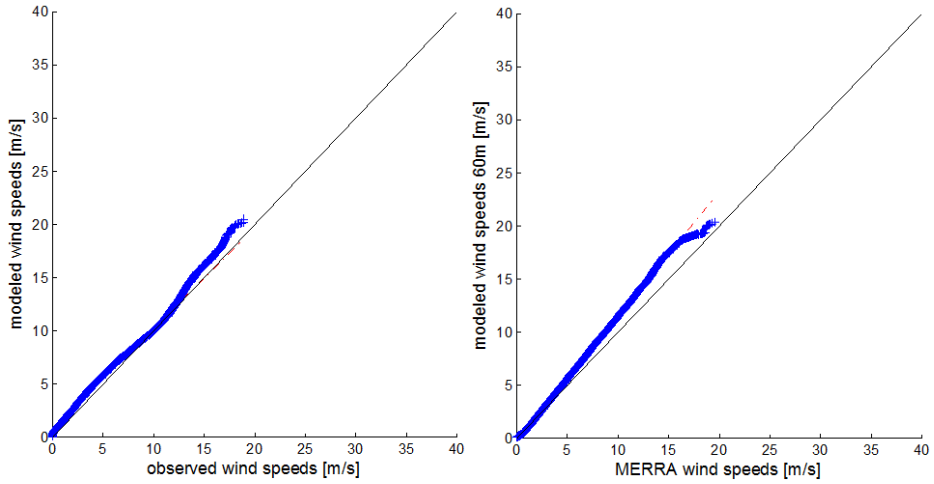

Figure 14. Quantile-quantile plot for Santa Maria at 10 m (left) and 50 m (right)

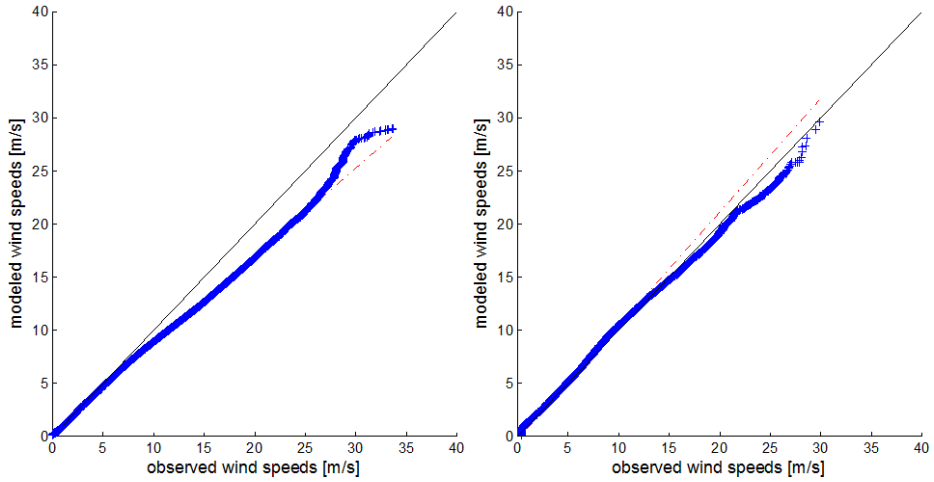

Figure 15. Quantile-quantile plot for Butler Grade (left) and Cape May (right)

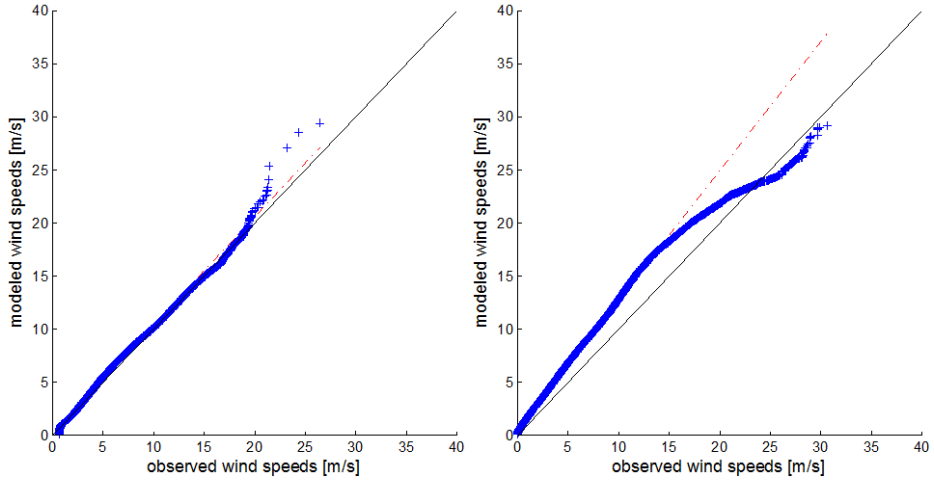

Figure 16. Quantile-quantile plot for Cochran (left) and Megler (right)

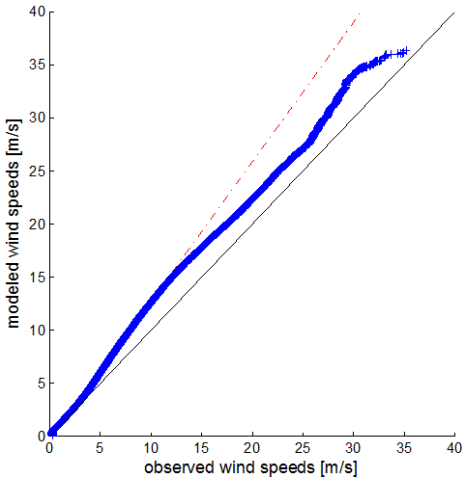

Figure 17. Quantile-quantile plot for NWTC

4.1.3 Wind Roses

Wind roses are plots that display wind speed, frequency, and direction. In addition, they show qualitatively whether the overall wind pattern was captured satisfactorily. For example, wind roses can provide information on whether or not channeling of a flow occurs, or if orographic winds are prevailing. Therefore, knowing prevailing wind directions and wind speed magnitudes helps find deficiencies in atmospheric modeling.

The model data used in the WIND Toolkit appears to capture the directional wind distribution quite well. The channeling at Butler Grade (Figure 27) is clearly visible; however, the winds are modeled to be not quite as strong as in the observations. This might be an indication that the model terrain is too smooth, so that the channeling in the model is not as strong as it is in reality. The modeled wind rose for Cape May (Figure 29) is inaccurate. Although the model has two major wind directions, northwest and south, the observations reveal the main wind directions to be west and around north. Note that there are no wind speeds recorded that are directly north, which might indicate an angle alignment error in the observation, or a tower shadowing effect. At the NWTC (Figure 32), modeled winds are much stronger than those observed during westerly winds, but the directional dependence is captured. Despite the flat terrain, the wind directions at Bovina (Figure 23 and Figure 24) were not easy for the WRF model to capture. The observations show stronger winds and a more pronounced southerly component than the model, which is similar to Cochran (Figure 30). The observed southeasterly component was not captured by the model. The directions at the Santa Maria buoy (Figure 28) were captured, even if the model shows more instances of northwesterly directions. The wind distribution at Portland (Figure 26); however, seems to be hard to capture for WRF, and the comparison at 50 m with MERRA data shows a different directional signal.

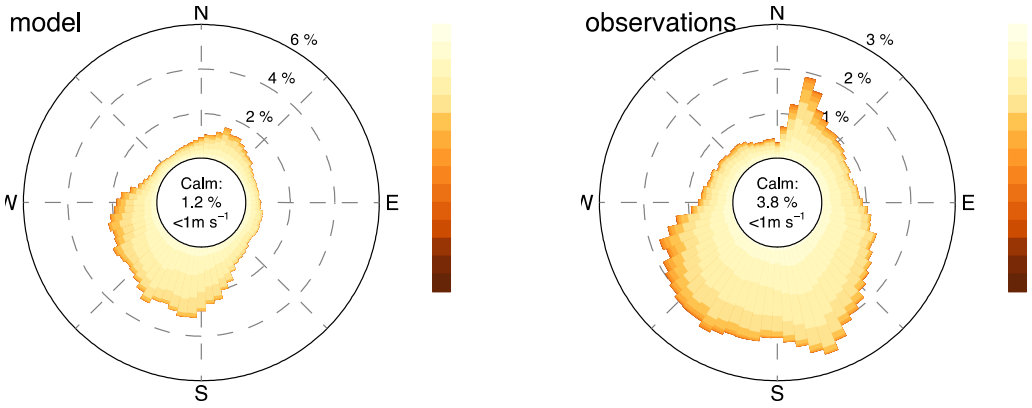

Figure 18. Wind roses for modeled (left) and observed wind speeds (right) for Bovina at 50 m

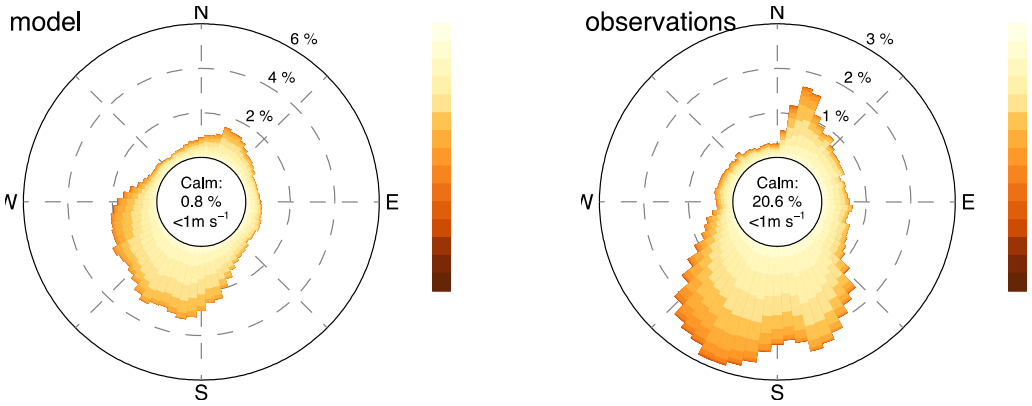

Figure 19. Wind roses for modeled (left) and observed wind speeds (right) for Bovina at 100 m

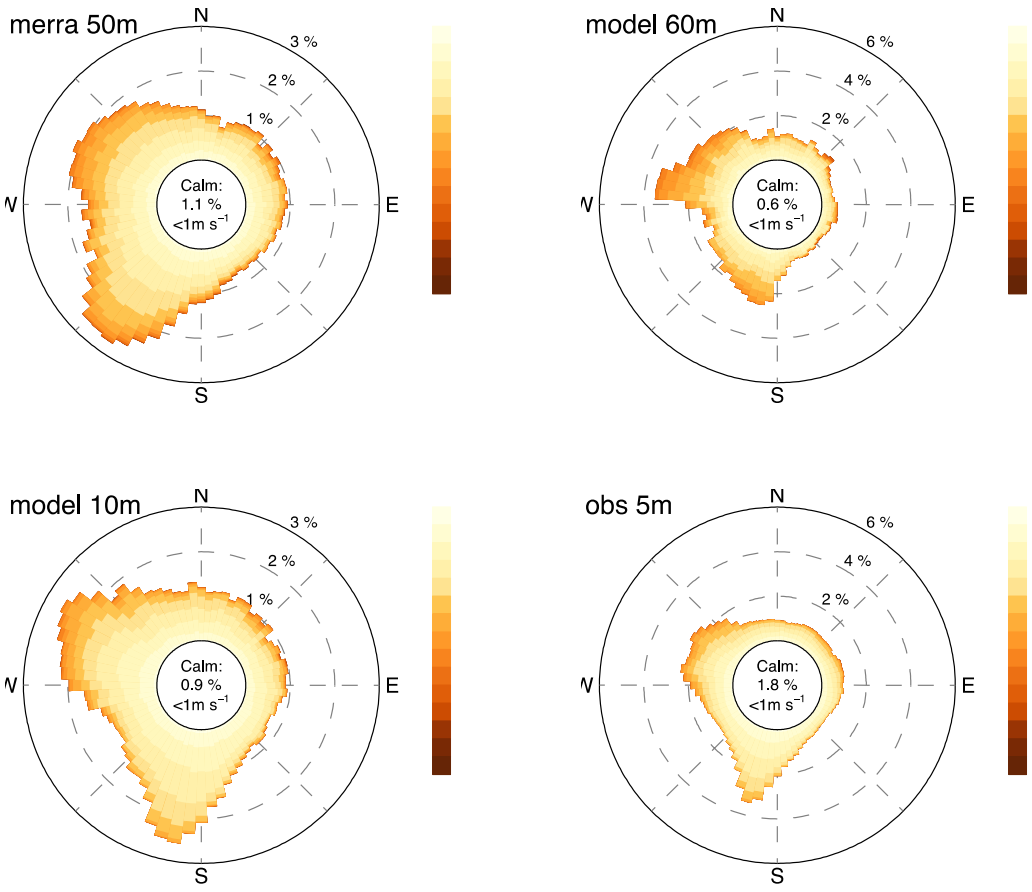

Figure 20. Wind roses for wind speeds modeled by MERRA (top left), the WIND Toolkit at 60 m (top right), the WIND Toolkit at 10 m (lower left), and observed wind speeds at 5 m (lower right) for New York Harbor

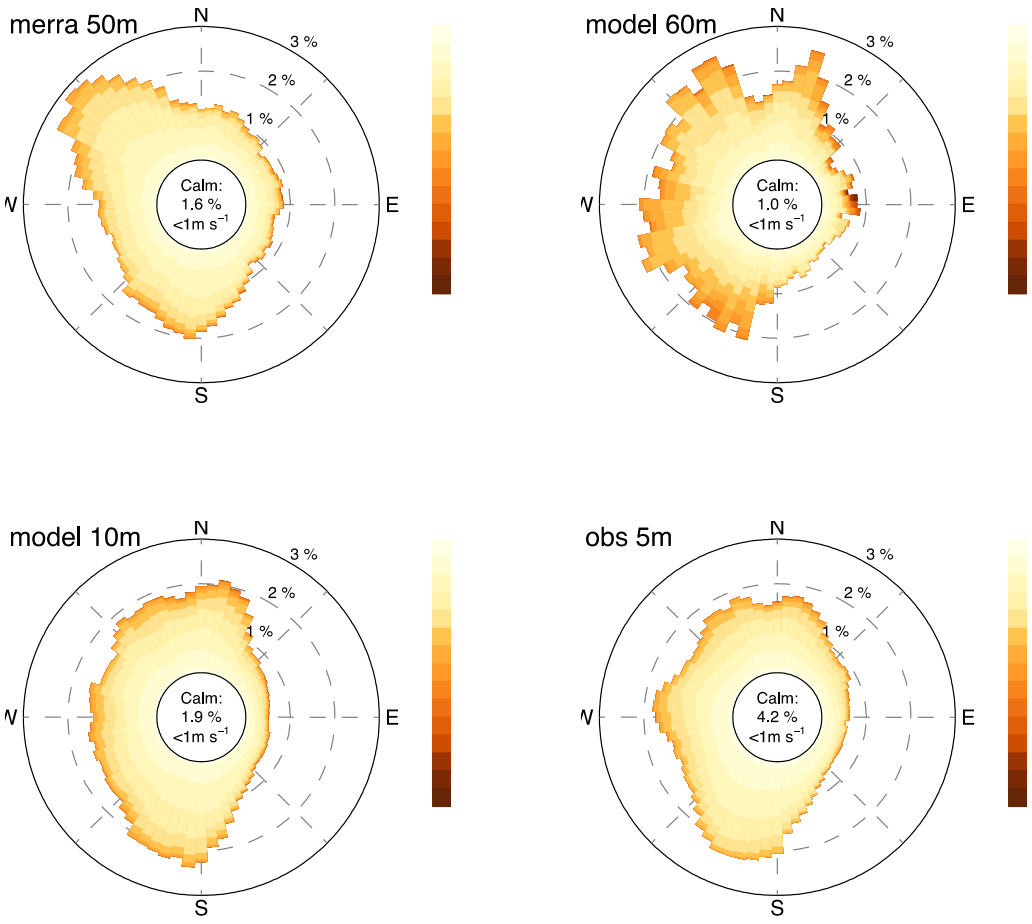

Figure 21. Wind roses for wind speeds modeled by MERRA (top left), the WIND Toolkit at 60 m (top right), the WIND Toolkit at 10 m (lower left), and observed wind speeds at 5 m (lower right) for Portland

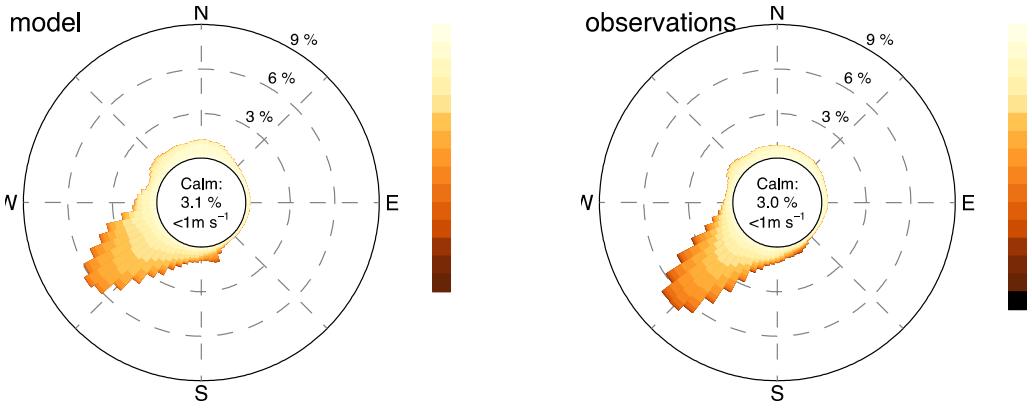

Figure 22. Wind roses for modeled (left) and observed wind speeds (right) for Butler Grade

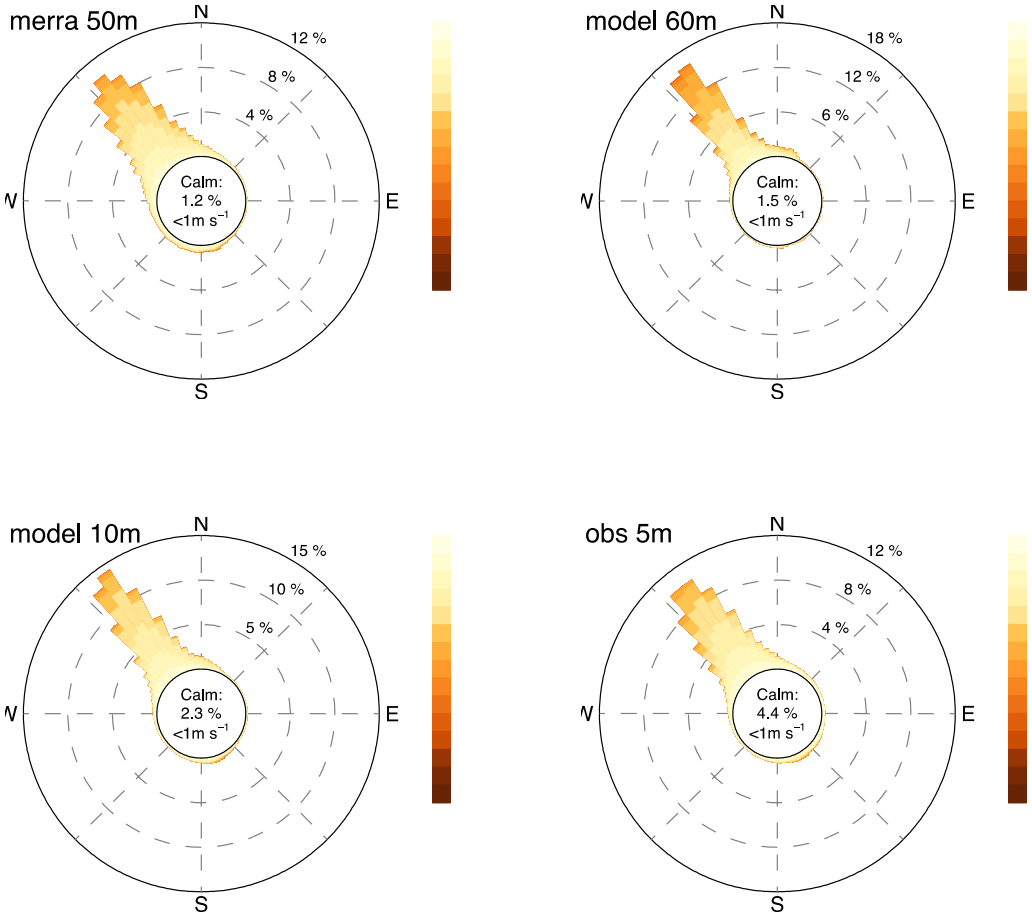

Figure 23. Wind roses for wind speeds modeled by MERRA (top left), the WIND Toolkit at 60 m (top right), the WIND Toolkit at 10 m (lower left), and observed wind speeds at 5 m (lower right) for Santa Maria

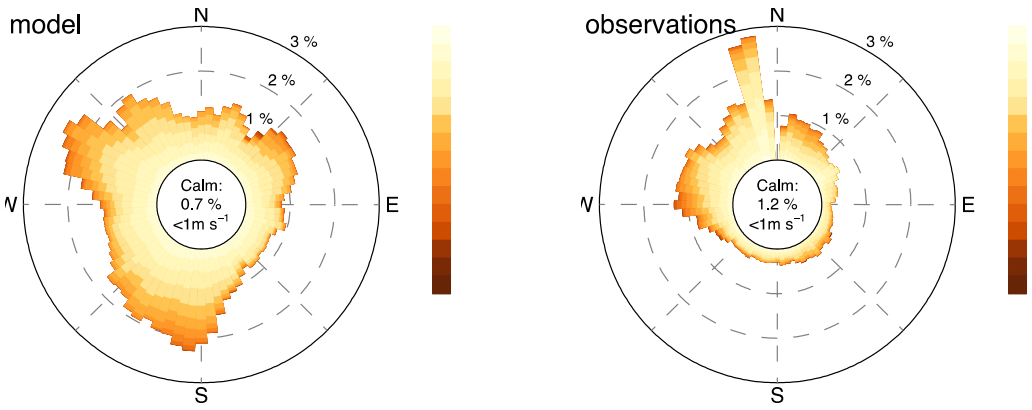

Figure 24. Wind roses for modeled (left) and observed wind speeds (right) for Cape May

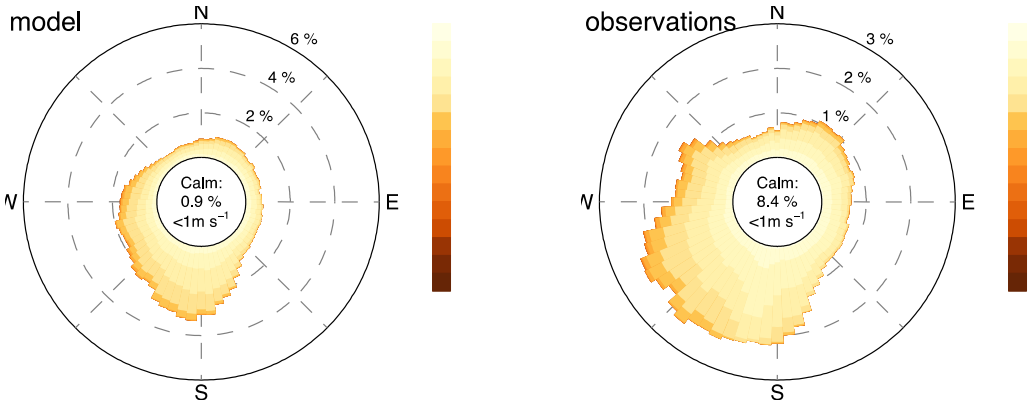

Figure 25. Wind roses for modeled (left) and observed wind speeds (right) for Cochran

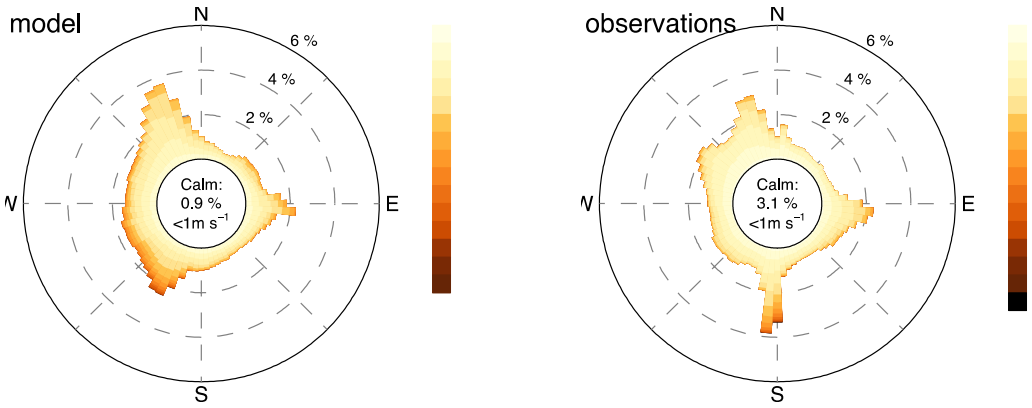

Figure 26. Wind roses for modeled (left) and observed wind speeds (right) for Megler

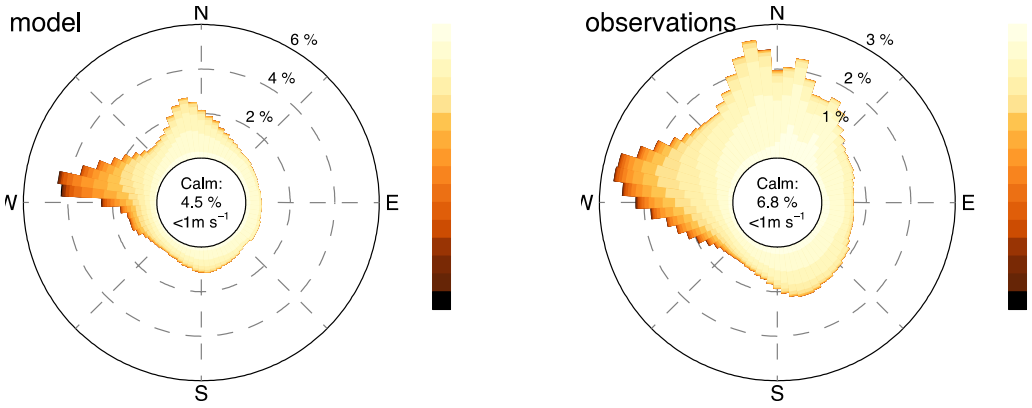

Figure 27. Wind roses for modeled (left) and observed wind speeds (right) for the NWTC

4.1.4 Wind Speed Error Metrics

The analyses in this report were calculated using the lowest resolution available, which in most cases is 5 or 10 minutes. The observations were compared to the 5-min model output. The observations are usually averages over the interval, whereas the model output is instantaneous. We did not anticipate major discrepancies because of this fact. We also performed analyses with hourly averages for both the observations and the model to compare equal values. The validation results did not change significantly when using hourly output, and the values varied only slightly. As expected, the error metrics at a higher resolution (Table 6) were slightly higher than the hourly averages (Table 5). We performed absolute error metrics in m/s and list the mean observed wind speeds as a reference, because wind power is the ultimate quantity of interest. For wind power, absolute values of wind speed are important.

The RMSE was highest for the NWTC among the land-based sites. In general, the RMSE for the buoys was higher than for the land-based sites. The bias was below 1 m/s for all sites except Megler, and negative biases occurred only for Bovina and Butler Grade. The CRMSE mirrored the behavior of the RMSE, and revealed that the random component of the model error is dominant, as opposed to the systematic error (the bias). The correlation was higher for the land-based sites; however, the 5/10 min interval comparison of the 5-m measurements were high as well. The MAE and the percentage error were higher for the buoy sites (up to 143%). The buoy sites exhibited lower mean wind speeds than the land-based sites, and high RMSE values. Note that the observed winds over the ocean were measured at 5 m, compared to the 10-m modeled wind speeds, which might be the reason for these high error values. The 50-m error metrics over the ocean were calculated with the WIND Toolkit and MERRA data, which, as mentioned before, are not to be seen as the truth. Correlation values were very low for the offshore sites as well, probably for the same reason that the measured 5-m wind is not representative of winds at higher measuring heights.

Table 5. Mean Observed Wind Speeds and Error Metrics Using Hourly Values

	Mean observed wind speed [m/s]	RMSE [m/s]	BIAS [m/s]	CRMSE [m/s]	CORR [-]	MAE [m/s]	Perc. Error [%]
BOVINA 100 m	8.04	2.36	-0.38	2.33	0.73	1.92	44.03
Butler Grade	8.17	3.05	-0.96	2.89	0.83	2.27	42.93
Cape May	7.74	2.14	0.20	2.13	0.79	1.73	34.25
Cochran	6.34	2.04	0.38	2.00	0.70	1.57	37.83
Megler	5.37	2.95	1.80	2.33	0.73	2.32	61.48
NWTC	4.82	3.89	0.98	3.77	0.52	2.71	78.87
NY HARBOR 10 m	6.62	4.27	-0.32	4.26	0.09	3.43	95.30
NY HARBOR 50 m	-	5.64	0.70	5.59	-0.03	4.49	104.73
Santa Maria 10 m	5.79	4.55	0.85	4.47	-0.03	3.63	142.99
Santa Maria 50 m	-	4.82	0.91	4.73	0.01	3.93	98.41
Portland 10 m	5.58	4.95	0.47	4.93	-0.12	3.91	142.92
Portland 50 m	-	5.31	1.67	5.04	-0.03	4.16	120.46

Table 6. Mean Observed Wind Speeds and Error Metrics Using 5/10-min Intervals

	Mean observed wind speed [m/s]	RMSE [m/s]	BIAS [m/s]	CRMSE [m/s]	CORR [-]	MAE [m/s]	Perc. Error [%]
Bovina	8.07	2.51	-0.42	2.47	0.71	2.06	46.65
Butler Grade	8.18	3.18	-0.97	3.03	0.81	2.38	56.01
Cape May	7.76	2.26	0.18	2.25	0.78	1.84	39.03
Cochran	6.36	2.15	0.35	2.12	0.68	1.67	39.27
Megler	5.37	3.09	1.80	2.52	0.70	2.41	76.64
NWTC	4.85	4.24	0.95	4.13	0.46	2.99	110.63
NY HARBOR 10 m	6.46	3.53	0.43	3.50	0.86	1.30	37.05
NY HARBOR 50 m	-	5.64	0.69	5.59	-0.03	4.49	104.73
Santa Maria 10 m	5.69	3.48	0.62	3.43	0.76	1.69	68.21
Santa Maria 50 m	-	5.31	1.67	5.04	-0.03	4.16	120.46
Portland 10 m	5.51	3.21	0.56	3.16	0.85	1.37	59.07
Portland 50 m	-	4.82	0.91	4.73	0.01	3.93	98.41

Bias and RMSE averaged for each month of the year at the lowest resolution available are shown in Table 7 and Table 9, respectively, and for hourly values in Table 8 and Table 10, respectively.

Table 7. Bias (Model – Obs) in m/s Per Month for All Sites Using the Lowest Resolution Available (5/10 min) in the Observations (Table 3)

	Jan	Feb	March	April	May	June	July	Aug	Sep	Oct	Nov	Dec
Bovina	-0.19	0.59	-0.8	-0.55	-0.97	-0.48	-0.09	-0.15	-0.4	-0.63	-0.8	-0.79
Butler Grade	-1.2	-0.83	-0.853	-1.43	-1.03	-1.25	-1.18	-1.24	-0.80	-0.82	-0.64	-0.24
Cape May	0.42	0.515	-0.809	0.31	-0.15	-0.14	-0.2	-0.07	-0.10	0.422	0.949	0.527
Cochran	-0.12	-0.10	0.173	0.22	0.29	0.64	0.826	0.812	0.464	0.482	-0.00	0.063
Megler	1.68	1.98	2.257	2.00	1.79	1.441	2.189	1.718	1.467	1.508	1.456	1.818
NWTC	0.94	0.713	0.686	1.00	0.951	1.103	1.303	1.235	1.067	0.892	0.726	0.749
NY Harbor 10 m	0.26	0.36	0.356	0.54	0.566	0.486	0.6	0.381	0.252	0.479	0.383	0.425
NY Harbor 50 m	-1.12	1.082	-0.176	0.64	1.8	4.095	3.32	3.165	0.622	-0.31	-2.16	-2.58
Portland 10 m	-0.21	-0.23	0.298	0.79	0.912	0.885	1.063	0.971	0.86	0.845	0.86	0.53
Portland 50 m	-0.25	1.735	1.067	1.68	2.493	5.083	4.931	2.963	1.157	1.418	0.031	-2.22
Santa Maria 10 m	0.58	0.31	0.458	0.43	0.545	0.556	0.654	0.73	0.874	0.592	0.492	0.54
Santa Maria 50 m	1.78	1.181	0.873	-0.94	-0.05	-0.51	1.736	1.55	0.825	1.623	0.616	2.155

Table 8. Bias (Model – Obs) in m/s Per Month for All Sites Using Hourly Averages

	Jan	Feb	March	April	May	June	July	Aug	Sep	Oct	Nov	Dec
Bovina	-0.12	0.68	-0.77	-0.44	-0.95	-0.47	-0.09	-0.13	-0.37	-0.61	-0.79	-0.77
Butler Grade	-1.16	-0.82	-0.85	-1.42	-1.02	-1.25	-1.18	-1.25	-0.80	-0.82	-0.63	-0.17
Cape May	0.44	0.51	-0.80	0.33	-0.14	-0.14	-0.18	-0.05	-0.08	0.45	1.00	0.53
Cochran	-0.11	-0.09	0.24	0.28	0.35	0.65	0.83	0.82	0.47	0.48	0.01	0.09
Megler	1.70	2.01	2.27	2.00	1.79	1.45	2.19	1.72	1.47	1.51	1.46	1.83
NWTC	0.99	0.78	0.71	1.02	0.96	1.11	1.31	1.24	1.08	0.91	0.75	0.80
NY Harbor 10 m	-0.2	2.54	-1.02	-1.06	-0.04	2.03	0.47	-0.45	-2.28	-0.9	-1.67	-0.93
NY Harbor 50 m	-1.19	1.15	-0.18	0.60	1.82	4.06	3.32	3.22	0.70	-0.28	-2.08	-2.53
Portland 10 m	0.82	2.81	-0.07	0.81	0.86	2.27	1.4	0.2	-1.45	-0.41	-0.53	-0.83
Portland 50 m	-0.21	1.81	1.08	1.73	2.5	5.17	4.91	3.04	1.21	1.42	0.03	-2.23
Santa Maria 10 m	-0.05	2.1	0.71	-0.38	3.31	1.40	2.29	1.26	-0.53	0.37	-1.60	1.49
Santa Maria 50 m	1.82	1.20	0.90	-0.94	-0.06	-0.53	1.74	1.53	0.85	1.60	0.59	2.13

Table 9. RMSE in m/s for Each Month at the Lowest Available Common Resolution (Table 3)

	Jan	Feb	March	April	May	June	July	Aug	Sep	Oct	Nov	Dec
Bovina	3.153	3.597	2.221	2.617	2.234	2.447	2.19	2.414	2.03	2.196	2.429	2.489
Butler Grade	3.539	3.121	3.579	3.275	3.112	2.977	2.884	2.961	2.543	2.918	3.182	4.012
Cape May	2.004	2.19	1.768	2.98	2.294	2.514	1.809	1.324	1.507	2.585	3.04	1.856
Cochran	1.91	1.972	2.185	2.298	2.179	2.488	2.204	2.313	2.049	2.006	1.897	2.019
Megler	3.378	3.316	3.745	3.223	2.794	2.368	3.004	2.698	2.688	3.089	3.354	3.459
NWTC	5.272	4.63	4.285	4.12	3.619	3.922	3.915	3.923	3.613	4.22	4.325	4.715
NY Harbor 10 m	7.816	1.837	1.674	1.852	1.739	1.773	1.798	1.618	1.459	1.639	7.031	1.694
NY Harbor 50 m	5.26	5.91	5.414	5.119	5.222	7.115	5.771	6.039	4.6	5.385	5.52	5.936
Portland 10 m	6.662	2.586	2.284	2.281	2.165	2.035	2.056	2.017	1.979	2.033	6.607	2.435
Portland 50 m	4.52	4.778	4.95	4.851	5.2	7.934	6.597	5.582	4.237	4.449	4.782	4.645
Santa Maria 10 m	6.996	1.77	1.753	1.669	1.882	1.66	1.604	1.666	1.84	1.873	6.631	2.017
Santa Maria 50 m	4.711	4.351	4.837	5.261	4.748	4.601	5.234	4.096	4.836	5.309	4.84	4.837

Table 10. RMSE in m/s for Each Month for Hourly Averages

	Jan	Feb	March	April	May	June	July	Aug	Sep	Oct	Nov	Dec
Bovina	3.071	3.548	2.128	2.611	2.063	2.201	1.946	2.195	1.859	2.028	2.263	2.334
Butler Grade	3.419	2.983	3.406	3.128	2.951	2.808	2.773	2.818	2.424	2.787	3.035	3.893
Cape May	1.911	2.058	1.654	2.867	2.119	2.316	1.69	1.223	1.414	2.496	2.966	1.742
Cochran	1.787	1.835	2.187	2.291	2.135	2.284	2.027	2.16	1.892	1.865	1.773	1.89
Megler	3.225	3.172	3.569	3.055	2.643	2.235	2.906	2.598	2.583	2.936	3.164	3.311
NWTC	4.929	4.296	3.959	3.775	3.247	3.511	3.462	3.538	3.308	3.925	4.002	4.389
NY Harbor 10 m	4.01	4.923	3.913	3.247	4.096	4.738	4.351	4.104	5.179	4.352	4.473	3.88
NY Harbor 50 m	5.278	5.942	5.394	5.161	5.264	7.118	5.762	6.087	4.625	5.416	5.548	5.908
Portland 10 m	4.745	4.744	4.049	5.259	4.572	7.33	6.03	4.121	4.167	4.479	4.937	3.714
Portland 50 m	4.578	4.79	4.919	4.871	5.209	7.987	6.533	5.585	4.202	4.465	4.696	4.653
Santa Maria 10 m	3.729	5.187	3.772	4.84	5.871	3.527	4.638	4.131	4.044	5.171	3.968	4.801
Santa Maria 50 m	4.656	4.308	4.861	5.26	4.709	4.611	5.246	4.051	4.814	5.283	4.822	4.827

4.1.5 Diurnal Cycles of Wind Speeds and Errors

Analyses of diurnal cycles can be useful in determining the time of the day when the model has the most difficulties in predicting wind speeds. This information can indicate whether or not the transition between stable boundary layers at night and convective ones during the day is captured correctly; if the model has more difficulties during the night or day; or if low-level jets are being modeled correctly. Further analysis could determine if there are difficulties with surface fluxes or specific weather patterns. Although an extensive analysis of these items is beyond the scope of this report, we present diurnal cycles of error metrics (e.g., bias, CRMSE, and RMSE per month). The plots are divided into summer months (April, May, June, July, August, and September) and winter months (October, November, December, January, February, and March) for better visualization. The signal of these diurnal cycles depends on the site. Furthermore, the months vary because they exhibit different behaviors and/or ranges of values.

As an example, we describe the diurnal cycles for Bovina (see the Appendix for the diurnal cycles for all other sites). The diurnal cycle of bias for Bovina at 100 m (Figure 33a) during the summer months shows that the bias is negative most of the time (i.e., the modeled wind speeds are lower than the observations). This is mostly the case from April to June. Although April shows variations in bias throughout the day with a lower bias after 13 UTC (after 8 h local time), May has the lowest bias from 0 to 5 UTC (16 to 21 h local time). The other months show a fairly homogeneous distribution during the course of a day. This finding could indicate that the model has difficulties during transition periods in April and May. In the winter months (Figure 34a), January has a bias of close to zero, and November and March show the lowest values during 16 UTC and 2-3 UTC, respectively.

The CRMSE, which is the random component of the wind speed error, tends to be lowest between 15 and 20 UTC (8 and 13 h local time, thus, the morning hours) in the summer (Figure 33b), especially in July, August, and September. In the winter months (Figure 34b), March and October show the lowest CRMSE, and in general the error is more homogeneously distributed throughout the day.

The RMSE shows the combined effects of bias and CRMSE. We observed that the CRMSE has the bigger contribution to it than the bias (i.e., the general pattern of the CRMSE is reflected in the RMSE).

What is valid for Bovina can be different for the other sites (Figures A1 through A22). Error metrics are different during different months and time of the day. At the offshore locations (Figures A11 through A22), when compared with MERRA data, the signals are very smooth compared to the land-based sites. Note that the range of wind speed values is different in each panel. The analysis of diurnal cycles shows that it depends on the site on whether or not the model captures the diurnal cycles accurately. Unfortunately, no general conclusion could be drawn based on the evaluation of the sites chosen.

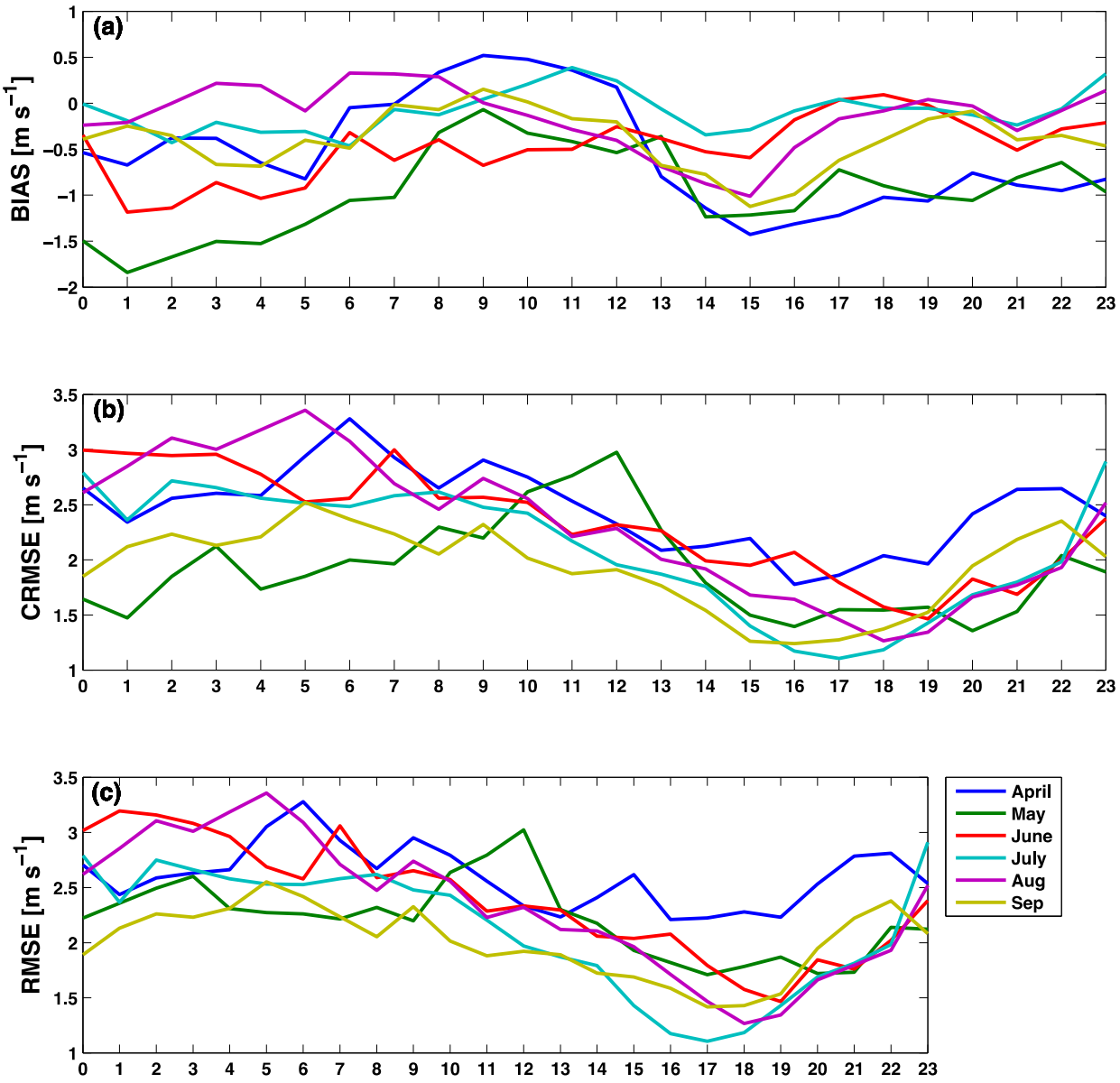

Figure 28. Diurnal cycle of wind speed bias (top), CRMSE (middle), and RMSE (bottom) for the summer months for Bovina at 100 m

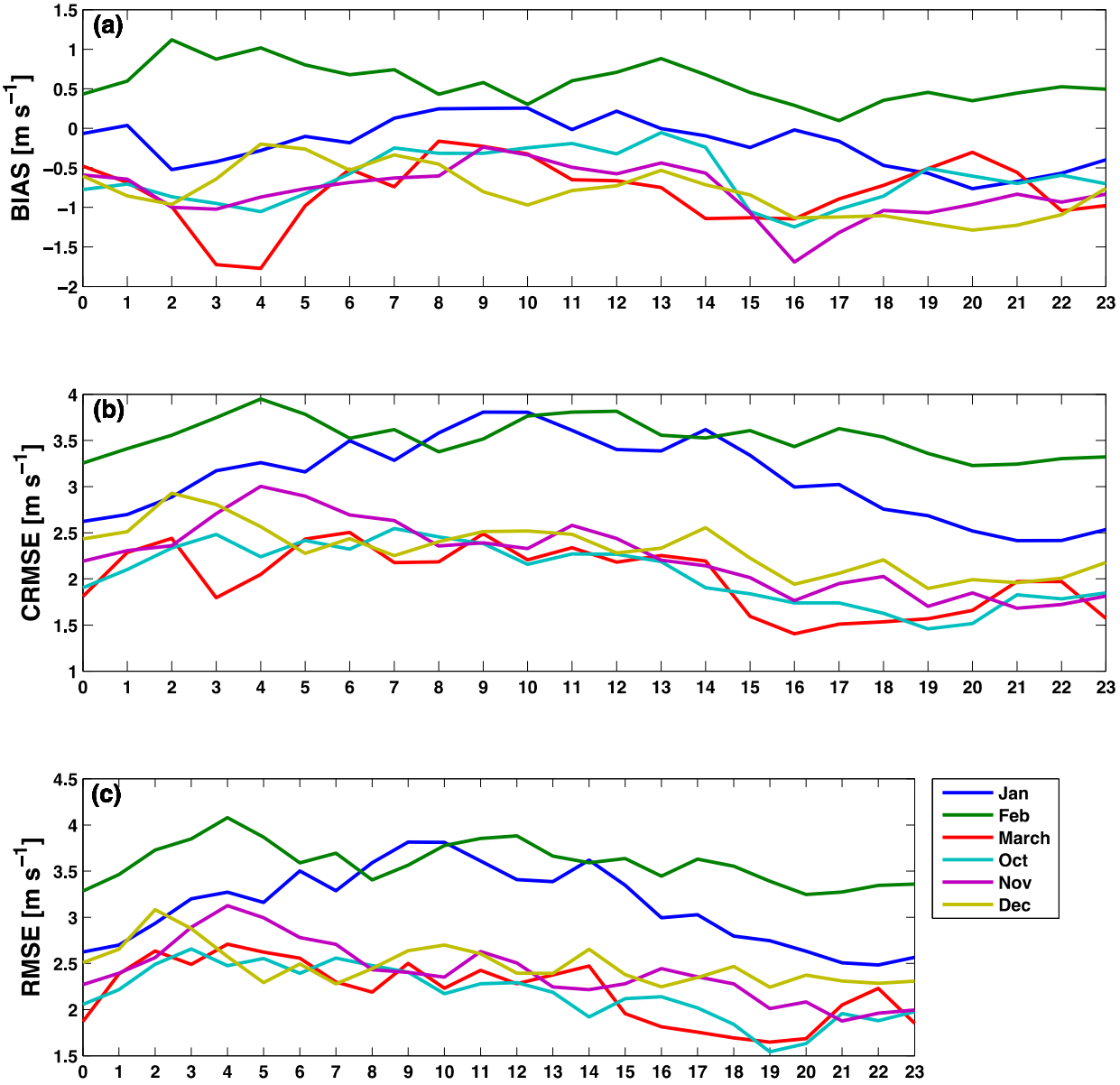

Figure 29. Diurnal cycle of wind speed bias (top), CRMSE (middle), and RMSE (bottom) for the winter months for Bovina at 100 m

4.1.6 Annual Cycles of Wind Speed Error

Annual cycles of bias, CRMSE, RMSE, and rank correlation for each site are presented in this section. Averaged values are portrayed for each month of the year. This approach helps indicate seasonal signals or challenges for the model.

Error metrics vary between months and differ from site to site. At the buoy sites (Figure 36 and Figure 37 [left]), the RMSE and CRMSE at 10 m is lower than at 50 m, and the rank correlation is higher at 10 m. The bias at 10 m is close to zero. The comparison with MERRA data at 50 m might not be accurate—errors are up to approximately 3 m/s higher for buoy sites than land-

based sites, and are in line with errors at land-based sites at 10 m throughout the year. There is less variation in the error metrics between each month at offshore locations compared to sites on land. At all land-based sites, except Butler Grade, the rank correlation drops in the summer.

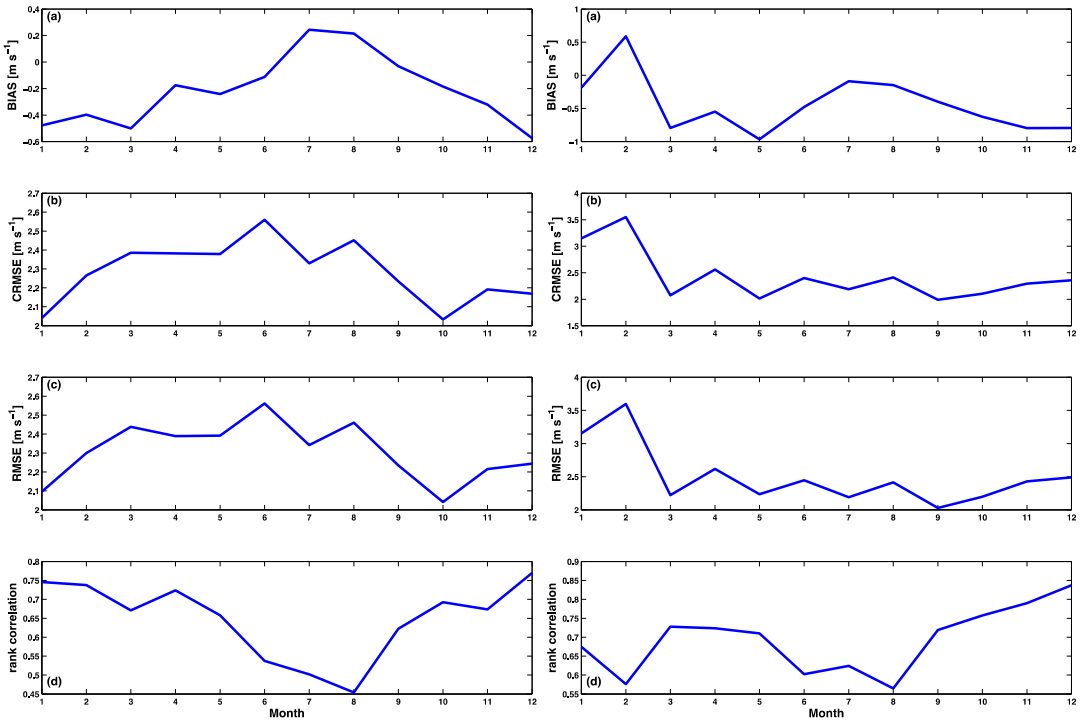

Figure 35. Annual cycle of wind speed bias (a), CRMSE (b), RMSE (c), and rank correlation (d) for Bovina at 50 m (left) and 100 m (right)

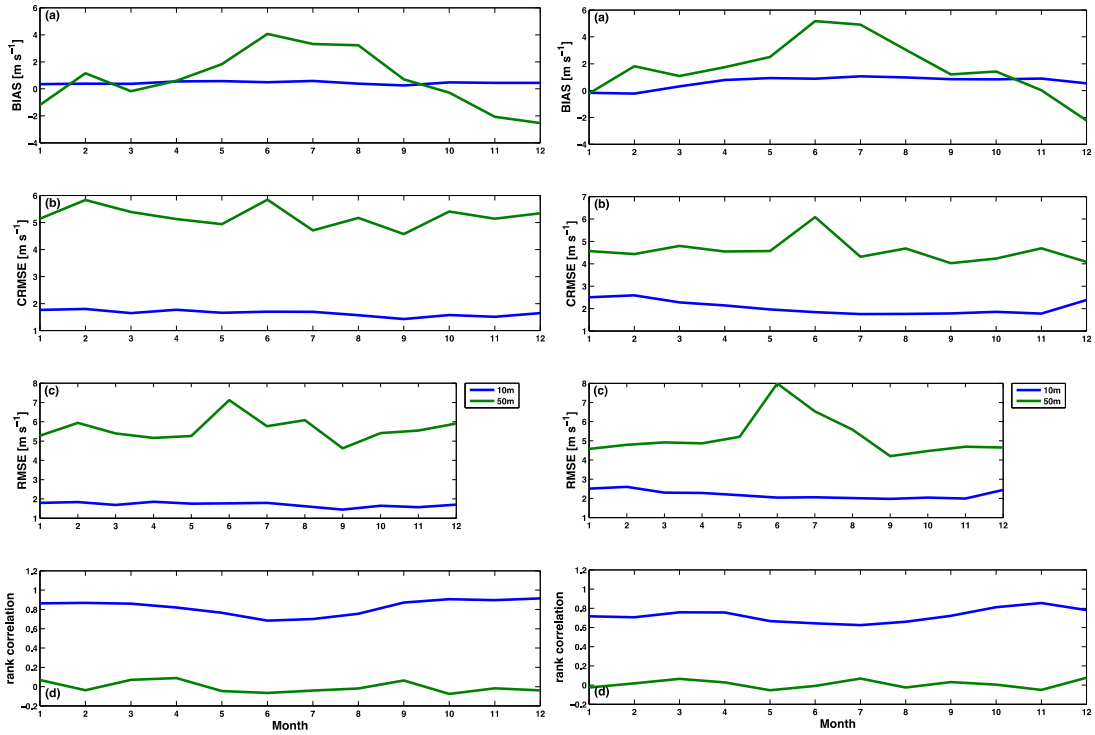

Figure 36. Annual cycle of wind speed bias (a), CRMSE (b), RMSE (c), and rank correlation (d) for New York Harbor (left) and Portland (right); the 50-m data are compared to MERRA.

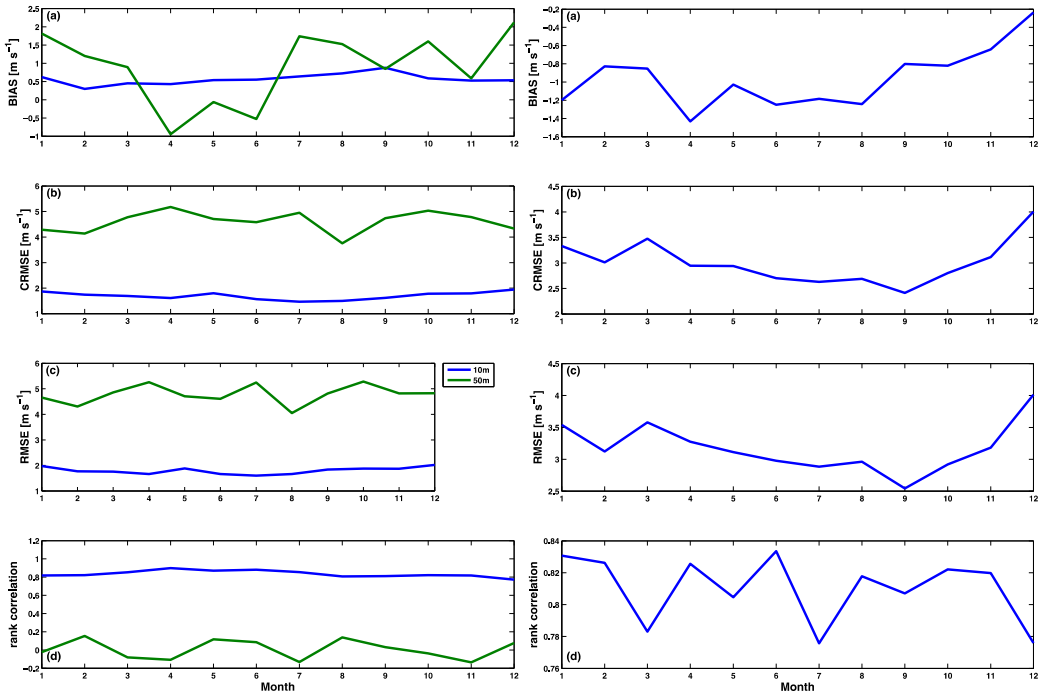

Figure 37. Annual cycle of wind speed bias (a), CRMSE (b), RMSE (c), and rank correlation (d) for Santa Maria (left) and Butler Grade (right)

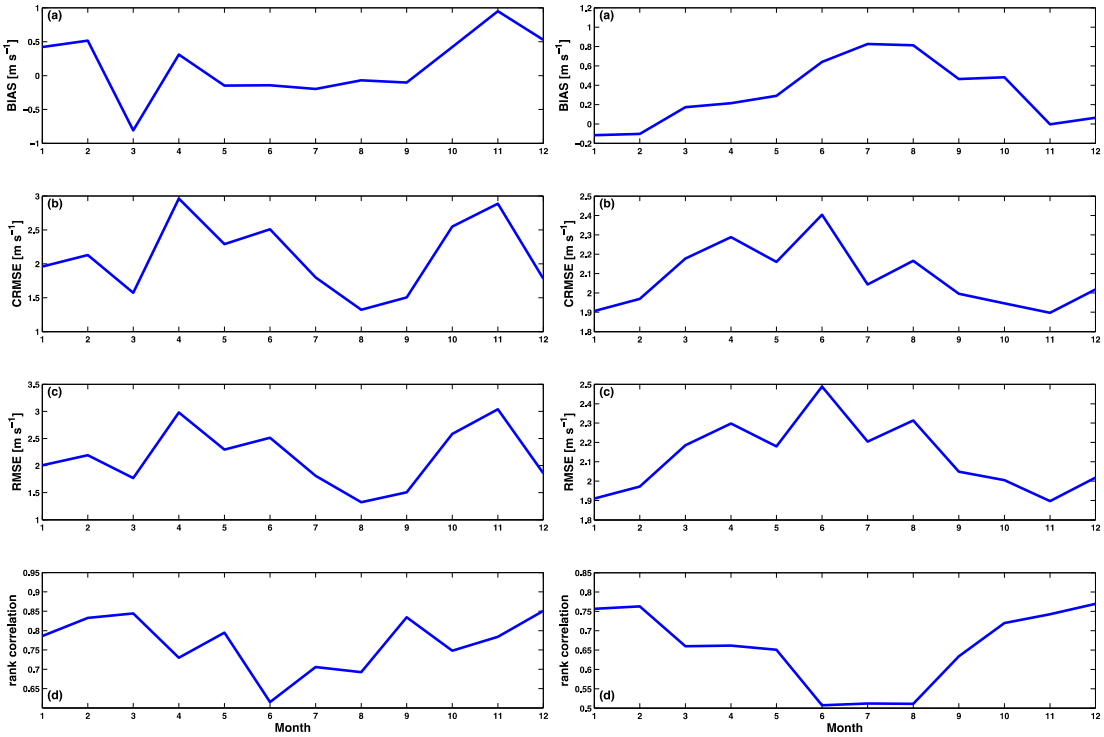

Figure 38. Annual cycle of wind speed bias (a), CRMSE (b), RMSE (c), and rank correlation (d) for Cape May (left) and Cochran (right)

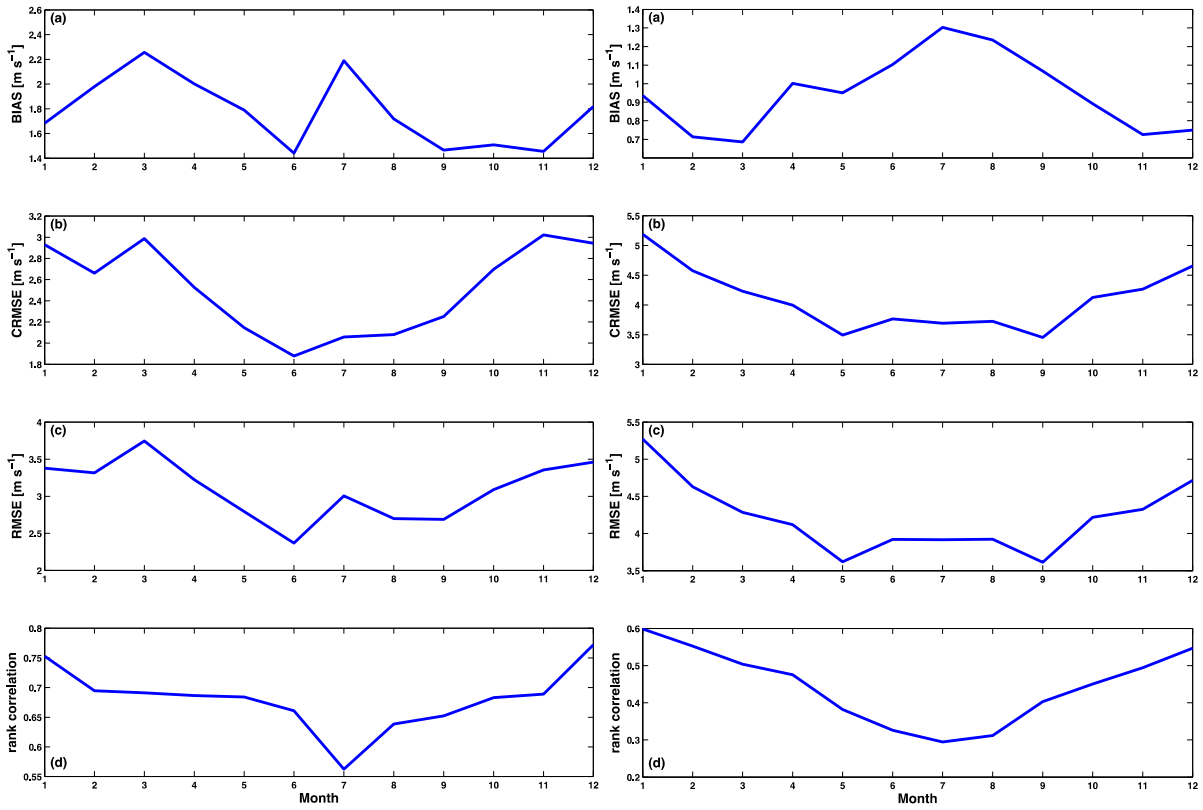

Figure 39. Annual cycle of wind speed bias (a), CRMSE (b), RMSE (c), and rank correlation (d) for Megler (left) and the NWTC (right)

As shown in the following sections and figures, the performance of the WIND Toolkit is highly dependent on the site. Given the limited number of validated sites, it is not possible to draw general conclusions for the whole United States, but rather give a hint as to how the model behaves in different areas. We strongly encourage users of the WIND Toolkit to perform their own validation before drawing conclusions for their sites. These validation results are intended as guidelines only.

4.2 Model Restarts

One of the problems with previous resource data sets was the presence of false wind ramps caused by model restarts. As a result, the WIND Toolkit was designed to avoid these problems. The WRF model was run continuously in cycles of ~36 days each, from January 2007 to December 2013. To avoid excessive drift, the model was cold-started every ~30 days and run with an overlap of ~ 2 days around these cold starts to eliminate temporal seams. The data that are publicly available through the data extraction tool have been cut at the beginning of each month. The user can request the overlapping data and interpolate them during these two overlapping days. Figure 40 shows an example of model runs around model restarts in January and February 2007 for the NWTC. The wind speeds before and after a cold start agreed well with each other. The same behavior could be seen for other sites (not shown).

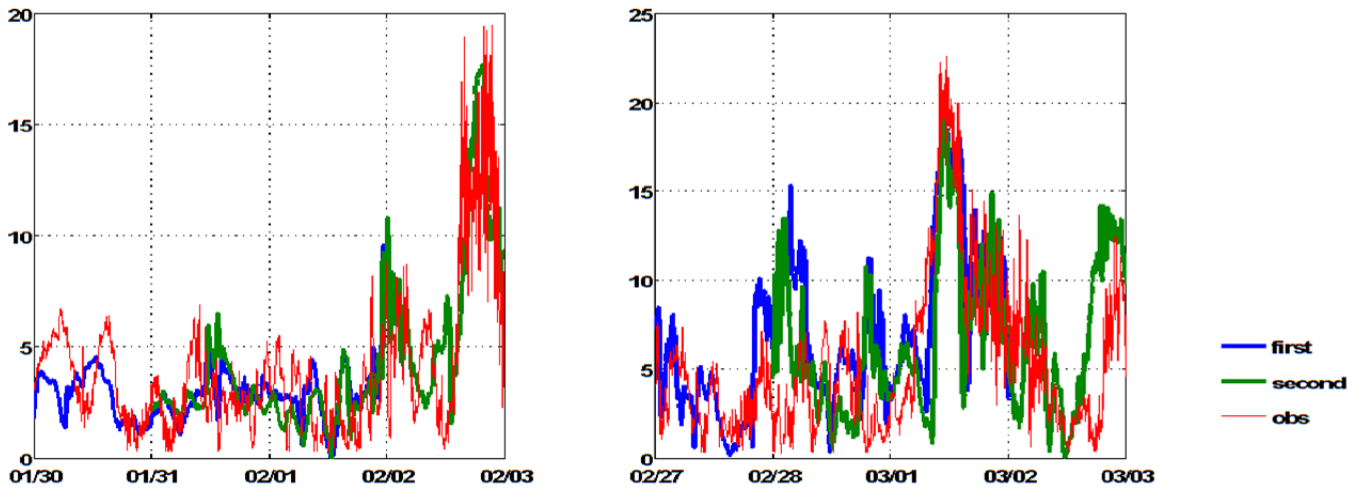

Figure 40. Times series during times of model restarts for 2 months in 2007 at the NWTC at 80 m; the model data at the nearest grid point from the NWTC are in blue and green, and the observations are in red

4.3 Validation of Power Production Simulations

This report outlines the validation of the meteorological reanalysis data set. The validation of the WIND Toolkit power data is addressed in a separate report (King et al. 2014), and the final report of the project (McCaa et al. 2015). King et al. compared the wind power production data (not the forecast data) at 284 sites, as converted from wind speed to power, and then to measured data from wind plants. That report includes a validation of the capacity factors, an examination of the variability in the power, and guidelines for use.

The main conclusions from the power validation include the following.

- The plant power curves used for the WIND Toolkit matched with the turbine curves for class 2 and the offshore turbines. Some discrepancies were found for class 3 turbines.
- Capacity factors from the WIND Toolkit were higher than those in both earlier simulated data sets (EWITS, WWSIS) and the measurement data available. That difference is explained by the use of advanced turbine power curves and the assumption that all turbines in the WIND Toolkit are at a hub height of 100 m.
- The power data set was found to acceptably model the power output of wind resources and can be trusted to represent production by modern turbines at a hub height of 100 m.

The results of the validation tests (quantified in the validation metrics) do not indicate if the WIND Toolkit is fit for a user's particular purpose. The results only provide a quantitative comparison with the real world and must be compared to the user's own requirements by conducting an "acceptance test" or "qualification test." The use of the validation results emphasizes the importance of selecting the appropriate validation metrics for specific use cases.

5 Discussion

The WIND Toolkit data set is primarily intended to provide the inputs to future wind integration studies. It is not a wind resource assessment tool. This is why the WIND Toolkit data are only available at 100 m. Compared to previous studies, the WIND Toolkit had higher computational requirements and covered a longer period of time over a larger geographical area. In addition, it reflects recent years, is time-synchronous with load profiles, covers 7 years, includes capacity factors of wind plant production, and is easily accessible. The WIND Toolkit has also had a more rigorous validation and was designed to detect and mitigate problems experienced in previous grid integration studies.

Storing big amounts of data, like the WIND Toolkit, is no small task. The current data storage amounts to ~ 0.5 Pb, which results in ~1 Pb including backup. Therefore, it was not possible to store many other variables that would be useful in exactly determining why the WRF model behaved a certain way (e.g., synoptic information, and turbulent kinetic energy), nor was it possible to store the whole original WRF gridded data. We do have information about the terrain and land-use types, WRF namelists, and boundary condition files to reproduce the study or run the WRF model for additional years, or to downscale further, extend the geographical domain, or rerun the model for comparison and research purposes.

A chief concern with any new integration data set is the accuracy of the WRF model data that are used to drive the power simulations. This report examines the accuracy of the wind speed and direction predicted by the WRF model, and compares them to observations and reanalysis data at nine sites. The motivation for this comparison is to point out deficiencies of the data set and to justify an extension of the data set. The use of many more towers would be desirable and would provide stronger results; however, finding and cleaning optimal data sets at hub heights for many sites is time consuming and beyond the scope of this project. Note that the WIND Toolkit analysis in this report is provided for heights other than 100 m above ground level at certain locations and was performed with WRF model output close to that height, even though only the 100-m wind speeds and wind directions are publically available. We responded to the following questions to determine potential deficiencies of the data set.

1. *Is there any apparent problem in the data set? Are the files intact? Did the model restarts create any apparent issues?*

   The data have been checked for integrity, and a file size check was performed to determine if the files were intact. The power validation (King et al. 2014) confirmed that model restarts did not create false ramps.

2. *Can the WRF model setup be justified?*

   An extensive sensitivity study was performed to select the optimal WRF configurations for the purpose of the WIND Toolkit. The validation results showed no apparent issue caused by selecting the WRF configuration.

3. *Terrain effects: To what extent is there any apparent effect of terrain on the wind speed distributions, wind roses, or wind speed error metrics?*

The validation results showed that even if some sites share similar terrain, their error metrics exhibit different characteristics. The NWTC and Butler Grade locations are both in complex terrain, Bovina and Cochran are in flat terrain, and Cape May and Megler are close to the ocean. The RMSE and CRMSE values among the land-based sites are highest for the sites in complex terrain; however, the bias is very different (Table 7 and Table 8). A breakdown of RMSE and bias into months did not show a common pattern for the complex sites. For a more detailed analysis of terrain effects, more sites would need to be validated. We conclude that the reason for the model behavior might not be dependent on terrain.

4. *Diurnal and seasonal effects: Is there any evidence for different diurnal/seasonal cycles in the WRF data than in the observations, and do errors show a diurnal/seasonal cycle?*

Figures 41 and 42 summarize the diurnal and annual bias, CRMSE, and RMSE for all of the land-based validated sites at the lowest available resolution (left column) and for hourly averages (right column). Although Megler shows the highest bias, the NWTC has the highest CRMSE and RMSE. Butler Grade has the lowest bias, and Cochran and Cape May show lower biases than the other stations most of the time. Again, these results show that it is not possible to generalize for certain terrain types, and that additional validation is needed before drawing general conclusions. Some sites exhibit a diurnal or seasonal cycle, whereas others do not. Hourly errors are generally lower, which is expected because errors are averaged out. Also, capturing features at scales of 5 or 10 min, which is the scale the observations are available for, is difficult if not impossible for a mesoscale model. This difficulty is reflected in higher errors at that temporal resolution. Given that the error values at the lowest available resolution are only slightly higher than the errors for the averages, small variations in wind speed were captured fairly accurately by the numerical simulations.

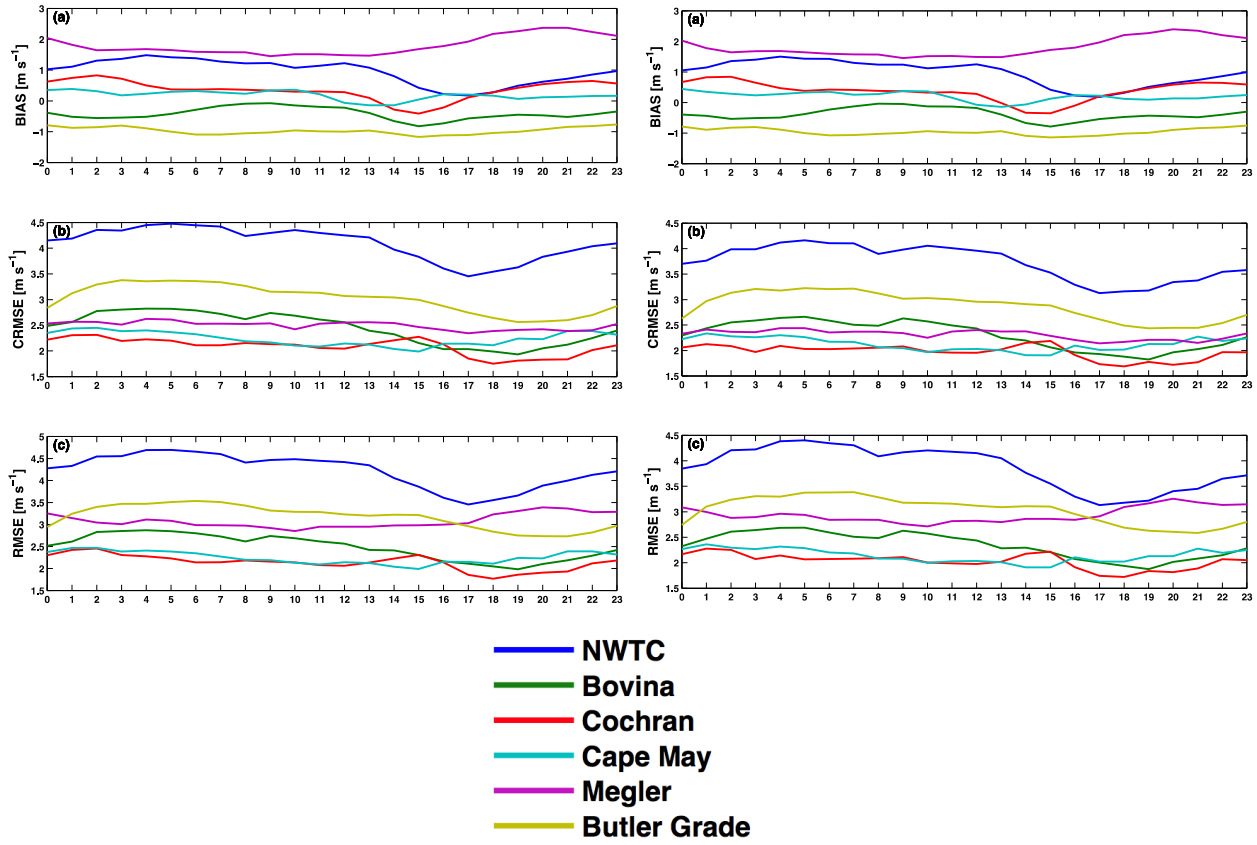

Figure 30. Diurnal cycles of wind speed at the lowest available resolution (left) and hourly averages (right)

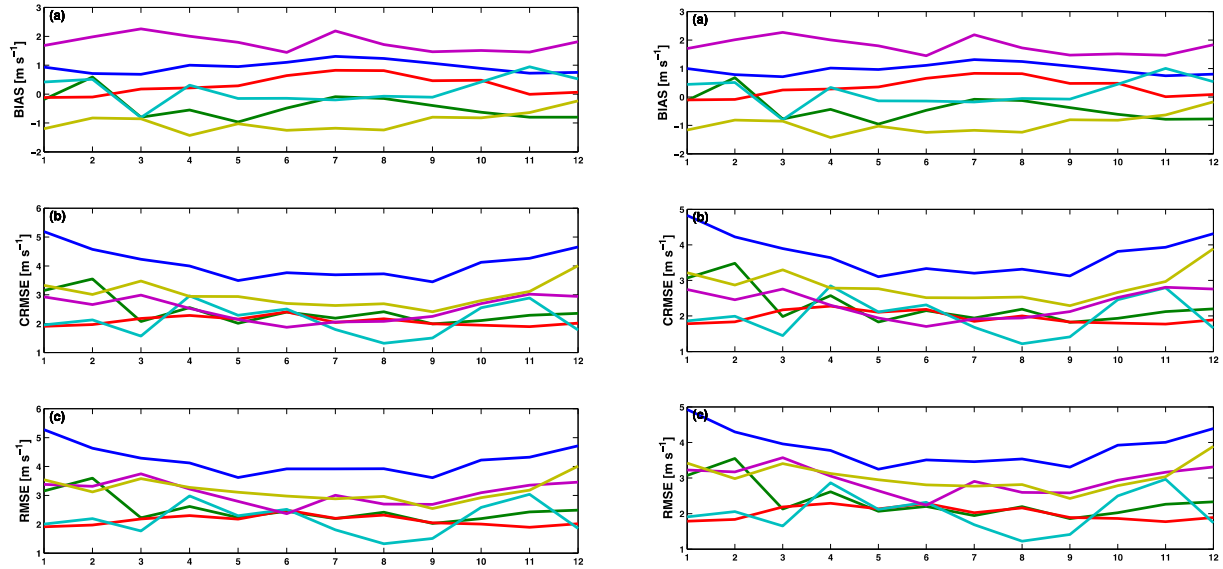

Figure 31. Annual cycle of wind speed at the lowest resolution (left) and hourly resolution (right); the same legend in Figure 41 applies

Even though we quality controlled the data, observations can still be erroneous. The most obvious errors can be seen in the wind rose for Cape May. Without sufficient information about the measurement practices and sensors, correction of these data is very time consuming and difficult, if not impossible. Except for the wind direction data of Cape May, we assumed the measurements to be fairly accurate.

There are many reasons for model behavior, and finding those for a big area like the United States is challenging. To find the reasons for this behavior, information about the terrain, roughness, local climate and wind conditions, surface fluxes, understanding of the model parameterizations, and boundary conditions, to name a few, is necessary. Such a detailed study was beyond the scope of this project. We wanted to give an overview of the quality of the data set by validating a few sites across the United States; however, the results of the validation tests (quantified in the validation metrics) do not tell a user if the WIND Toolkit is fit for their particular needs. The results only provide a quantitative comparison with the real world and must be compared to the user's own requirements to establish if the data are fit for purpose. The use of the validation results to determine if the data are acceptable emphasizes the importance of selecting the appropriate validation metrics for each use case.

Together with the WIND Toolkit, the SIND Toolkit will be released. This toolkit was funded to create a new national solar database at a higher temporal and spatial resolution and to provide public access to this data to reduce the costs and risks of integrating solar power systems into the electric power grid. Stakeholders have been requesting a solar data set that complements a wind data set for use with grid integration studies.

6 Summary and Conclusion

Regional wind integration studies in the United States require detailed wind power output data at many locations to perform simulations of how the power system will operate under high-penetration scenarios. The wind data sets that serve as inputs into these studies must realistically reflect the ramping characteristics, spatial and temporal correlations, and capacity factors of the simulated wind plants, as well as be time synchronized with available load profiles. From what has been shown in this study and in the validation of the power data set in a separate report, the WIND Toolkit fulfills these requirements as a state-of-the-art, national wind resource, power production, and forecast data set. It is a freely available wind speed and power data set that can be used for wind resource assessments as well as grid integration and grid planning studies.

In this report, a team of researchers describe the importance of creating this data set; the challenges associated with creating numerical weather prediction simulations for a large geographical area such as the continental United States; the numerical simulations themselves; how the simulated wind speeds are converted into power; and the initial validation results from the raw meteorological data set. The meteorological validation confirms the need for further validation at different sites or different variables and potentially regional post-processing approaches, especially if the meteorological data are used for wind resource assessments and siting. For the analyzed sites, we concluded that the model captures the wind conditions satisfactorily; the validation study shows a tendency of WRF to overpredict wind speeds. We believe the results are within the usual limits of errors. Note that the purpose of the WIND Toolkit was not to create the most accurate data set possible, but one that would best reflect current forecast errors.

The validation results are limited and should be used with caution. We strongly recommend carrying out additional validation steps before using the data or drawing general conclusions. These results have shown that every site has its own characteristics and is represented differently by the numerical model. R-code for the validation is available upon request.

References

Clifton, A.; Schreck, S.; Scott, G.; Kelley, N.; Lundquist, J. (2012). *Turbine Inflow Characterization at the National Wind Technology Center*. NREL/CP-5000-53525. Golden, CO: National Renewable Energy Laboratory. Accessed 26 November 2014: http://www.nrel.gov/docs/fy12osti/53525.pdf.

Clifton, A.; Daniels, M.H.; Lehning, M. (2014). "Effect of winds in a mountain pass on turbine performance." *Wind Energy*; Vol 17 (10). pp.1543–1562, http://onlinelibrary.wiley.com/doi/10.1002/we.1650/pdf.

Draxl, C.; Mayr, G.J. (2010). "Meteorological wind energy potential in the Alps using ERA40 and wind measurement sites in the Tyrolean Alps." *Wind Energy*; 14 (4), 471–489, http://onlinelibrary.wiley.com/doi/10.1002/we.436/abstract.

Hong, S.-Y; Noh, Y.; Dudhia, J. (2006)."A new vertical diffusion package with an explicit treatment of entrainment processes." *Mon. Wea. Rev.*; 134, pp. 2318–2341.

International Electrotechnical Commission (IEC). (2005). IEC 61400-1: Wind turbines - Part 1: Design requirements. International Electrotechnical Commission, Geneva, Switzerland, 3rd PPUB edition.

Jimenez, P.; Dudhia, J. (2012). "Improving the Representation of Resolved and Unresolved Topographic Effects on Surface Wind in the WRF Model." *Journal of Applied Meteorology and Climatology*; Vol. 51.

King, J.; Clifton, A.; Hodge, B.-M. (2014). *Validation of Power Output for the WIND Toolkit*. NREL/TP-5D00-61714. Golden, CO: National Renewable Energy Laboratory. Accessed 26 November 2014: http://www.nrel.gov/docs/fy14osti/61714.pdf.

Lew, D.; Alonge, C.; Brower, M.; Frank, J.; Freeman, L.; Orwig, K.; Potter, C.; Wan, Y.-H. (2011). "Wind Data Inputs for Regional Wind Integration Studies." *IEEE Power & Energy Society Annual Meeting*; Detroit, Michigan.

Li, J.; Liao, W.-k; Choudhary, A.; Ross, R.; Thakur, R.; Gropp, W.; Latham, R.; Siegel, A.; Gallagher, B.; Zingale, M. (2003). "Parallel netCDF: A High-Performance Scientific I/O Interface." *ACM/IEEE Supercomputing 2003 Conference*; Phoenix, Arizona.

McCaa, J.; Harrold, S.; Stoelinga, M.; Grimit, E.; Fowler, P.; Dunsmuir, M.; George, R.; Storck, P.; Hodge, B.; Jones, W.; Orwig, K. (2015). "Creation of the WIND Toolkit Dataset and API". NREL Technical Report (in progress).

National Center for Atmospheric Research. (2010). "Developmental Testbed Center." Accessed November 2014: http://www.dtcenter.org/eval/meso_mod/wrfrr_vl/WRFRR-VL_FINAL_report.pdf.

National Oceanic and Atmospheric Administration (NOAA). (2014a). "National Buoy Data Center." Accessed August 2014: http://www.ndbc.noaa.gov/.

NOAA (2014b)."NCEP Reanalysis." Accessed November 2014: http://www.esrl.noaa.gov/psd/data/gridded/reanalysis/

National Renewable Energy Laboratory. (2014). "Dynamic Maps, GIS Data, & Analysis Tools." Accessed August 2014: http://www.nrel.gov/gis/wind.html.

Patton, E.G.; Sullivan, P.P.; Kosovic, B.; Mahrt, L.; Zagar, M.; Dudhia, J.; Gulstad, L. (2014). "Non-equilibrium winds/waves: Impact of wave-propagation direction and wave age on hub-height winds and turbulence." 21st Symposium on Boundary Layers and Turbulence; Leeds, United Kingdom.

Potter, C.; Lew, D.; McCaa, J.; Cheng, S.; Eichelberger, S.; Grimit, E. (2008). "Creating the Dataset for the Western Wind and Solar Integration Study." *Wind Engineering*; Vol. 32, pp. 325–338.

Pryor, S.; Barhelmie, R.; Young, D.; Takle, E.; Arritt, R.; Flory, D.; Gutowski, W.; Nunes, A.; Roads, J. (2009). "Wind speed trends over the contiguous United States." *Journal of Geophysical Research: Atmospheres*; Vol. 114.

Rienecker, M.M.; Suarez, M.J.; Gelaro, R.; Todling, R.; Bacmeister, J.; Liu, E.; Bosilovich, M.G.; Schubert, S.D.; Takacs, L.; Kim, G.-K. (2011). "MERRA: NASA's modern-era retrospective analysis for research and applications." *Journal of Climate*; 24, pp. 3624−3648.

Skamarock, W.; Klemp, J.; Dudhia, J.; Gill, D.; Barker, D.; Duda, M.; Huang, X.-Y.; Wang, W.; Powers, J. (2008). *A Description of the Advanced Research WRF Version 3*. Boulder, CO: National Center for Atmospheric Research.

Taylor, K. (2012). "Summarizing multiple aspects of model performance in a single diagram." *Journal of Geophysical Research: Atmospheres*; Vol. 106, pp. 7183– 7192.

Wilks, D.S. (2005). "Statistical Methods in the Atmospheric Sciences." *Elsevier Inc*., ISBN-13: 978-0127519661.

Appendix

WRF Namelist

```
 &domains
  time_step                  =  300,|
  s_we                       =  1,  1,  1,  1,
  e_we                       =  151,355,
  s_sn                       =  1,  1,  1,  1,
  e_sn                       =  100,202,
  s_vert                     =  1,  1,  1,  1,  1, 1,
  e_vert                     =  41,41,41,41,
  num_metgrid_soil_levels     =  4 ,
  num_metgrid_levels          =  38 ,
  eta_levels                 =  1.0000, 0.9958, 0.9916, 0.9874, 0.9832,0.9790, 0.9749, 0.9707, 0.9661,
 0.9609,0.9549, 0.9480, 0.9398, 0.9303, 0.9189,0.9054, 0.8894, 0.8704, 0.8481, 0.8221,0.7922, 0.7583, 0.7205,
 0.6791, 0.6346,0.5877, 0.5393, 0.4900, 0.4407, 0.3922,0.3450, 0.2996, 0.2564, 0.2156, 0.1773,0.1417, 0.1086,
 0.0755, 0.0475, 0.0224,0.000
  p_top_requested            = 5000,
  dx                         = 54000,18000,
  dy                         = 54000,18000,
  i_parent_start             = 1,17,
  j_parent_start             = 1,17,
  parent_grid_ratio          = 1,  3,  3,  3,  3,  3,
  parent_time_step_ratio     = 1,  3,  3,  3,  3, 3,
  feedback                   = 0,
  smooth_option              = 2
  use_adaptive_time_step     = .false.
  step_to_output_time        = .false.
 /

 &physics
  topo_wind                  = 1,1,
 num_land_cat                = 33,
  mp_physics                 = 5, 5,
  ra_lw_physics              = 1, 1,
  ra_sw_physics              = 1, 1,
  radt                       = 15,    15,    15,    15,    15,    15,
 sf_sfclay_physics           = 1, 1,
 sf_surface_physics          = 2, 2,
  bl_pbl_physics             = 1, 1,
  bldt                       = 0,     0,     0,     0,     0,     0,
  cu_physics                 = 1,     1,     0,     0,     0,     0,
 cudt                        = 5,     5,     5,     0,     0,     0,
  cam_abs_freq_s             = 21600,
  levsiz                     = 59,
  paerlev                    = 29,
  cam_abs_dim1               = 4,
  cam_abs_dim2               = 41,
  isfflx                     = 1,
  ifsnow                     = 0,
  icloud                     = 1,
  surface_input_source       = 1,
  num_soil_layers            = 4,
  sf_urban_physics           = 0,0,0,0,0,0,0,0
```

```
 mp_zero_out                 = 0,
 maxiens                     = 1,
 maxens                      = 3,
 maxens2                     = 3,
 maxens3                     = 16,
 ensdim                      = 144,
 slope_rad                   = 0,
 topo_shading                = 0,
 /

 &fdda
 grid_fdda                  = 2, 2, 0,
gfdda_interval_m            = 360, 360, 0,
 gfdda_end_h                = 768, 768, 0,
 io_form_gfdda              = 2,
 fgdt                        = 0,     0,     0,
 if_no_pbl_nudging_uv       = 1, 1, 0, 0, 0, 0,
if_no_pbl_nudging_t         = 1, 1, 0,
 if_no_pbl_nudging_q        = 1, 1, 0,
 if_zfac_uv                  = 0,     0,     0,
  k_zfac_uv                  = 10,   10,    10,
 if_zfac_t                  = 1, 1, 0,
  k_zfac_t                  = 10,   10,    10,
 if_zfac_q                  = 1, 1, 0,
  k_zfac_q                  = 10,   10,    10,
 guv                         = 0.0003,     0.0001,     0.0001,
 gt                          = 0.0003,     0.0001,     0.0001,
 gq                          = 0.000003,   0.000001,   0.000001,
 xwavenum                    = 20, 16, 0,
 ywavenum                    = 14, 9, 0,
 if_ramping                 = 0,
 dtramp_min                  = 0.0,
/

 &dynamics
use_baseparam_fr_nml        = .true.
 w_damping                  = 1,
 diff_opt                   = 1,
 km_opt                     = 4,
 diff_6th_opt               = 0,
 diff_6th_factor            = 0.12,
 base_temp                  = 290.
 damp_opt                   = 0,
 zdamp                      = 5000.,  5000.,  5000.,5000.,
 dampcoef                   = 0.01,   0.01,   0.01,   0.01
 khdif                      = 0,      0,      0,      0,
 kvdif                      = 0,      0,      0,      0,
 non_hydrostatic            = .true., .true., .true.,.true.
 /

 &bdy_control
spec_zone                   = 1,
 relax_zone                 = 4,
```

Diurnal Cycles Per Month

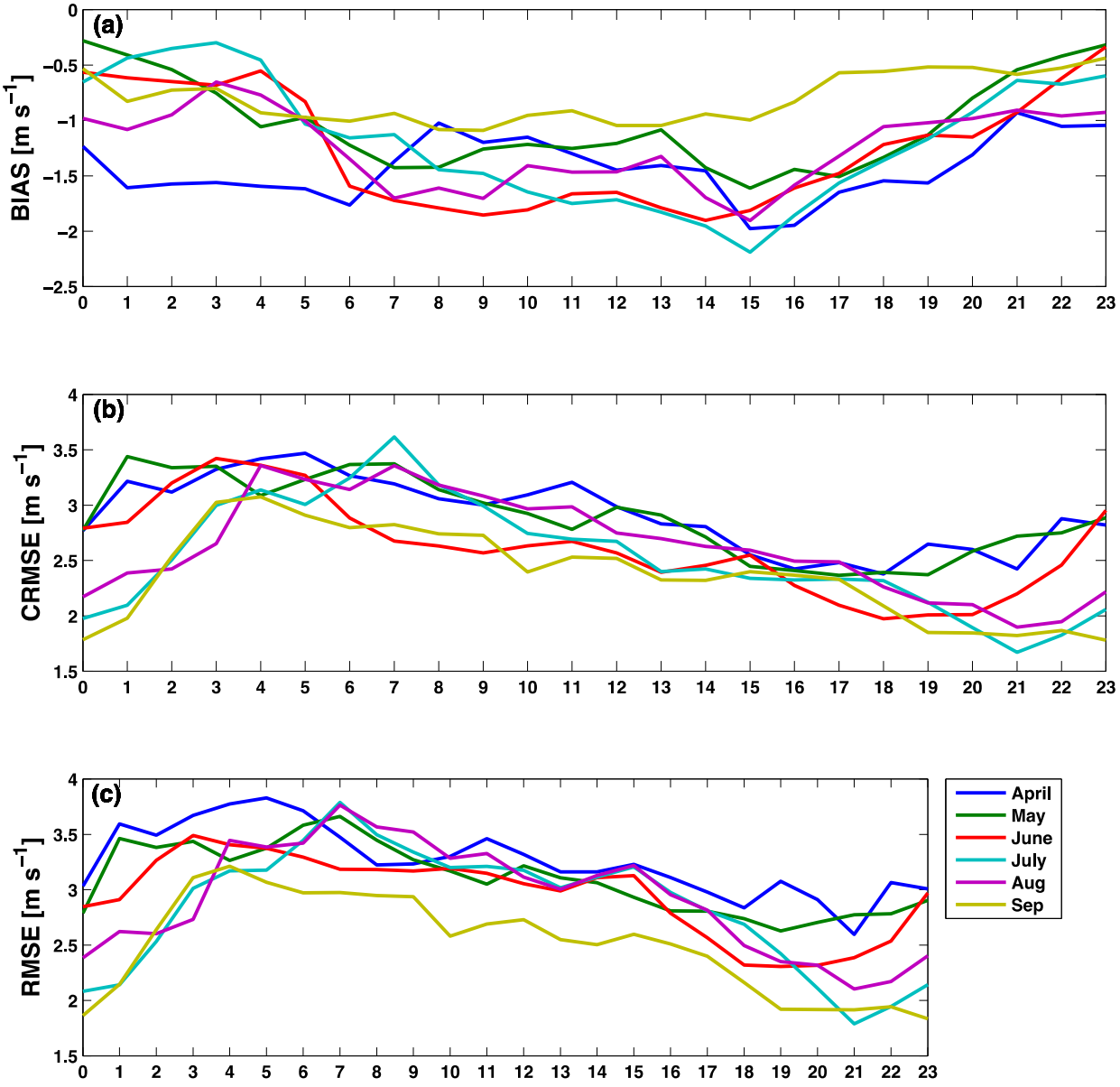

Figure A1. Diurnal cycle of wind speed bias (top), centered-root-mean-square error (CRMSE) (middle), and root-mean-square error (RMSE) (bottom) for the summer months for Butler Grade

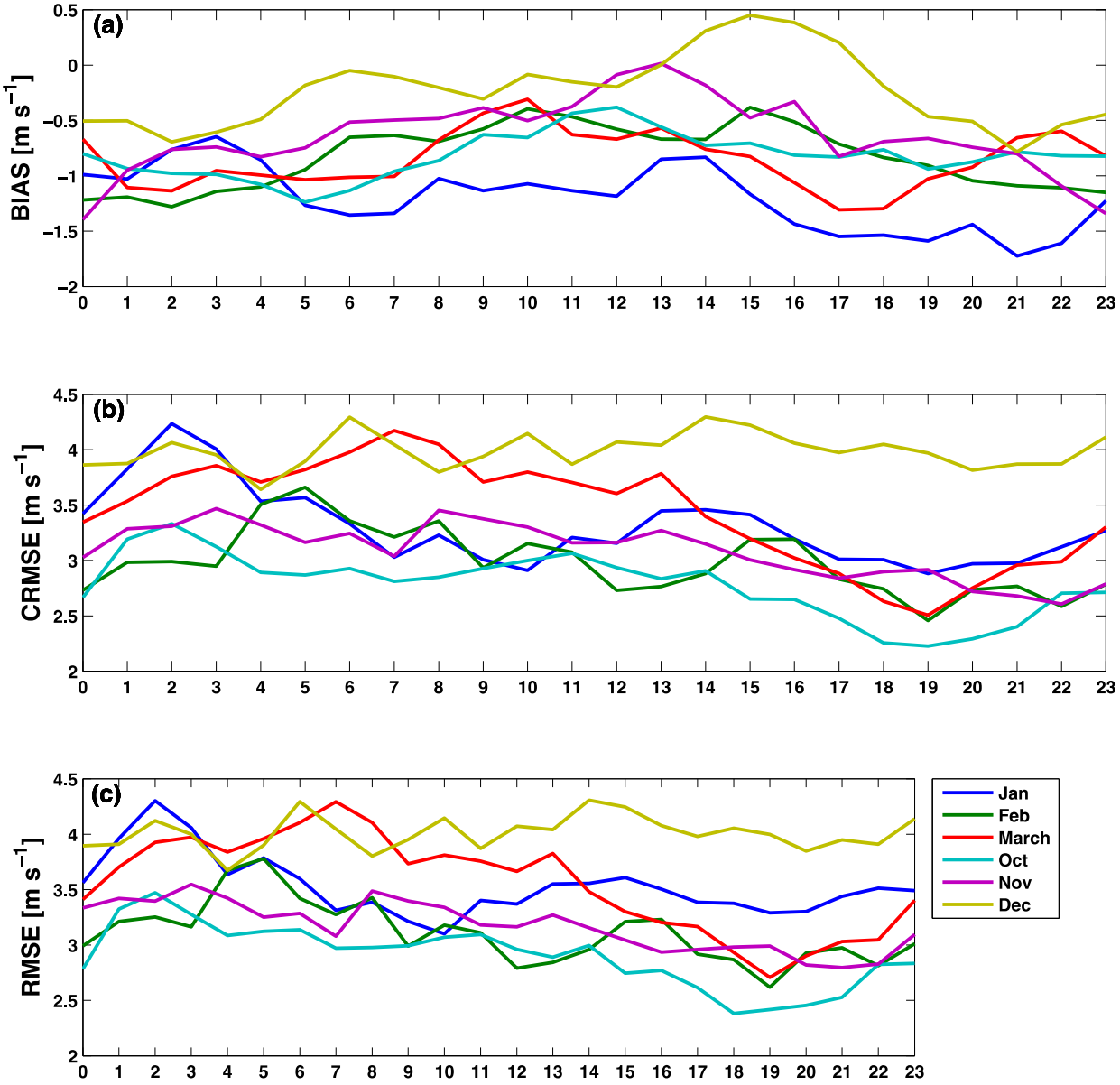

Figure A2. Diurnal cycle of wind speed bias (top), CRMSE (middle), and RMSE (bottom) for the winter months for Butler Grade

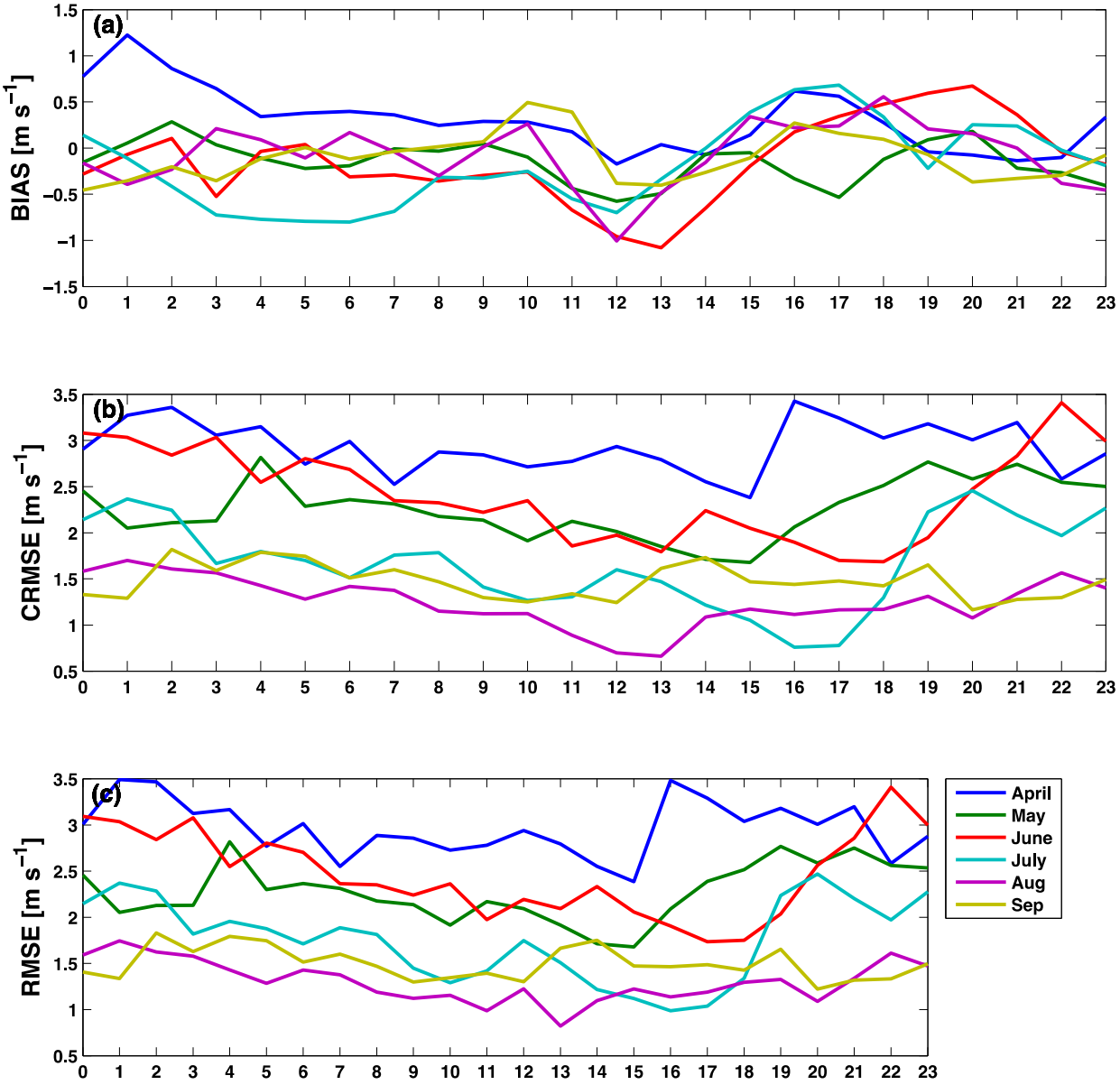

Figure A3. Diurnal cycle of wind speed bias (top), CRMSE (middle), and RMSE (bottom) for the summer months for Cape May

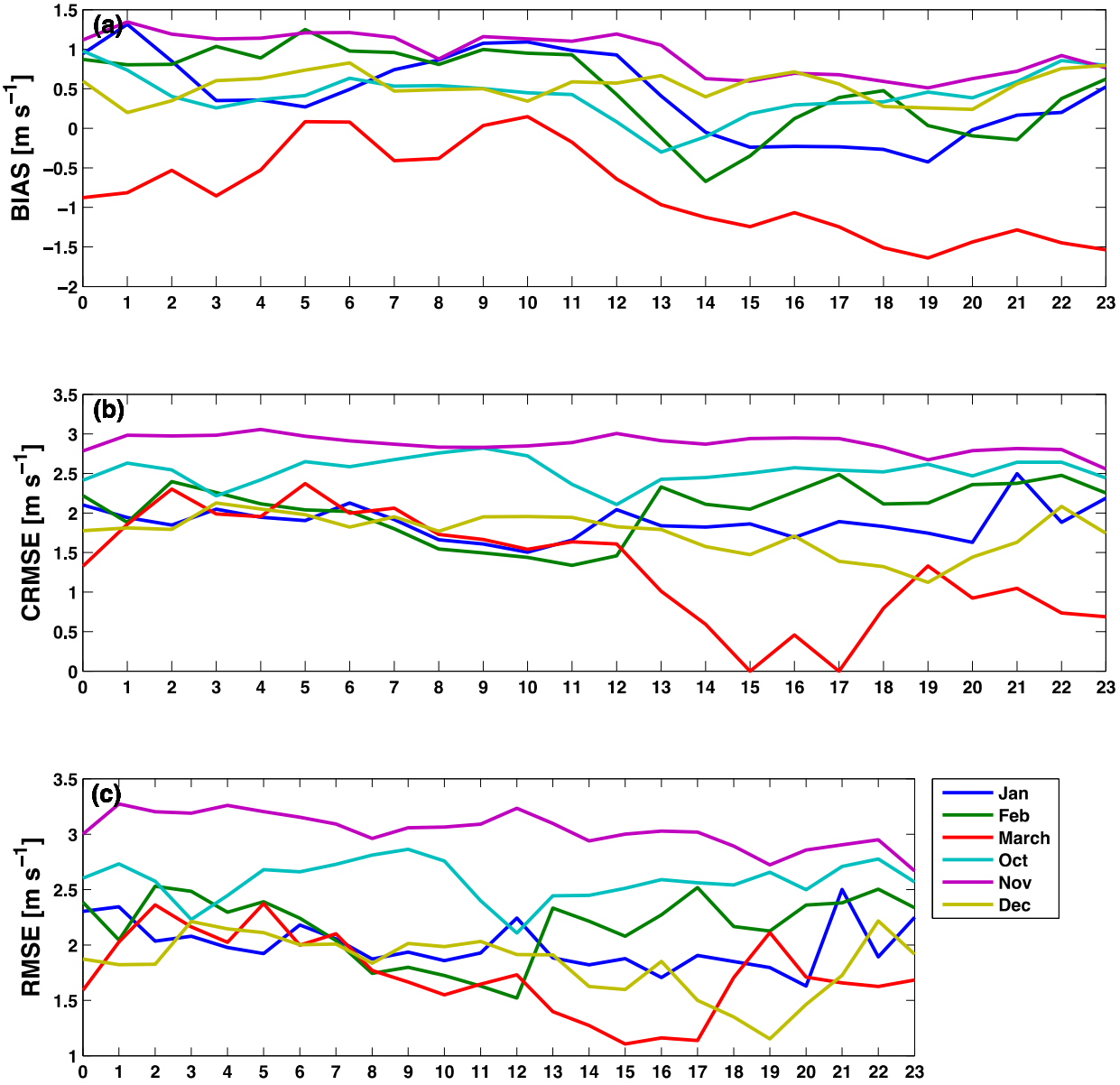

Figure A4. Diurnal cycle of wind speed bias (top), CRMSE (middle), and RMSE (bottom) for the winter months for Cape May

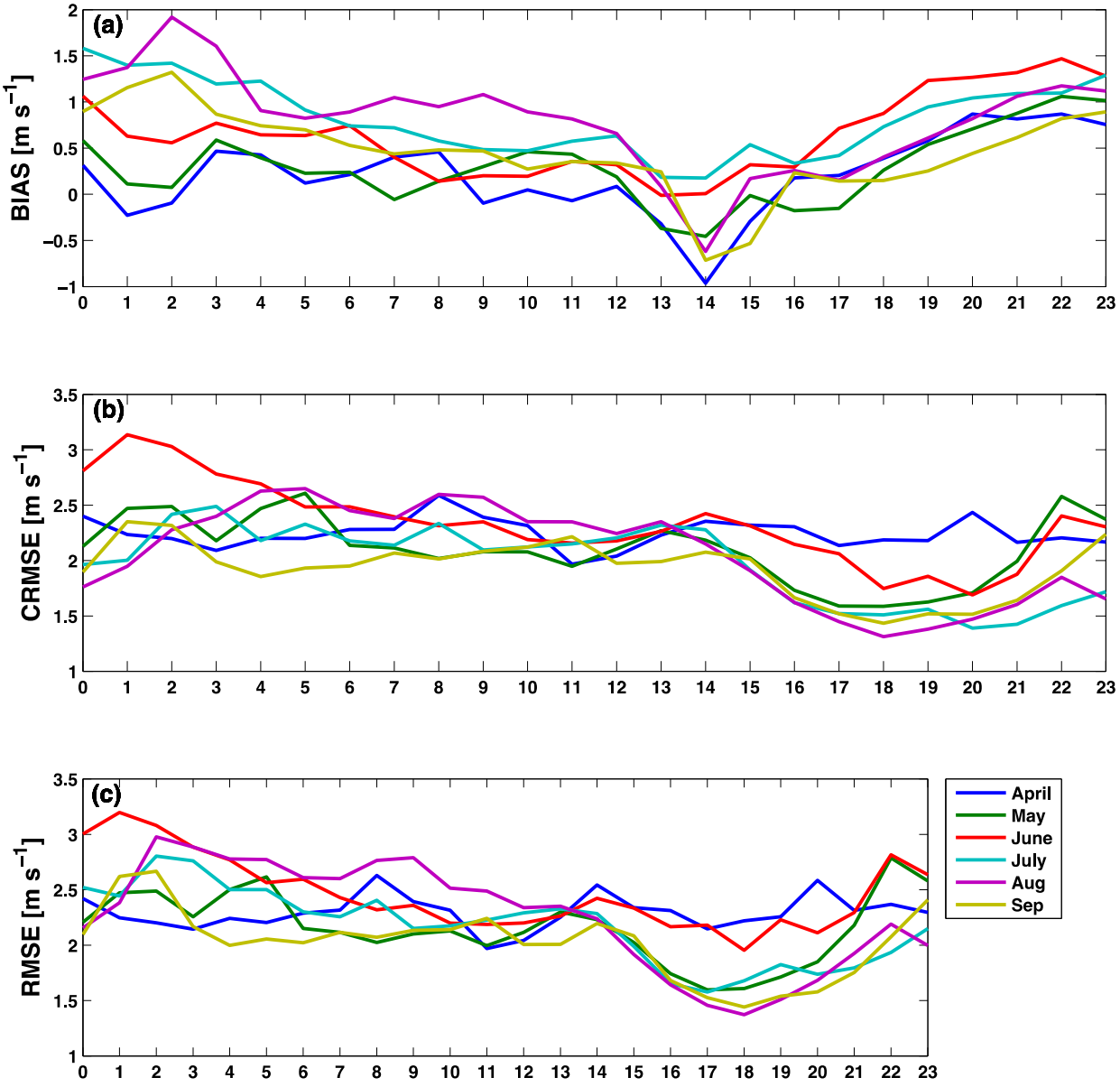

Figure A5. Diurnal cycle of wind speed bias (top), CRMSE (middle), and RMSE (bottom) for the summer months for Cochran

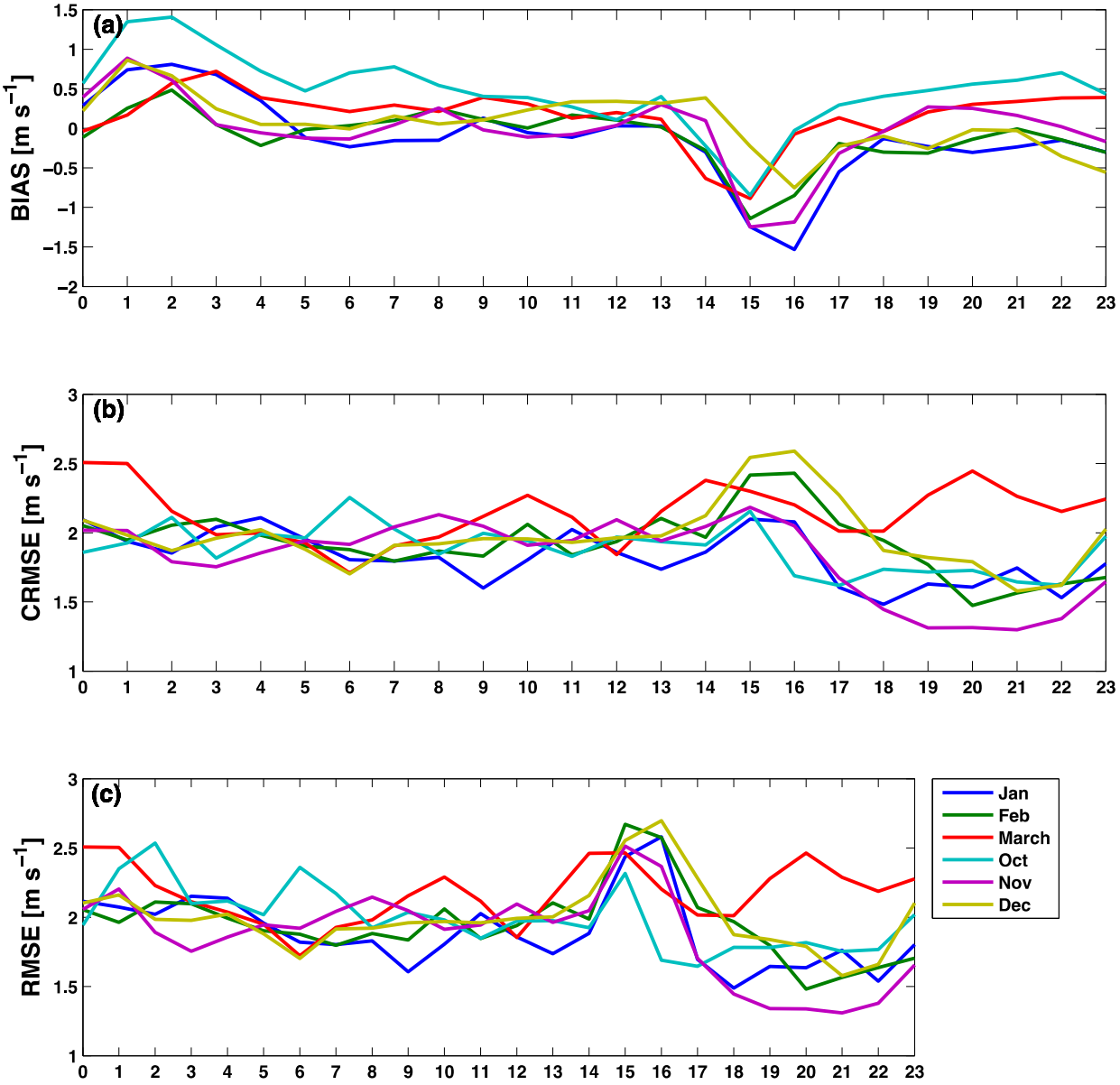

Figure A6. Diurnal cycle of wind speed bias (top), CRMSE (middle), and RMSE (bottom) for the winter months for Cochran

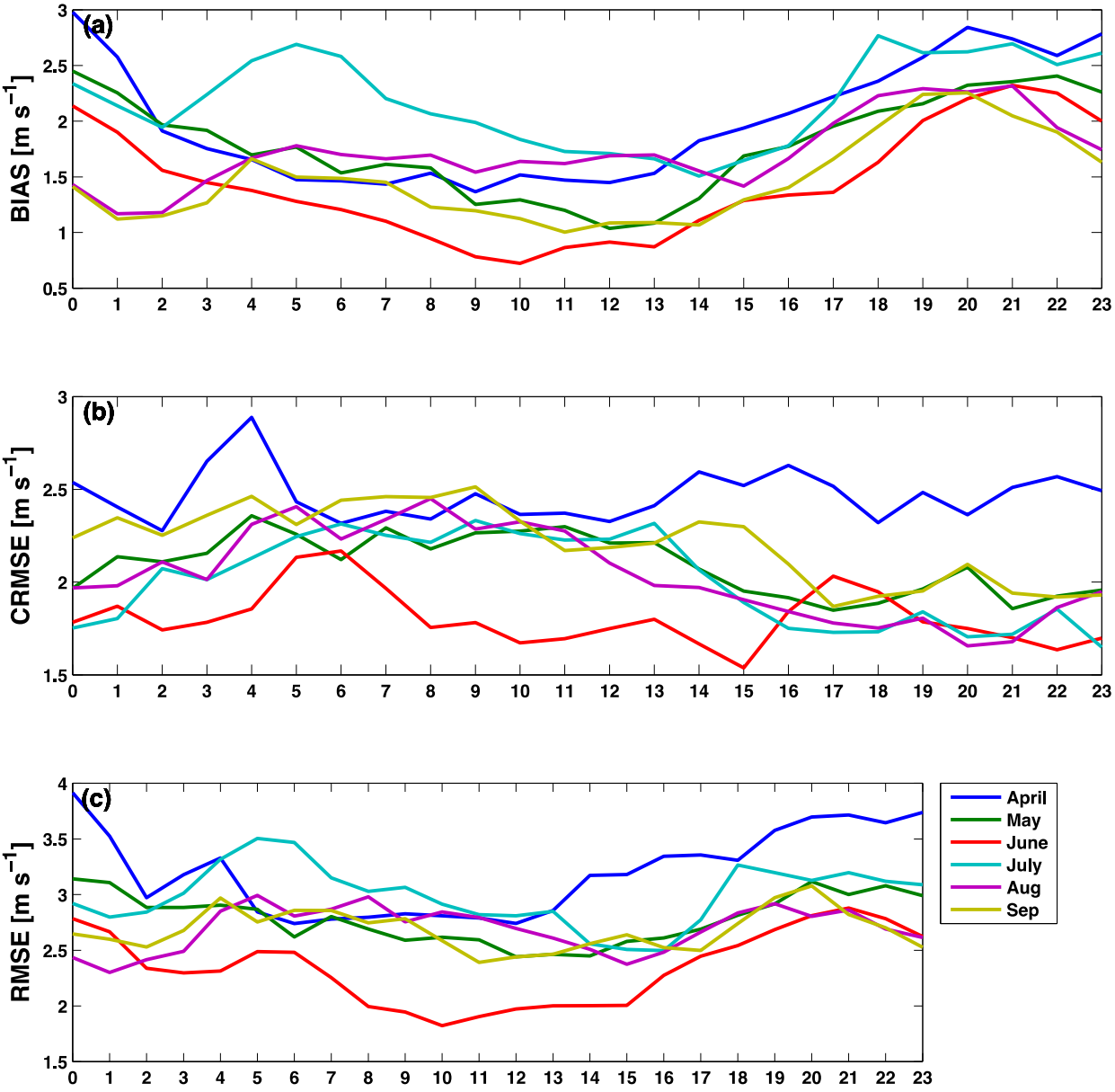

Figure A7. Diurnal cycle of wind speed bias (top), CRMSE (middle), and RMSE (bottom) for the summer months for Megler

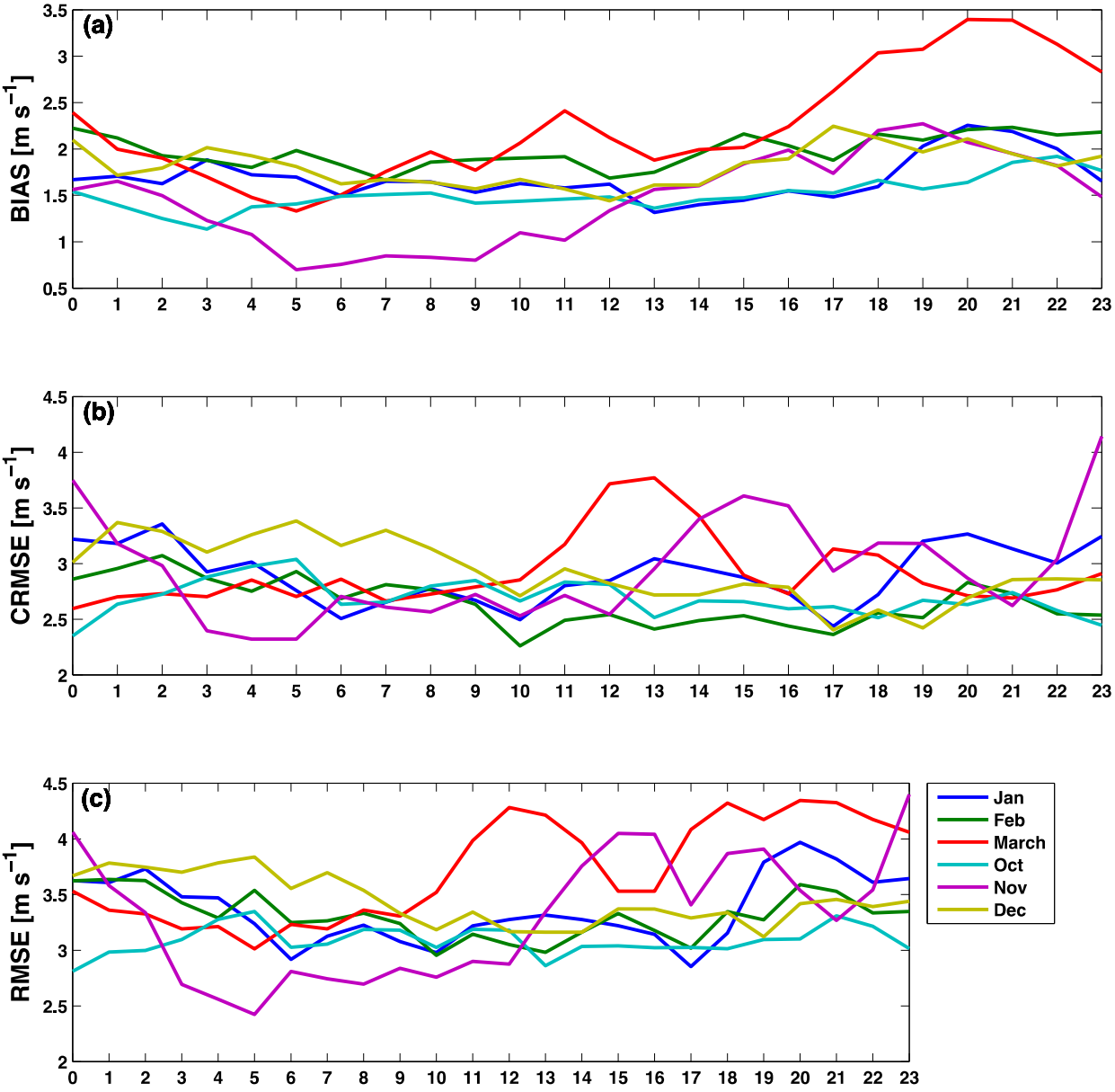

Figure A8. Diurnal cycle of wind speed bias (top), CRMSE (middle), and RMSE (bottom) for the winter months for Megler

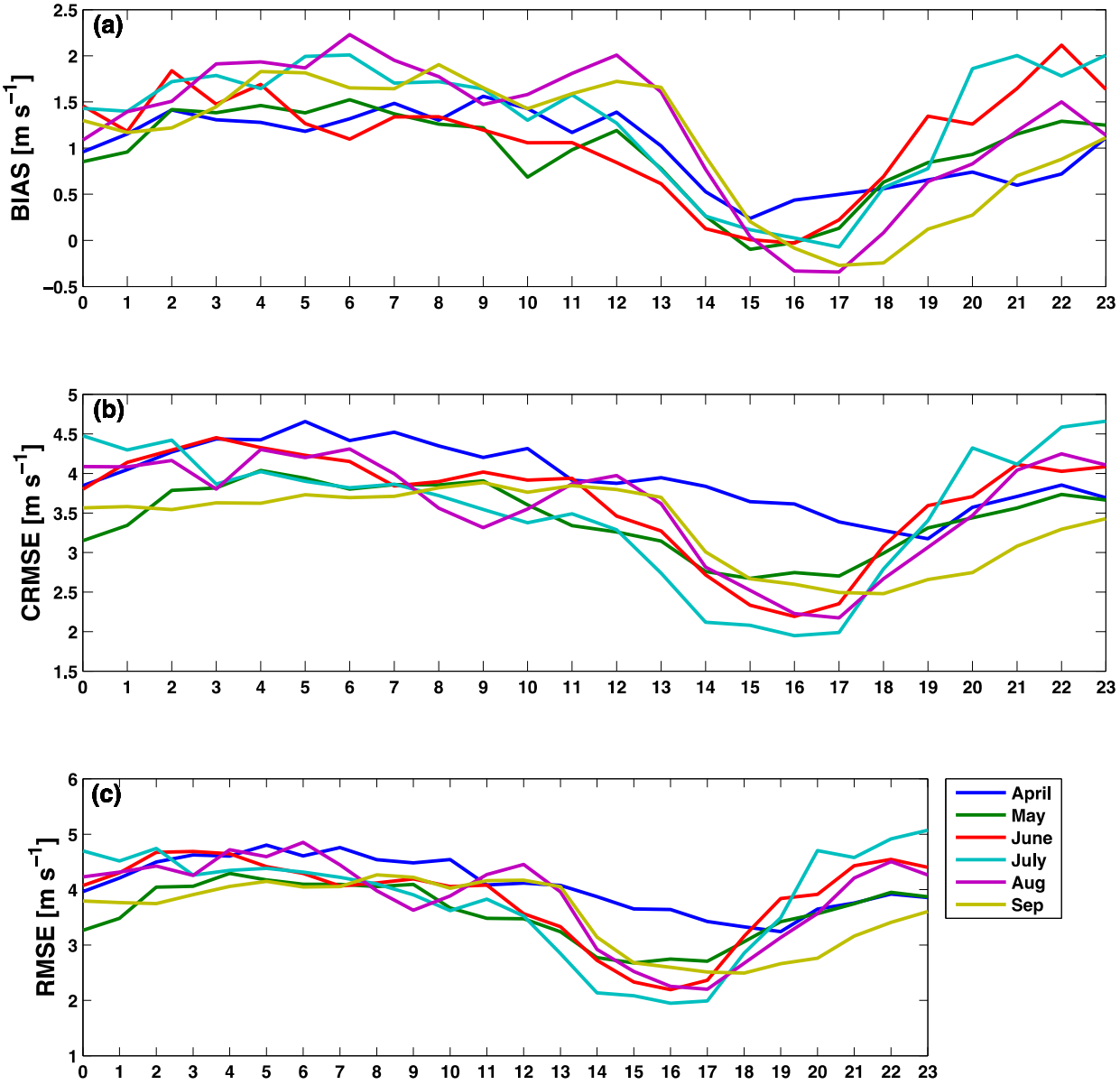

Figure A9. Diurnal cycle of wind speed bias (top), CRMSE (middle), and RMSE (bottom) for the summer months for the National Wind Technology Center (NWTC)

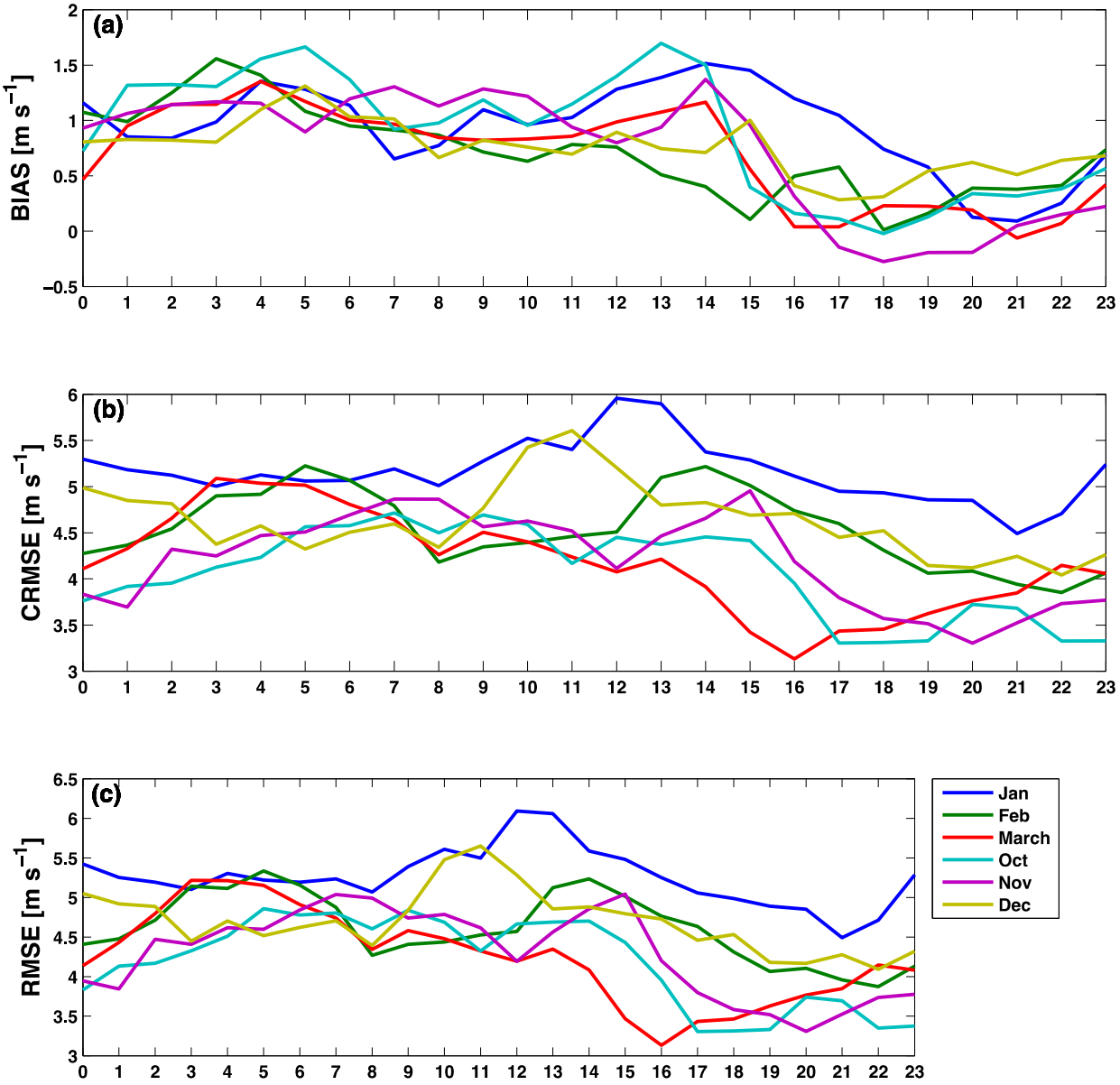

Figure A10. Diurnal cycle of wind speed bias (top), CRMSE (middle), and RMSE (bottom) for the winter months for the NWTC

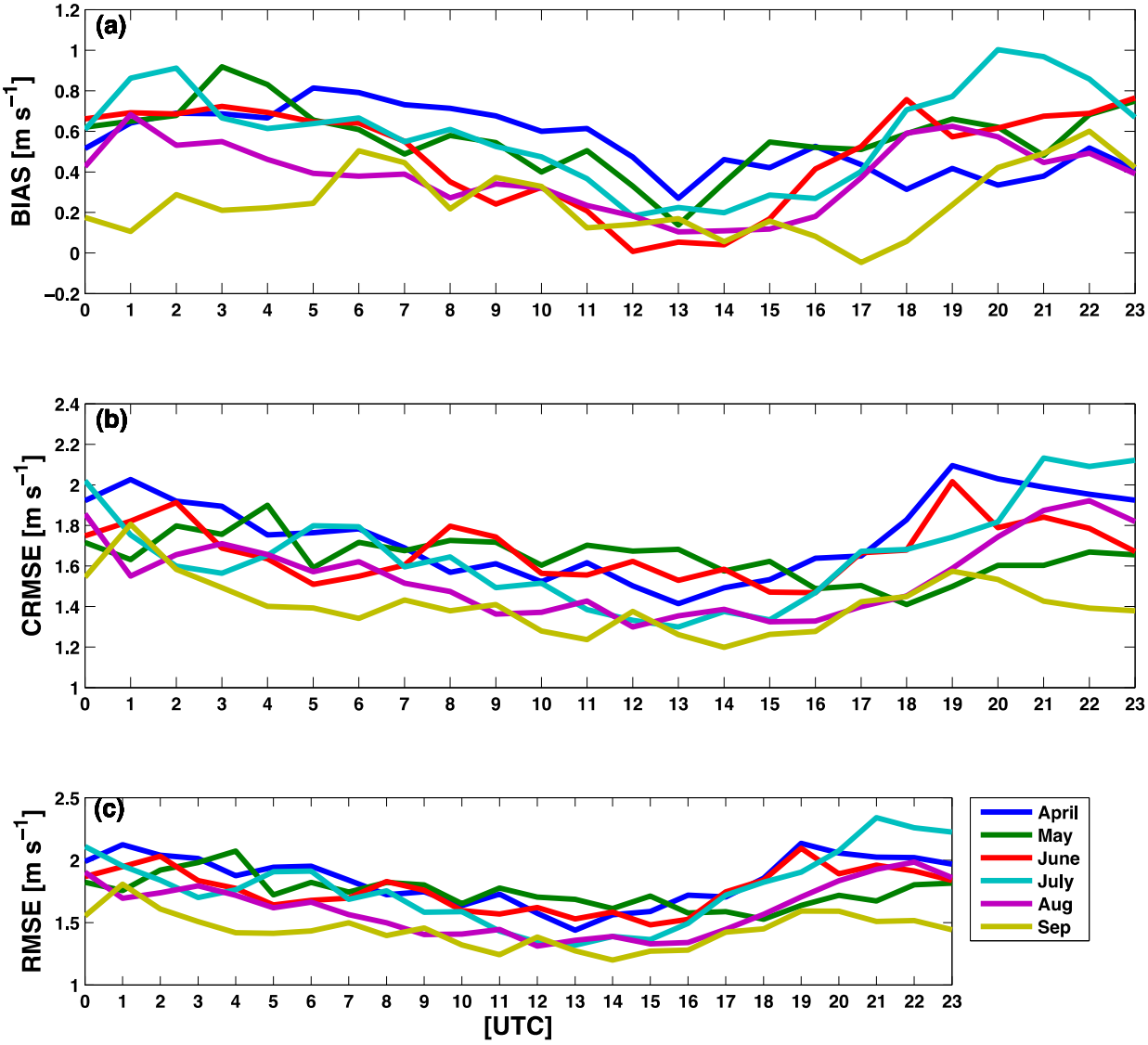

Figure A11. Diurnal cycle of wind speed bias (top), CRMSE (middle), and RMSE (bottom) for the summer months for New York Harbor at 10 m

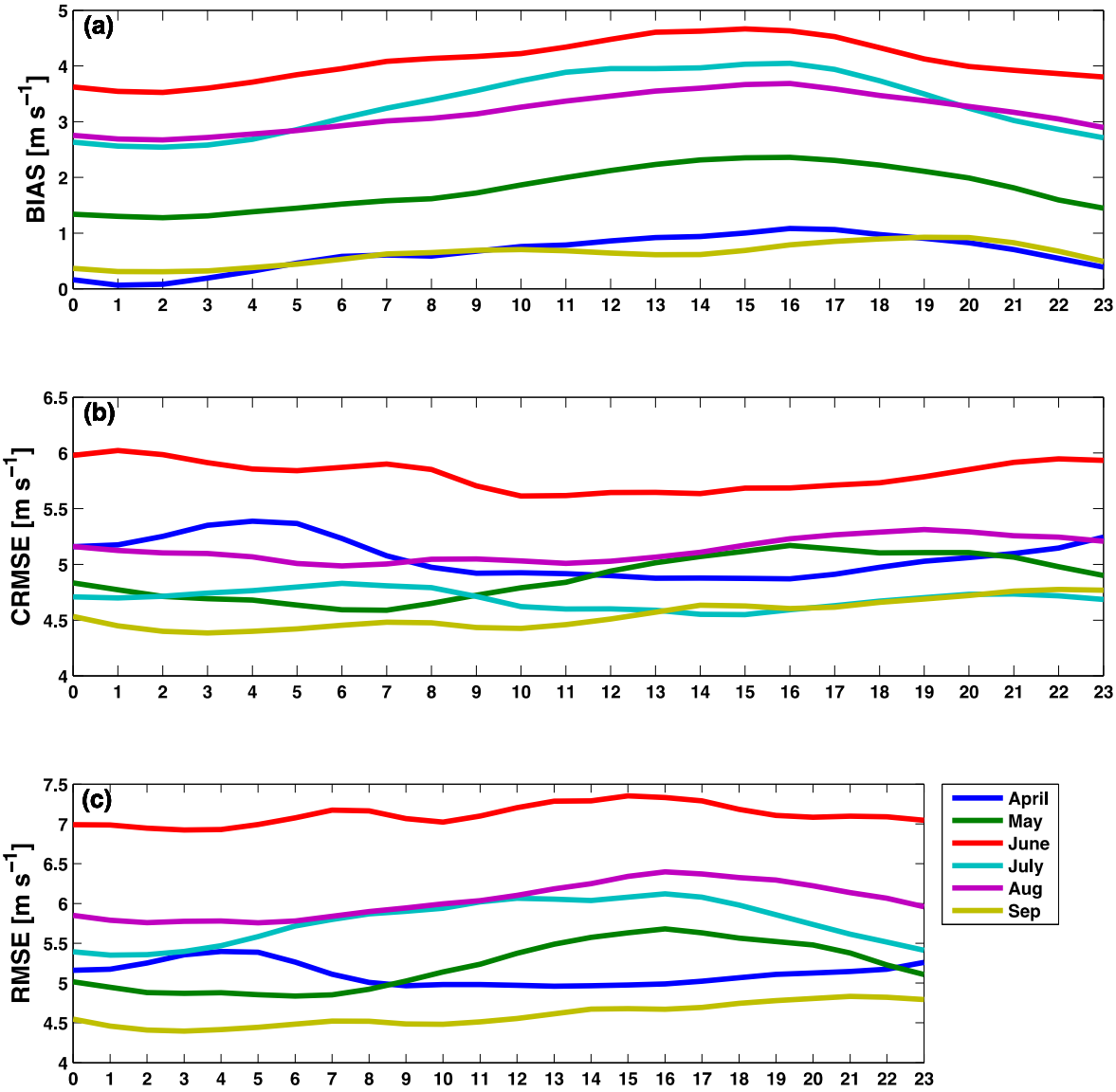

Figure A12. Diurnal cycle of wind speed bias (top), CRMSE (middle), and RMSE (bottom) for the summer months for New York Harbor at 50 m; WIND Toolkit model data are compared to Modern-Era Retrospective Analysis (MERRA)

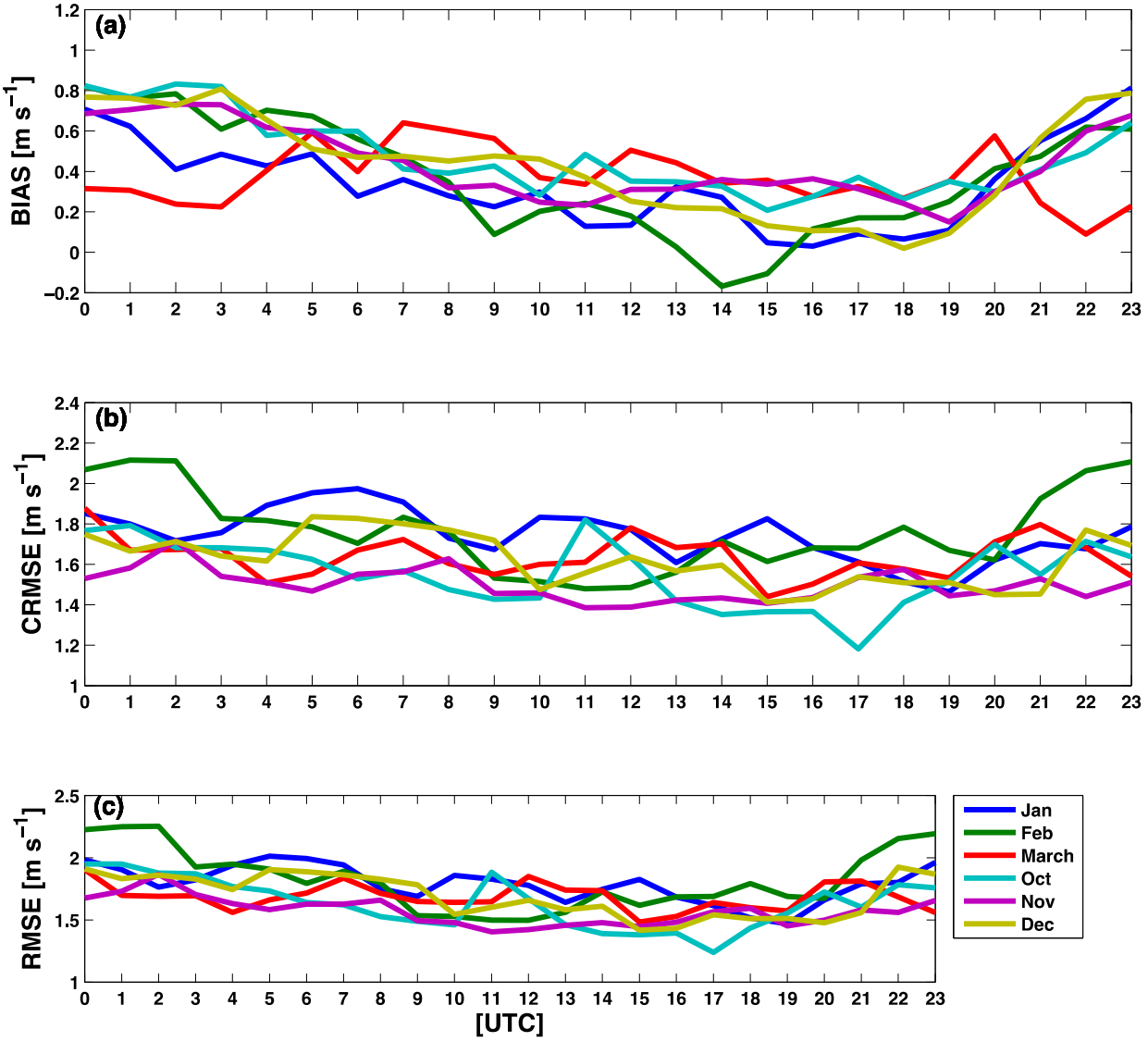

Figure A13. Diurnal cycle of wind speed bias (top), CRMSE (middle), and RMSE (bottom) for the winter months for New York Harbor at 10 m

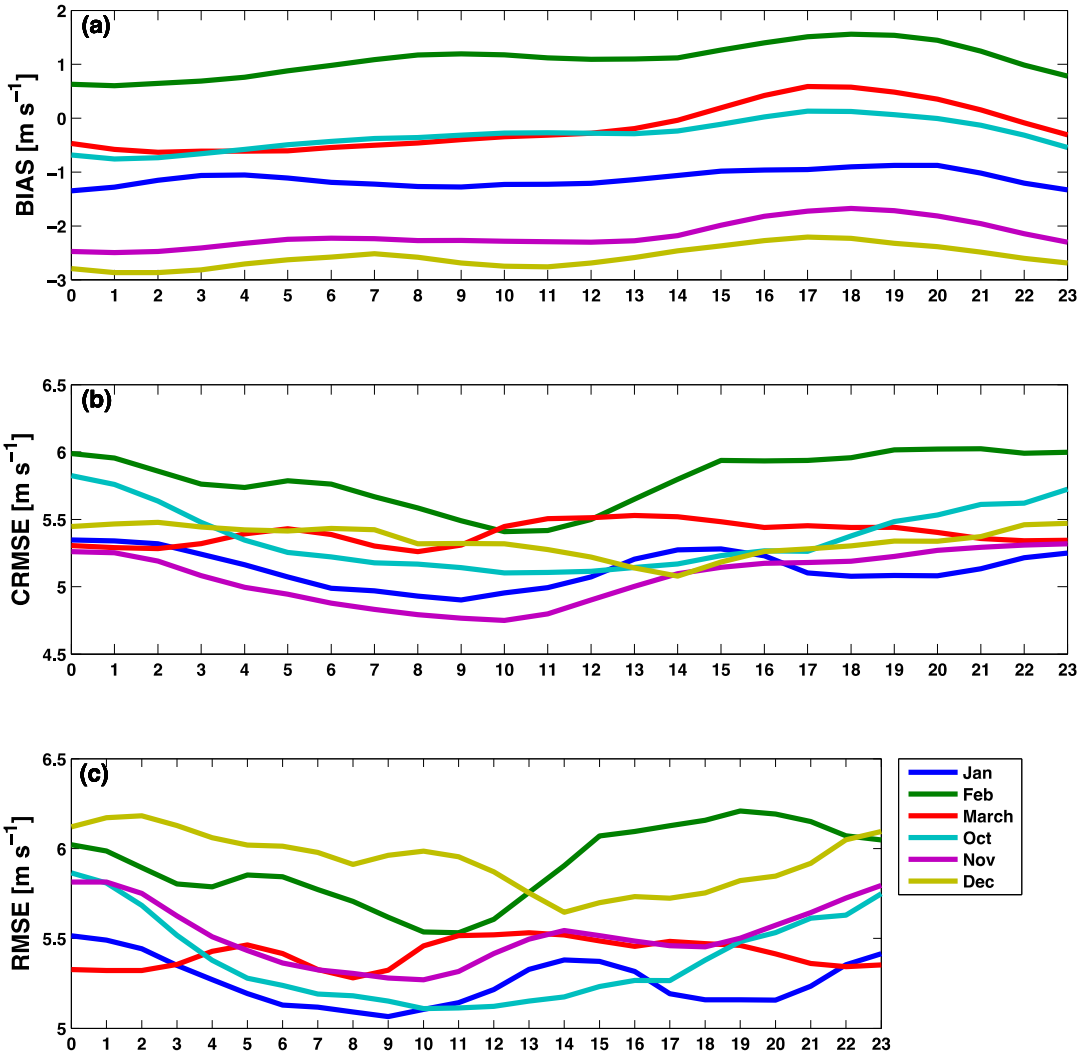

Figure A14. Diurnal cycle of wind speed bias (top), CRMSE (middle), and RMSE (bottom) for the winter months for New York Harbor at 50 m; WIND Toolkit data are compared to MERRA

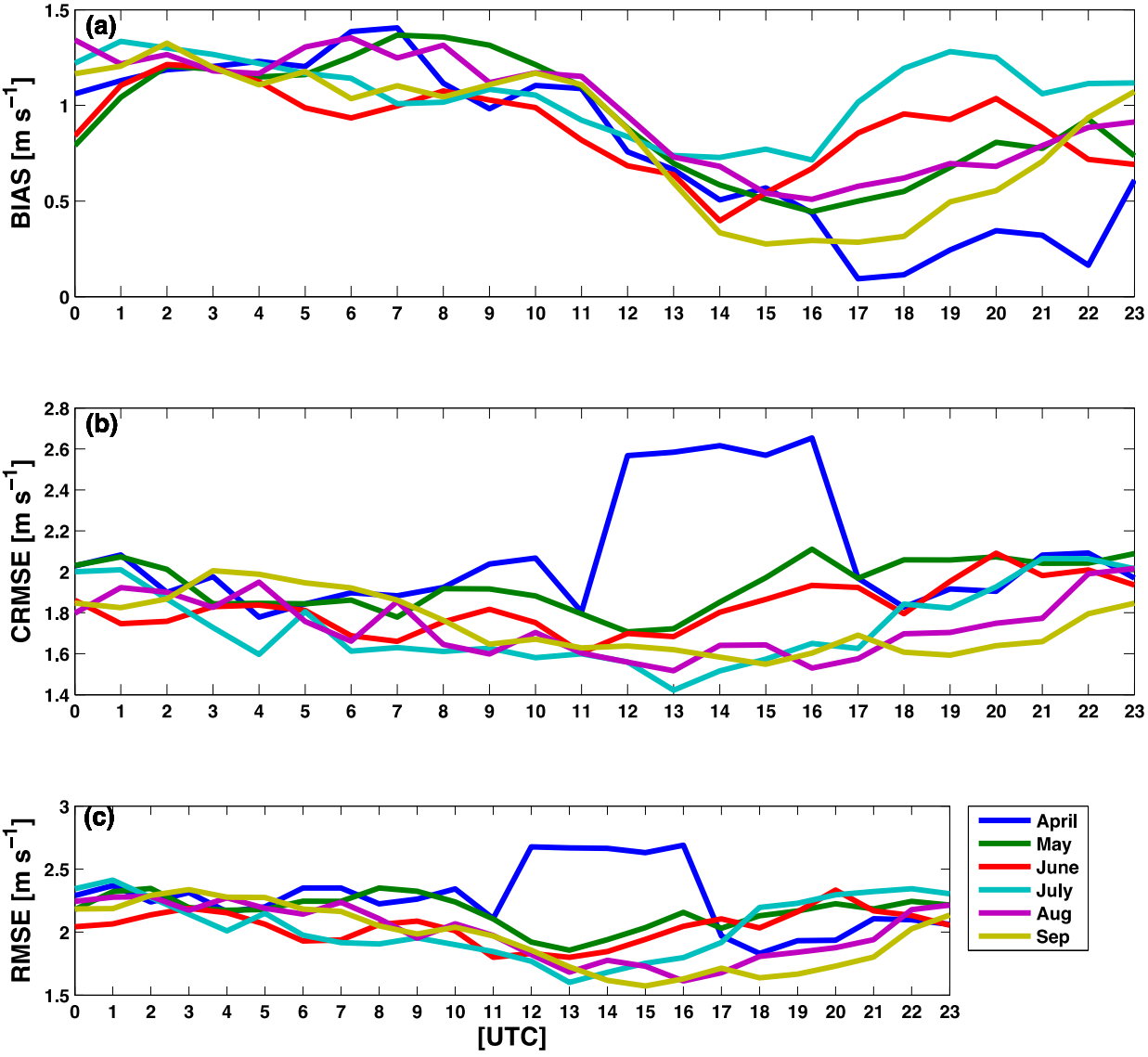

Figure A15. Diurnal cycle of wind speed bias (top), CRMSE (middle), and RMSE (bottom) for the summer months for Portland at 10 m

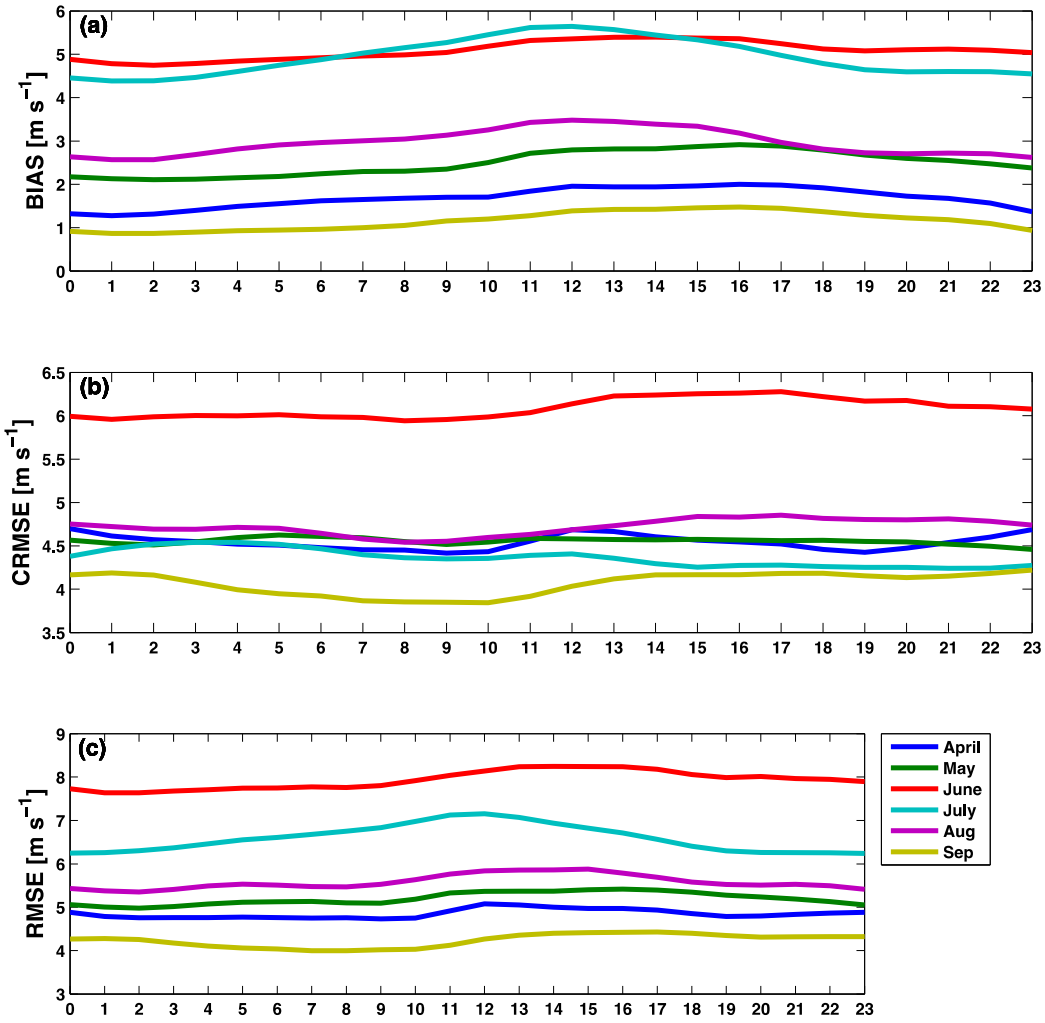

Figure A16. Diurnal cycle of wind speed bias (top), CRMSE (middle), and RMSE (bottom) for the summer months for Portland at 50 m; WIND Toolkit data are compared to MERRA

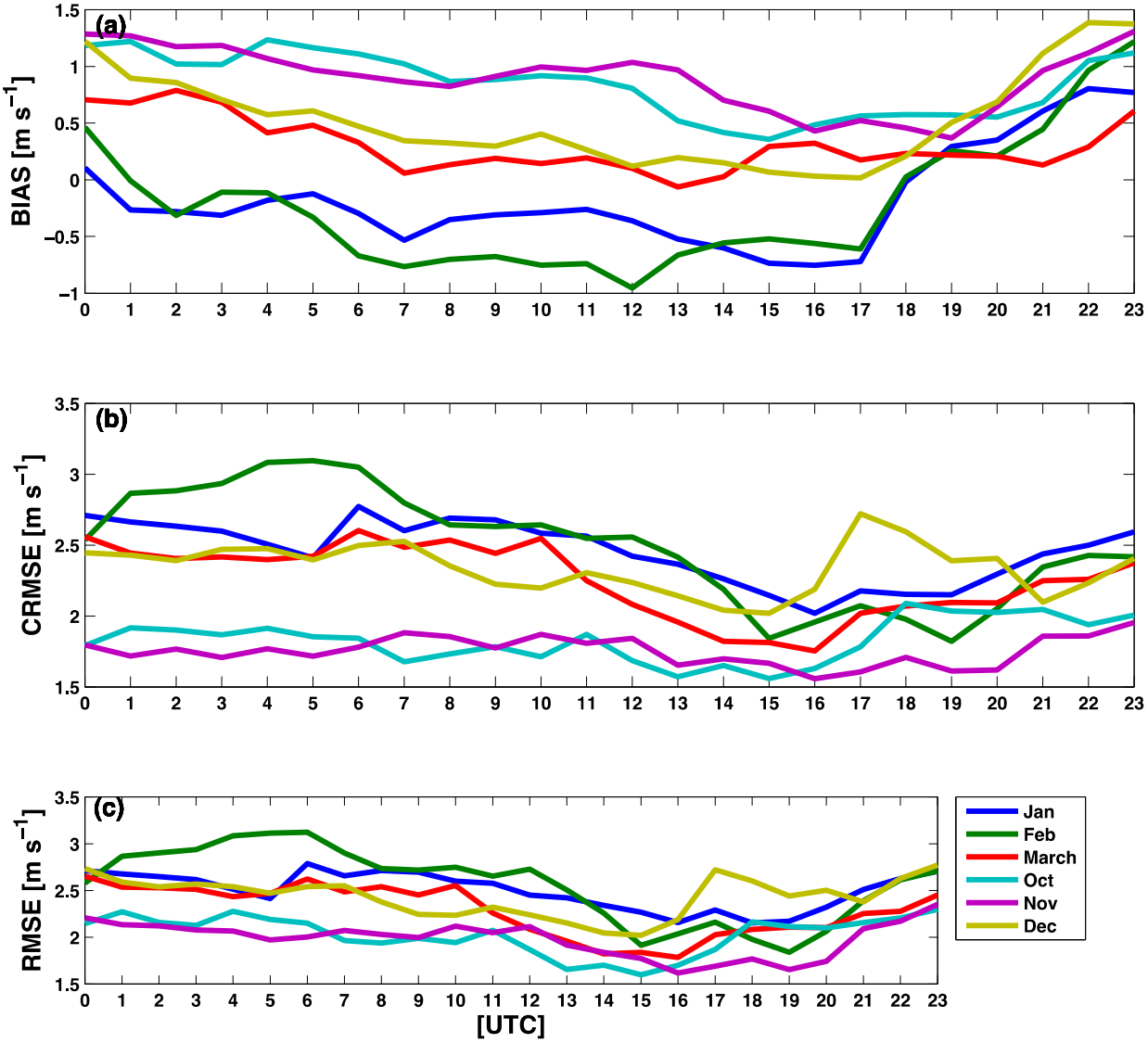

Figure A17. Diurnal cycle of wind speed bias (top), CRMSE (middle), and RMSE (bottom) for the winter months for Portland at 10 m

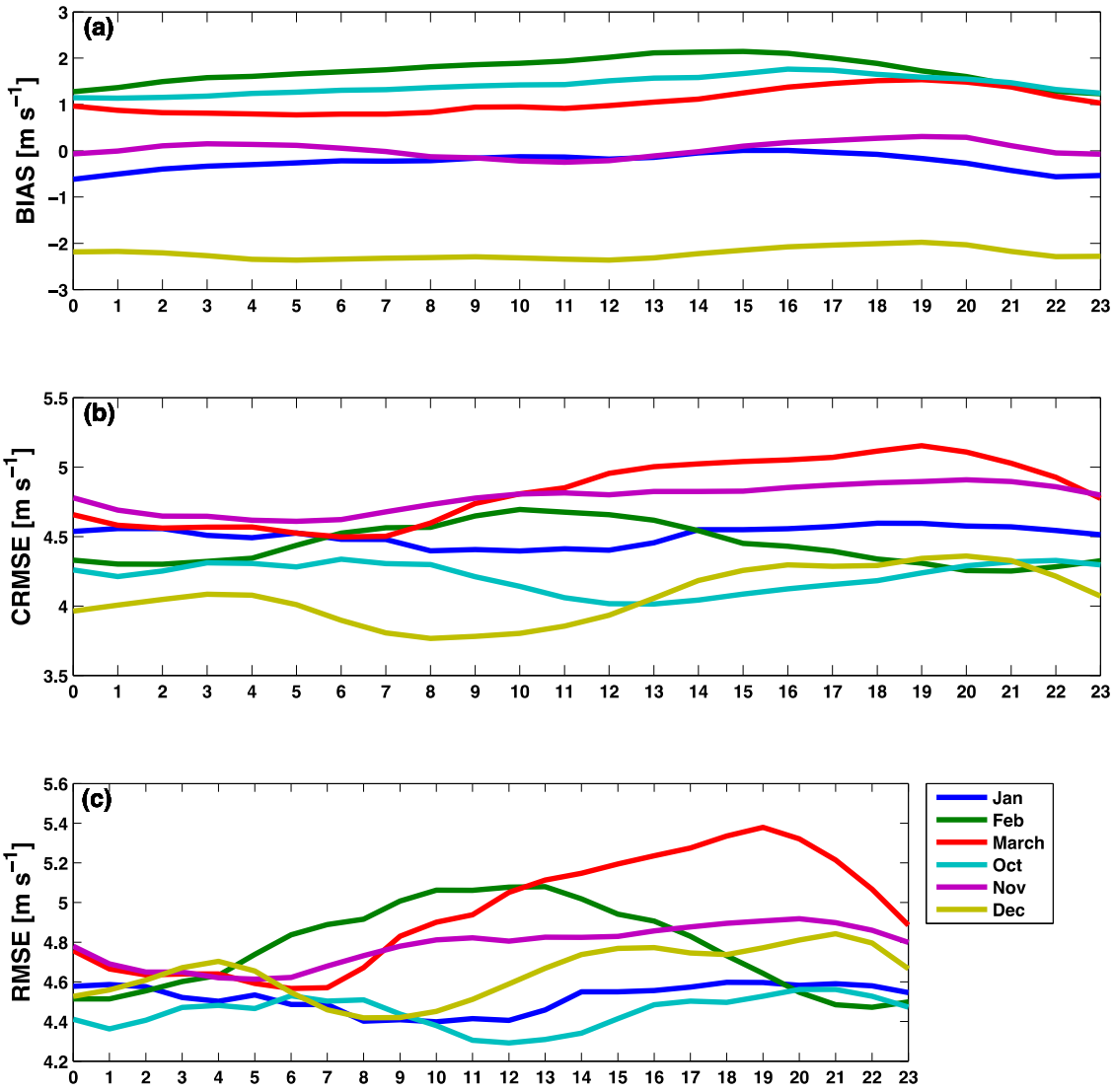

Figure A18. Diurnal cycle of wind speed bias (top), CRMSE (middle), and RMSE (bottom) for the winter months for Portland at 50 m; WIND Toolkit data are compared to MERRA

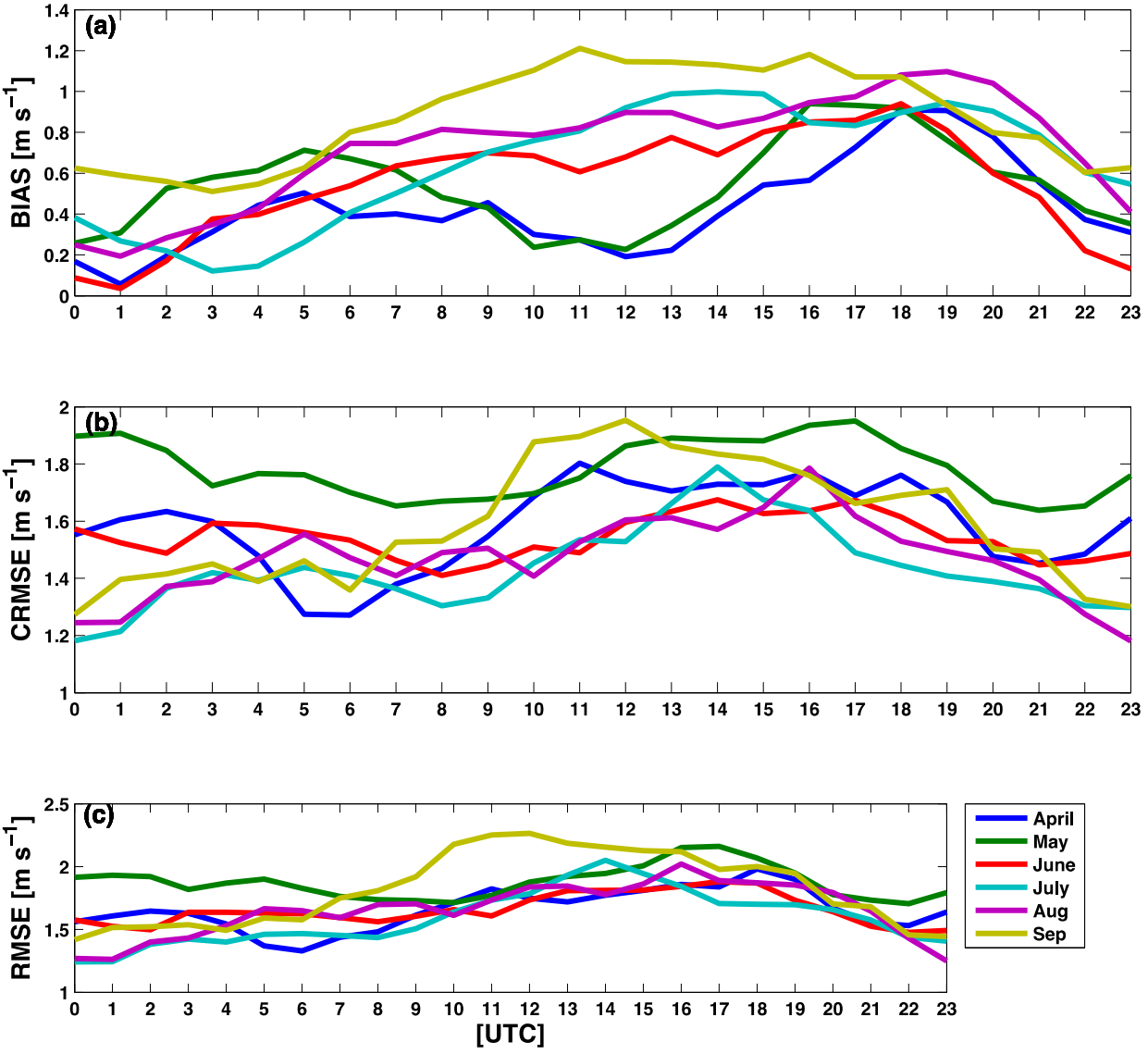

Figure A19. Diurnal cycle of wind speed bias (top), CRMSE (middle), and RMSE (bottom) for the summer months for Santa Maria at 10 m

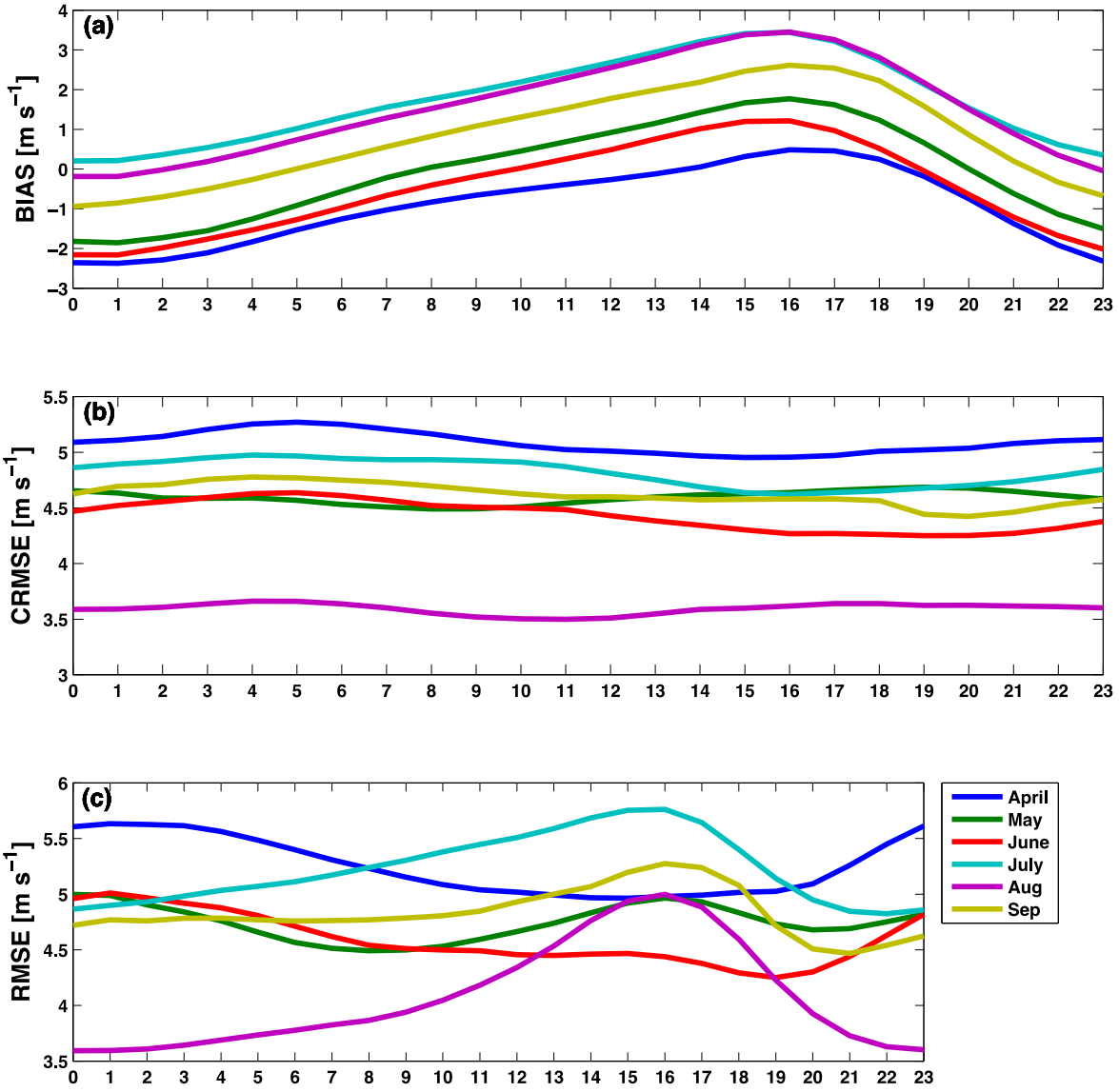

Figure A20. Diurnal cycle of wind speed bias (top), CRMSE (middle), and RMSE (bottom) for the summer months for Santa Maria at 50 m WIND Toolkit data are compared to MERRA

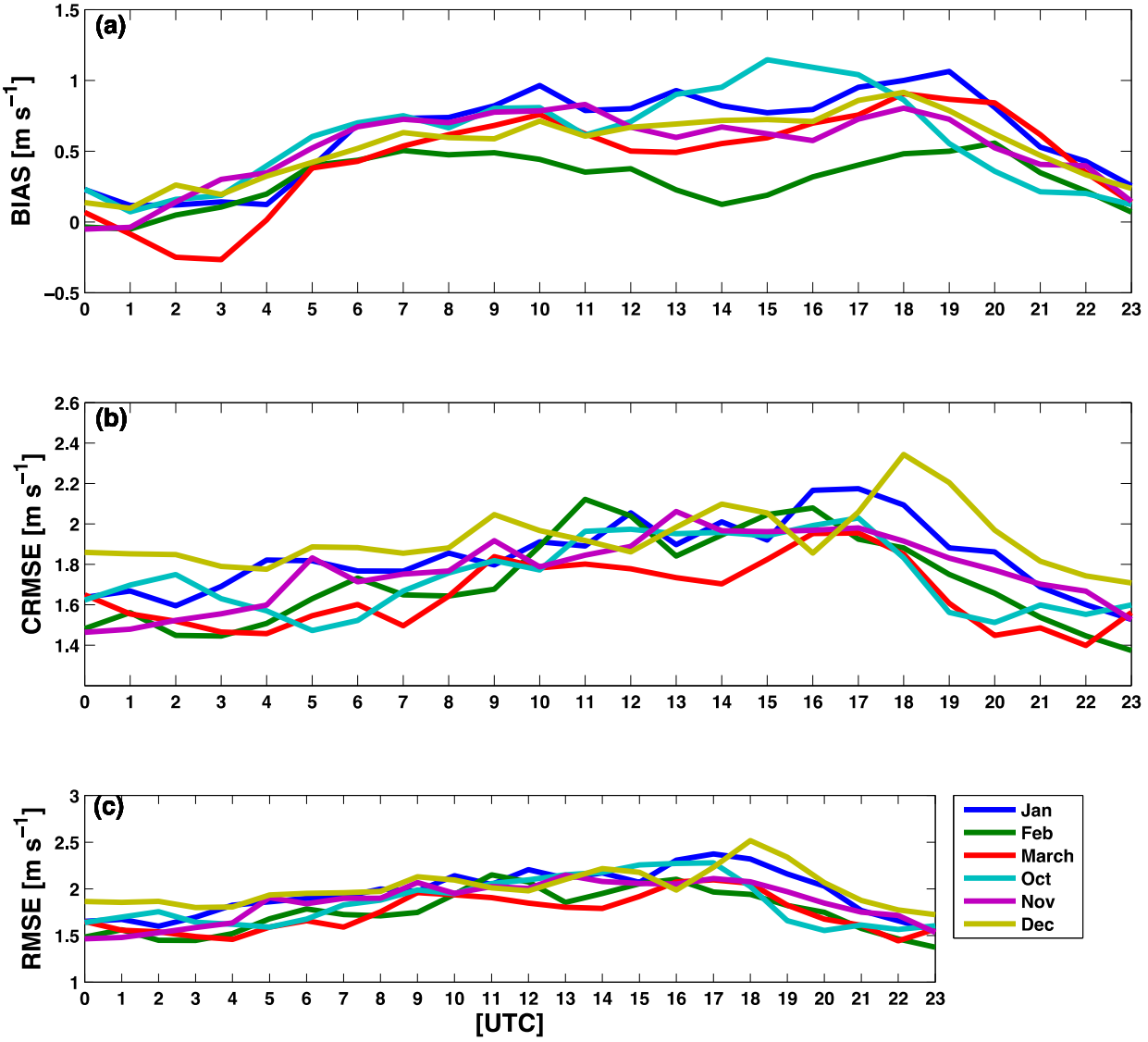

Figure A21. Diurnal cycle of wind speed bias (top), CRMSE (middle), and RMSE (bottom) for the winter months for Santa Maria at 10 m

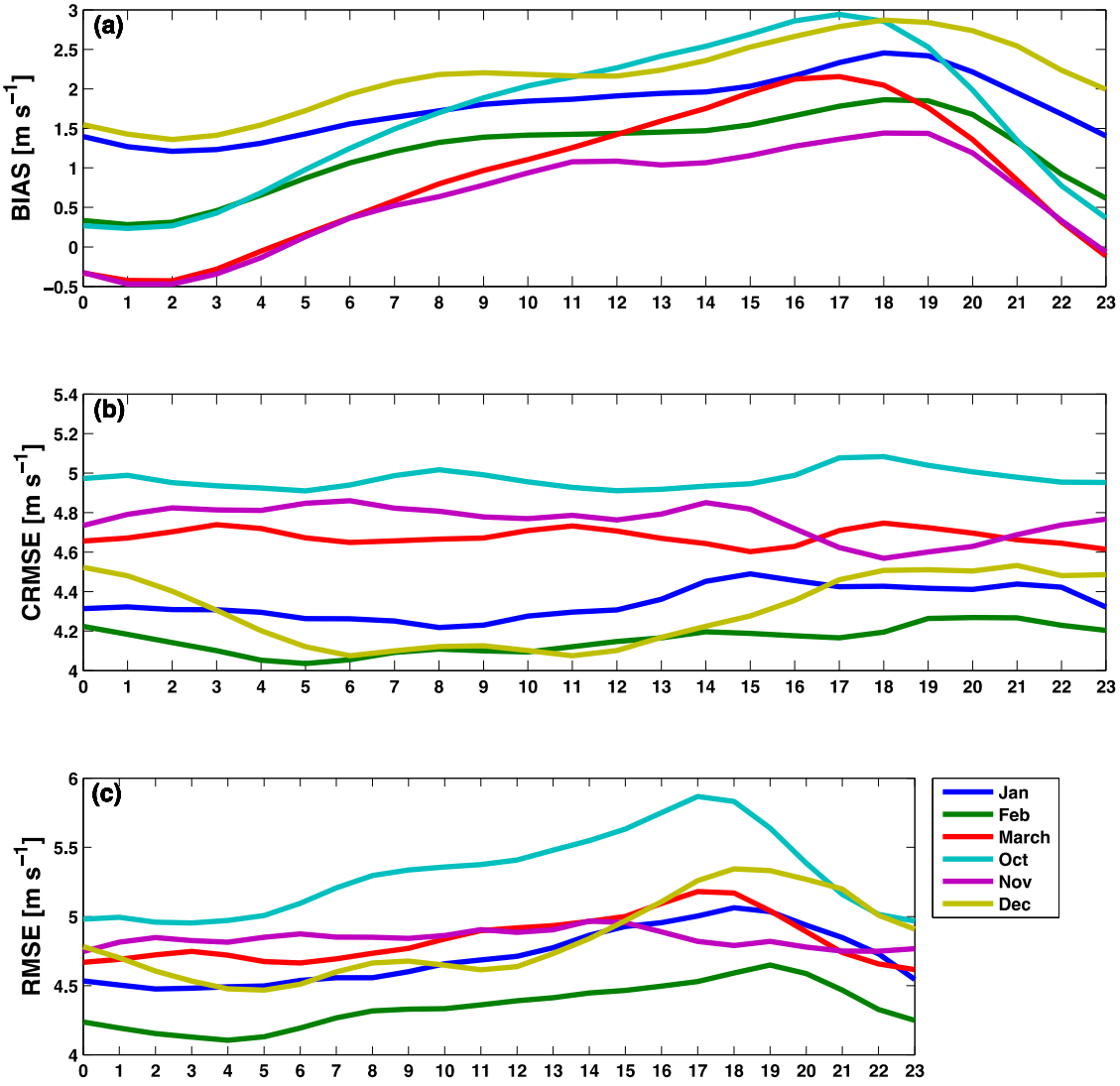

Figure A22. Diurnal cycle of wind speed bias (top), CRMSE (middle), and RMSE (bottom) for the winter months for Santa Maria at 50 m WIND Toolkit data are compared to MERRA